12-2010

Synthesis and Characterization of Diamond-like Carbon Thin Films for Biomedical Applications

Russell Lee Leonard
UTSI, rleonard@utsi.edu

To the Graduate Council:

I am submitting herewith a thesis written by Russell Lee Leonard entitled "Synthesis and Characterization of Diamond-like Carbon Thin Films for Biomedical Applications." I have examined the final electronic copy of this thesis for form and content and recommend that it be accepted in partial fulfillment of the requirements for the degree of Master of Science, with a major in Materials Science and Engineering.

Jacqueline Johnson, Major Professor

We have read this thesis and recommend its acceptance:

George Murray, Trevor Moeller

Accepted for the Council:
Carolyn R. Hodges

Vice Provost and Dean of the Graduate School

(Original signatures are on file with official student records.)

To the Graduate Council:

I am submitting herewith a thesis written by Russell Lee Leonard entitled “Synthesis and Characterization of Diamond-like Carbon Thin Films for Biomedical Applications.” I have examined the final electronic copy of this thesis for form and content and recommend that it be accepted in partial fulfillment of the requirements for the degree of Master of Science, with a major in Materials Science and Engineering.

Jacqueline A. Johnson, Major Professor

We have read this thesis
and recommend its acceptance:

George M. Murray

Trevor M. Moeller

Accepted for the Council:

Carolyn R. Hodges
Vice Provost and Dean of the
Graduate School

(Original signatures are on file with official student records.)

SYNTHESIS AND CHARACTERIZATION OF DIAMOND-LIKE CARBON THIN FILMS FOR BIOMEDICAL APPLICATIONS

A Thesis Presented for the
Master of Science
Degree
The University of Tennessee, Knoxville

Russell Lee Leonard
December 2010

DEDICATION

This thesis is dedicated to my father, John C. Leonard, Jr.

ACKNOWLEDGEMENTS

I would like to give special thanks to my advisor, Dr. Jacqueline Johnson, for all of her support and encouragement during this endeavor. She and her husband, Dr. Charles Johnson, have been incredibly kind and generous to me during my time at the University of Tennessee Space Institute.

I would also like to thank Dr. George Murray and Dr. Trevor Moeller for their participation in my Thesis Committee.

There are many other people that I would like to acknowledge for their help with the research required for writing this thesis. Alexander Terekhov, Kathleen Lansford, and Doug Warnberg provided invaluable technical assistance. Dr. Saad Hassan, Dr. James Dickerson, and Dr. Carol Thompson contributed greatly to the AFM results. Dr. Robert Erck provided the entirety of the tribological measurement data. Dr. William Hofmeister and Dr. Lino Costa offered many helpful ideas for solving problems that I encountered. Christian Paßlick and Dr. Richard Weber gave me very valuable comments after reviewing early drafts of my thesis.

My time at UTSI has been a pleasant one. Many people have helped me transition into my role as a Graduate Research Assistant and student. I am grateful to Deepak Rajput and Matt Parrish for “showing me the ropes” when I first arrived at UTSI. I also wish to thank Carole Thomas, Rebecca Layman, Betsy Harbin, and all the rest of the UTSI staff for all their hard work which made my life as a student and GRA much easier. I am also grateful to the Materials Science Club for being such a wonderful group of guys and giving me a welcome diversion from my studies when needed.

ABSTRACT

Diamond-like carbon (DLC) thin films were produced by pulsed laser deposition (PLD) on silicon, fused silica, and silicon nitride substrates. The films produced were either undoped, made using a pure graphite target, or doped, using multi-component targets made from a combination of graphite and silicon, silicon nitride, titanium dioxide, or silicon monoxide. These films were evaluated for their potential use in biomedical applications, including coatings for artificial joints, heart stents, and bronchoscopes. The films were characterized by Raman spectroscopy, atomic force microscopy, ball-on-flat tribometry, contact angle measurements, and spectrophotometry. Film thickness was determined by optical profilometry. Film adhesion was checked by soaking the films in simulated body fluid (SBF) and monitoring the quality of the film surface at varying time intervals using an optical microscope. DLC coatings were produced with a root mean square surface roughness of less than 1 nm and a 0.08 lubricated coefficient of friction. Contact angles of water on the undoped films varied with deposition conditions, ranging from 65 to 88 degrees. Contact angles as low as 25 degrees were achieved by incorporating silicon monoxide dopant. DLC coatings were produced on fused silica having high transparency and showing no delamination after forty-three weeks of immersion in SBF. These results indicate that these films have potential as biomedical coatings.

TABLE OF CONTENTS

LIST OF TABLES

Table Page

LIST OF FIGURES

Figure Page

CHAPTER I
INTRODUCTION

Diamond-like Carbon

Diamond-like carbon (DLC) films are amorphous carbon films with a mixture of sp^2 and sp^3 hybrid bonding [1] [2]. DLC films have properties similar to that of diamond, including high hardness, low coefficient of friction, optical transparency, and chemical inertness [3]. These properties make DLC an ideal protective coating for such applications as automotive parts, optical windows, magnetic storage devices, micro-electromechanical devices (MEMS), and biomedical implants and instruments [4-6].

Diamond-like carbon films can be made by a wide range of methods including ion beam, dc or rf sputtering, cathodic arc, pulsed laser deposition (PLD), and plasma enhanced chemical vapor deposition (PECVD) [7]. DLC film properties can vary greatly, depending upon the deposition method used.

DLC is commonly doped with other elements that induce a change in material properties. Hydrogen is the most commonly used dopant in DLC films, with films generally being classified as hydrogenated or non-hydrogenated [8]. Other dopants used to modify the properties of DLC include fluorine, nitrogen, oxygen, boron, chromium, copper, platinum, silver, titanium, and silicon [9-19].

Post processing techniques such as surface treatments and annealing can further modify the properties of DLC films. Plasma treatments with oxygen, nitrogen, hydrogen, and carbon tetrafluoride can change contact angle [20-22]. Laser and thermal annealing can reduce residual stresses [23] [24].

Biomedical Applications of Diamond-like Carbon

Currently there is much interest in developing DLC films for biomedical applications. As DLC has been shown to be biocompatible with the human body, it has potential as a coating for cardiovascular, orthopedic, ophthalmic, MEMS, and biosensor implants [6] [25]. The primary goal of this work is to develop DLC coatings for coronary stents, artificial joints, and bronchoscope lenses.

Coronary Stents

Coronary stents are devices surgically implanted into a patient's restricted artery to support the walls of the artery and allow for greater blood flow as shown in Figure 1. Two problems associated with stents are thrombosis, the formation of a thrombus or clot along the inside of the stent and cytotoxicity, which is an unfavorable reaction of cells in the body to metal ions released from the stent. DLC, being inert and hemocompatible, has shown promise as a coating for reducing thrombosis and preventing cytotoxicity [26]. These films can also be used in conjunction with drug-eluding materials to improve their effectiveness [27]. DLC films which exhibit antibacterial properties have also been produced [28].

Artificial Joints

Joint replacement surgery is a common surgical procedure to reduce chronic joint pain or replace a badly damaged joint. In this procedure, the unhealthy joint is replaced with a new man-made joint. Wear and debris formation are the two largest problems with today's joint replacement materials. Wear can lead to joint failure, causing revisionist surgery to be required. Debris can accumulate in the body, causing adverse reactions. DLC could potentially reduce wear and debris formation, making joint replacement safer and longer lasting [29].

The hip joint is a spherical joint, consisting of a femoral head and an acetabular cup, as shown in Figure 2. The complicated motions within this joint, the high load requirements, and the large number of cycles required in its lifetime make it a challenging joint to replace. An example of an artificial hip joint is shown in Figure 3.

Bronchoscopes

The bronchoscope is a medical device which can look into the airways of a patient's lungs, called the bronchi and bronchioles. An example of a bronchoscope in use is shown in Figure 4. Within the lungs, a warm moist environment, the bronchoscope lens has a tendency to fog over. By applying a transparent, super-hydrophilic DLC coating to the lens, the lens may become anti-fogging, eliminating the need to wipe clean the lens during use.

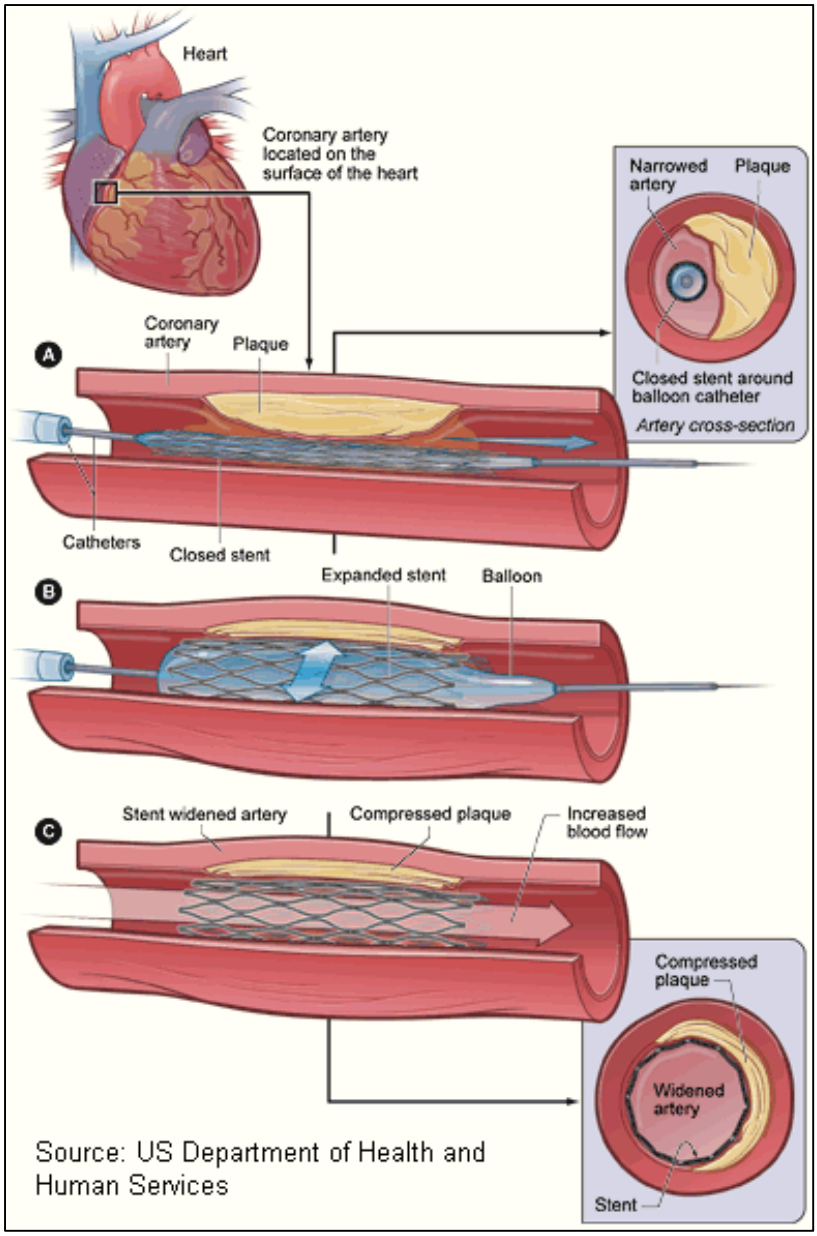

Figure 1 Coronary Artery Stent Placement [30]

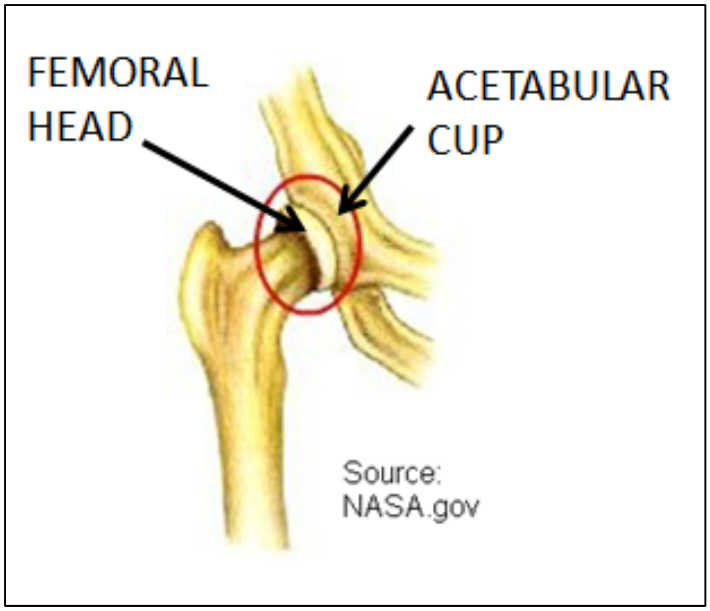

Figure 2 The Hip Joint [31]

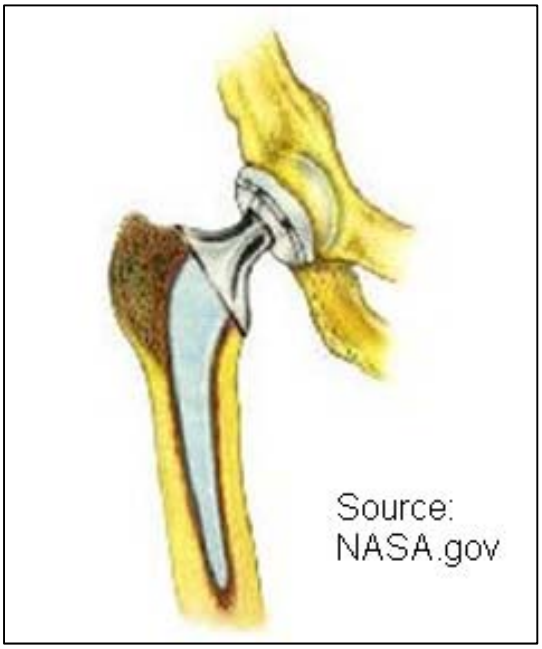

Figure 3 An Artificial Hip Joint [31]

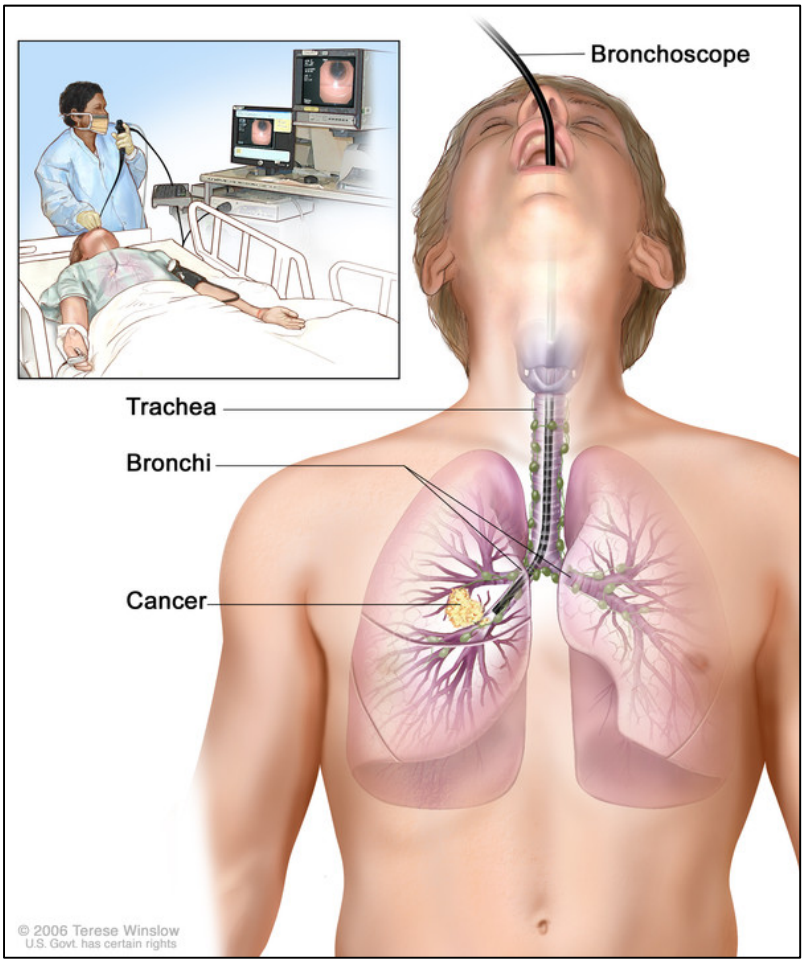

Figure 4 Example of a Bronchoscope in Use [32]

CHAPTER II
EXPERIMENTAL DETAILS

DLC films were produced by pulsed laser deposition (PLD) on three types of substrates: silicon, fused silica, and silicon nitride. The films were characterized by Raman spectroscopy, atomic force microscopy (AFM), ball-on-flat tribometry, contact angle measurement (CAM), and spectrophotometry. To gain an understanding of how these films might be affected within the human body, soaking experiments were performed with the films immersed in simulated body fluid (SBF). Film thickness was obtained by optical profilometry.

Substrates

Silicon

The silicon substrates used were diced into 1"x1" squares from 4" diameter wafers, whose specifications are shown in Table 1.

The silicon wafers were cleaned before use to remove any surface contaminants. The wafers were ultrasonically cleaned in acetone for ten minutes, rinsed with ultrapure water, and dried with compressed nitrogen. This was followed by ultrasonic cleaning in methanol for ten minutes, subsequent rinsing with ultrapure water and drying with compressed nitrogen. Each substrate was then dipped into a buffered oxide etch solution (6:1 volume ratio of 40% NH_4F in water to 49% HF in water) for 20 seconds to remove any oxides remaining on the surface, followed by a rinse in ultrapure water and drying with compressed nitrogen.

The substrates were then mounted on a holder as shown in Figure 5, if silicon wafers were the only substrates to be used. Figure 6 shows the mounting arrangement for silicon wafers paired with silicon nitride spheres.

Table 1 Silicon Wafer Specifications

Characteristic	Specification
Diameter	4"
Thickness	400-500 μm
Flats	2 semi-standard
Type	P/Boron
Resistivity	1-25 ohm-cm
Orientation	(100)
Grade	test
Polishing	single side

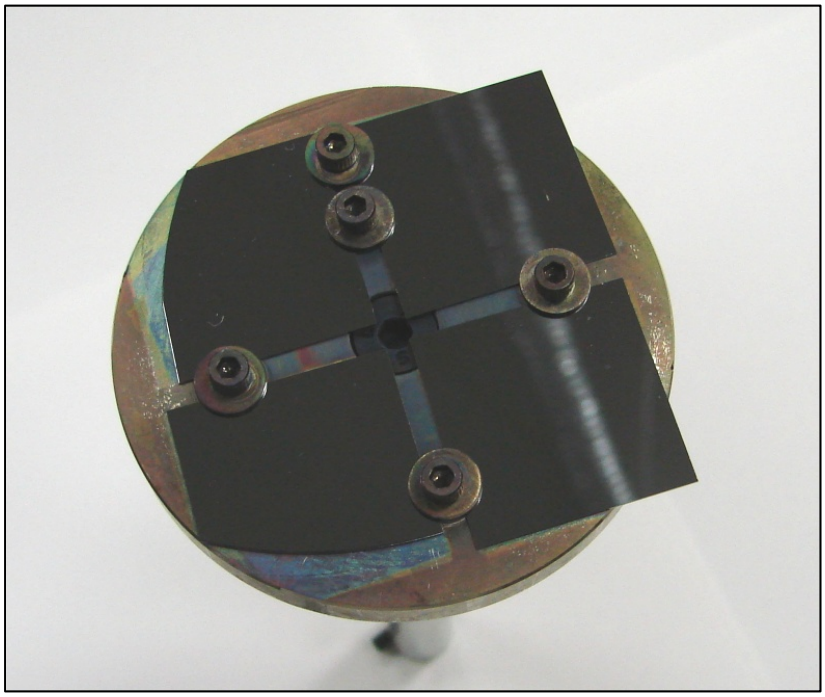

Figure 5 Silicon Wafers Mounted on the Substrate Holder

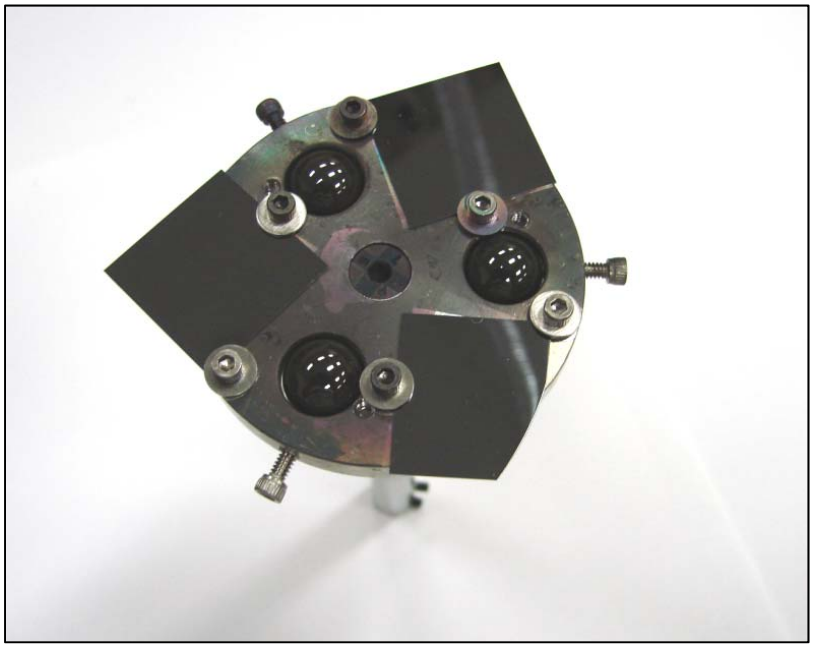

Figure 6 Silicon Wafers and Silicon Nitride Spheres Mounted on the Substrate Holder

Fused Silica

The fused silica substrates used were diced from 4” diameter wafers into 1” x 1” squares. The properties of the wafers are shown in Table 2.

As with silicon, the fused silica substrates required cleaning before use. The fused silica substrates were ultrasonically washed in acetone for ten minutes then rinsed with ultrapure water and dried with compressed argon. The substrates were then ultrasonically cleaned in methanol for ten minutes, rinsed with ultrapure water, and dried with compressed argon. This was followed by a two minute dip in piranha solution (1:1 volume ratio of H_2SO_4 and H_2O_2) rinsing with ultrapure water. The substrates were then dried with compressed argon. Figure 7 shows the substrates mounted onto the substrate holder.

Silicon Nitride

The silicon nitride substrates were ½ inch diameter spheres. Before use, the silicon nitride spheres were ultrasonically cleaned in acetone for ten minutes then rinsed with ultrapure water before drying with compressed nitrogen. The process was then repeated with methanol. The substrates were mounted as shown in Figure 6.

Pulsed Laser Deposition

The DLC films were produced using a PLD system with an ArF excimer laser with a wavelength of 193 nm. The repetition rate of the laser was 50 Hz with a pulse length of 15 ns. The laser beam was focused onto a target, which was rotated and translated. The substrates were affixed to a rotating holder for more even film coating. After initial rough pumping to 15 mTorr with a rotary piston oil-sealed mechanical pump, a cryopump was used to pump the vacuum chamber to $1x10^{-6}$ Torr or lower pressure. An ionization gage was used to monitor chamber pressure. For depositions with substrate heating, an incandescent lamp radiatively heated the backside of the substrate holder. A thermocouple in contact with the substrate holder was used to monitor deposition temperature. The pulsed laser deposition system is shown in Figure 8. Properties of the laser and optical system are shown in Table 3. A schematic of the laser and system optics with relevant dimensions is shown in Figure 9.

Table 2 Fused Silica Wafer Specifications

Characteristic	Specification
Diameter	4”
Thickness	500 µm
Grade	UV
Polishing	double side
Surface Roughness	Ra<1.5 nm

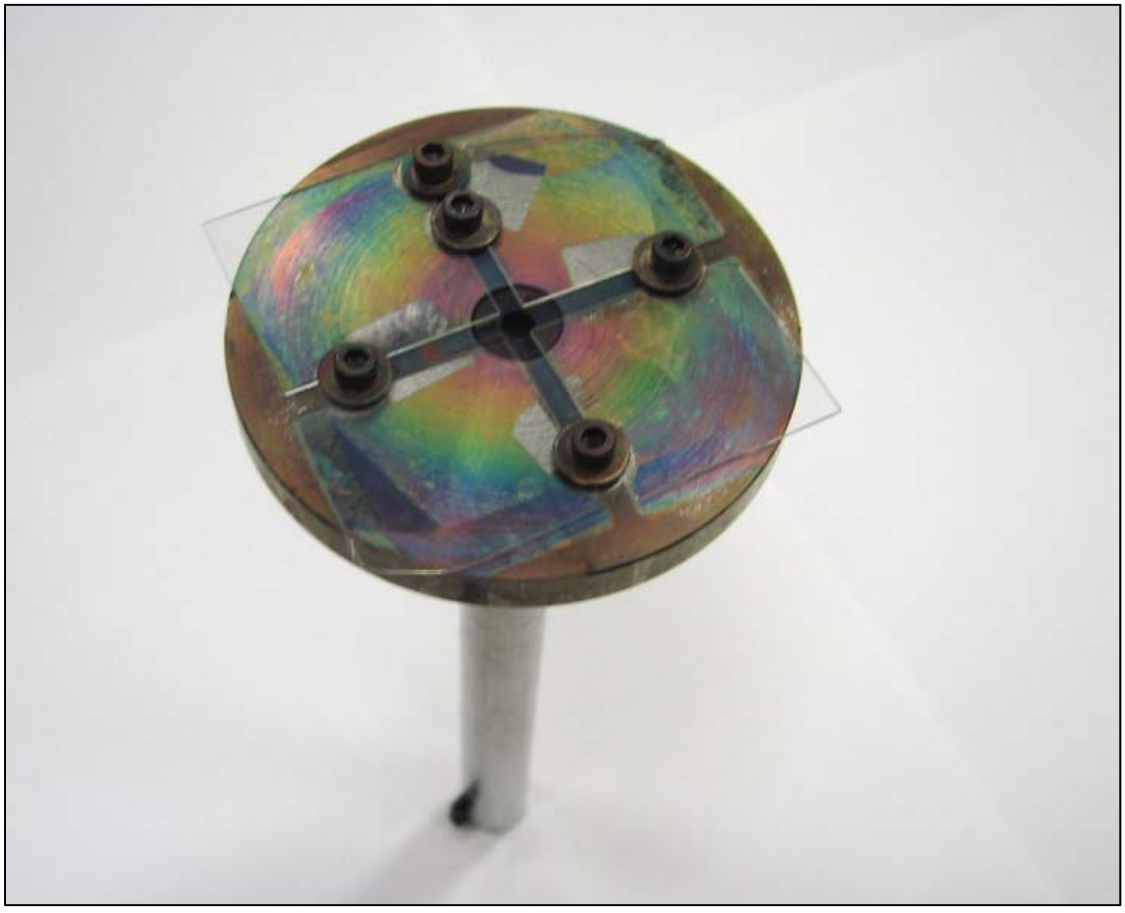

Figure 7 Fused Silica Wafers Mounted on the Substrate Holder

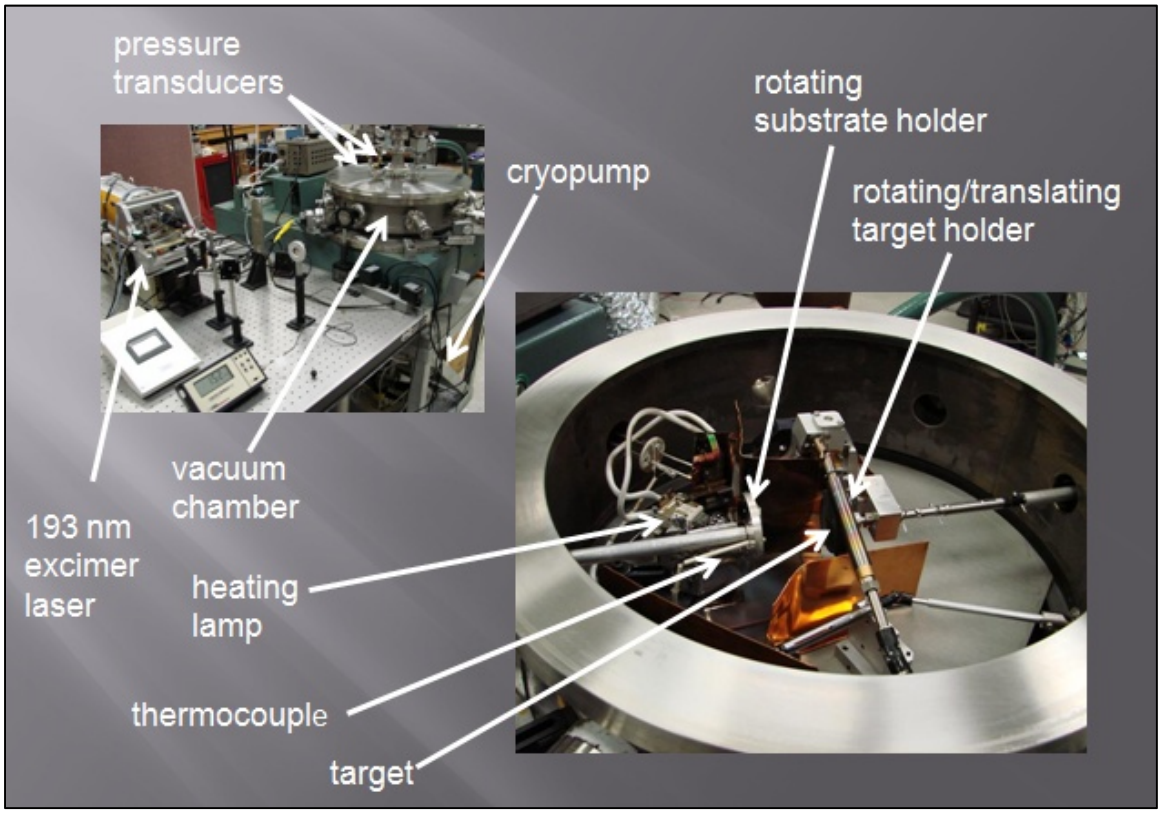

Figure 8 Pulsed Laser Deposition System

Table 3 Laser and Optical System Properties

Property	Value
wavelength	193 nm
pulse duration	15 ns
beam shape/size	elliptical; a=3.4 mm, b=2.0mm, Area = 21 mm^2
focal length of lens	31 cm
area of beam at target surface	0.13 mm^2

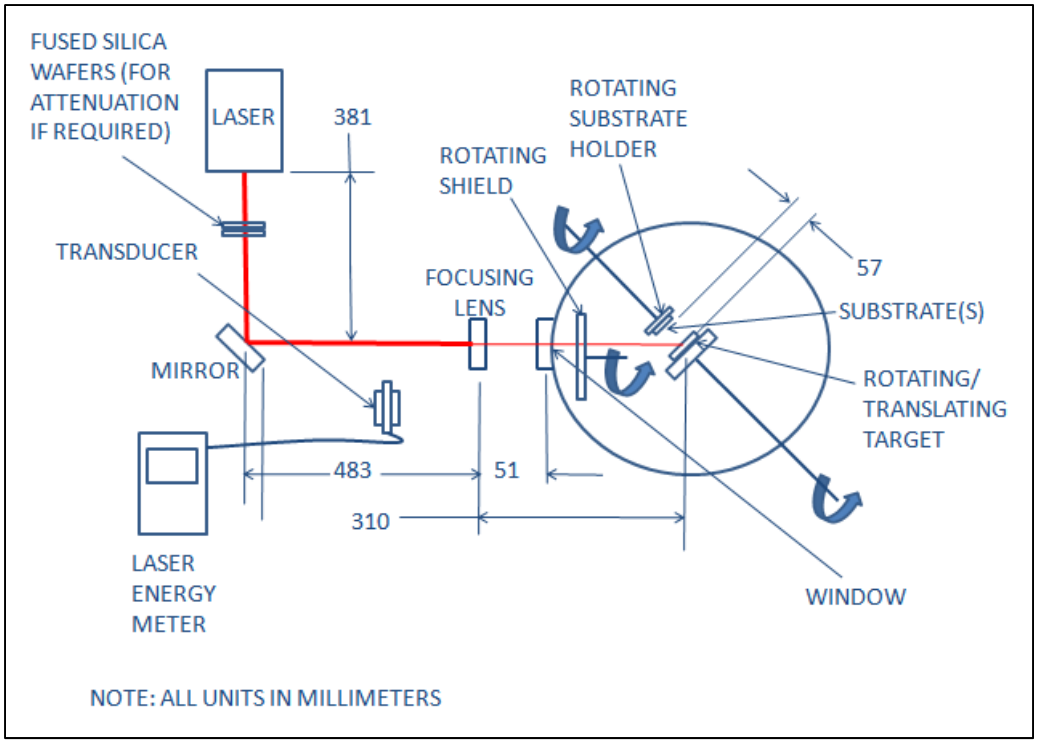

Figure 9 Schematic of the Laser and System Optics with Relevant Dimensions

The laser pulse energy reaching the focusing lens was measured using a meter between the mirror and focusing lens. The beam energy was attenuated to the desired value by placing 200 μm thick fused silica wafers between the laser and the mirror. During depositions lasting longer than fifteen minutes, the laser pulse energy was monitored periodically. This was to ensure that the energy of the beam did not change significantly during the course of the deposition.

Between depositions, the sum of the attenuation due to the focusing lens, chamber window, and shield was measured by placing the meter between the shield and target in the PLD chamber. It was found that the attenuation from the lens and window remained constant throughout the course of this study. The attenuation due to the debris shield, however, slowly increased over time due to the effects of the laser beam. If the attenuation approached a significant amount, the shield was shifted to move the beam to a new, unaltered location along the shield radius. Because of the attenuation effect of the lens, window, and shield was reasonably constant across all depositions made, pulse laser energy as opposed to fluence, will be reported throughout this work for convenience. The calculated fluence for each deposition, as well as all other deposition parameters, can be found in the Appendix in Table 19.

Graphite Target

For undoped films, a 2” diameter round target made from semiconductor grade graphite was used.

Multi-component Targets

In order to add dopants to the DLC produced during pulsed laser deposition, multi-component targets, comprised of graphite and the desired doping material were used. In general, a 2” diameter graphite target with a 90° cut-out was paired with a wedge shaped piece of the desired doping material and a wedge-shaped graphite spacer. The doping material was machined to a pre-determined angle to control the percentage of doping material; the spacer was machined to the corresponding angle that would complete the 360° target. If the doping material was thinner than the graphite, a graphite or copper shim was inserted behind the dopant to place the two materials on the same plane. The components were held in-place by graphite tape. An example of this arrangement is shown in Figures 10 and 11.

By having a series of dopant materials cut at different angles and corresponding graphite spacers to complete the target circle, the composition of the multi-component target could be easily controlled. An example of a series of dopant targets cut to different angles is shown in Figure 12. The corresponding graphite filler wedges are shown in Figure 13.

Because silicon nitride dopant material was only readily available in spherical form, a different multi-component target arrangement was used. First, a hole with matching diameter (.500”) was machined into a 90° wedge-shaped graphite insert. The silicon nitride sphere then had two flats machined into it on opposite ends. The silicon nitride sub-insert was then placed within the 90° wedge-shaped graphite insert and combined with the larger graphite target with the 90° cut-out. The components of this set-up are shown in Figure 14. The assembled multi-component target is shown in Figure 15.

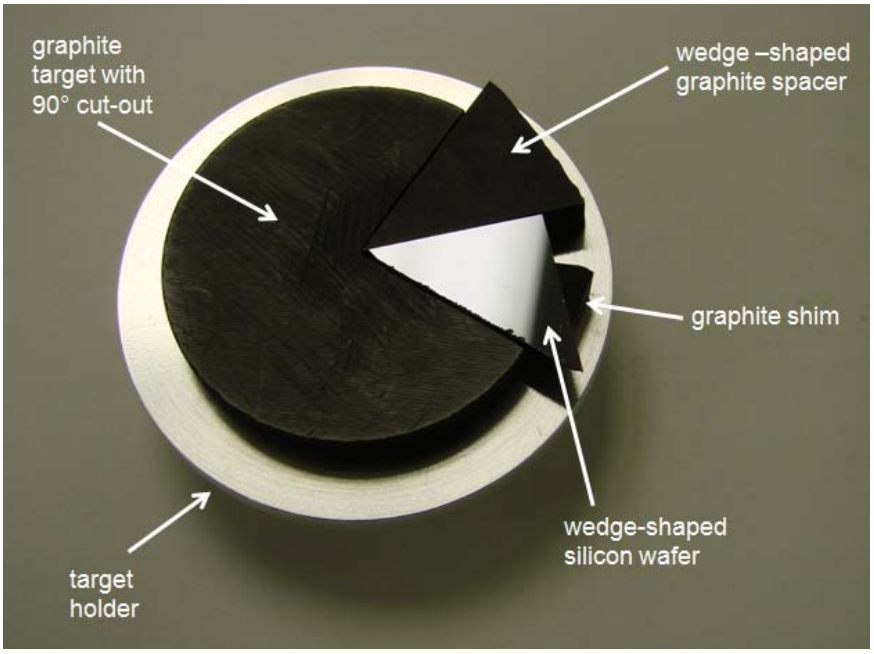

Figure 10 Components of a Silicon/Graphite Target

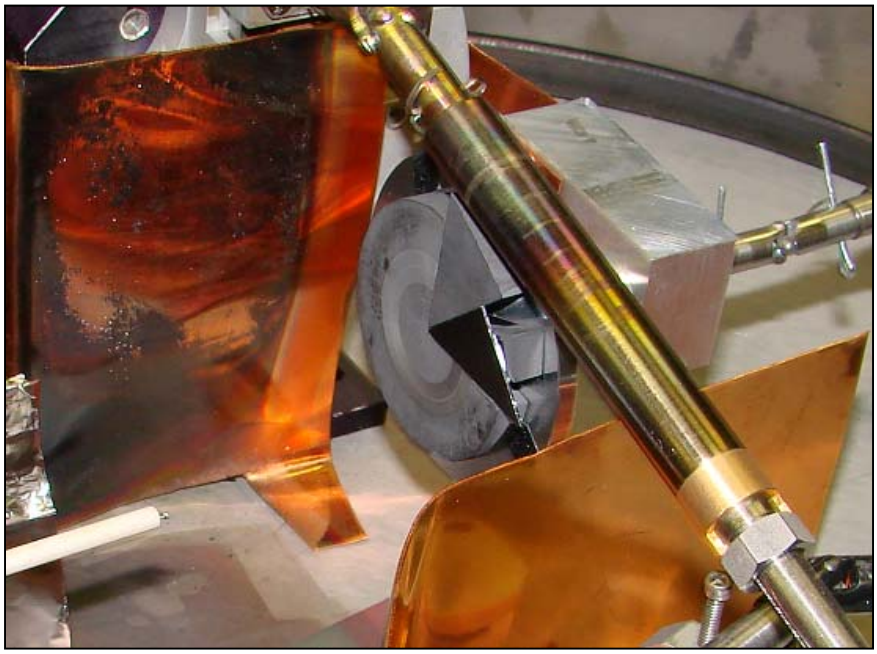

Figure 11 Assembled Silicon/Graphite Multi-Component Target Installed in the PLD Chamber

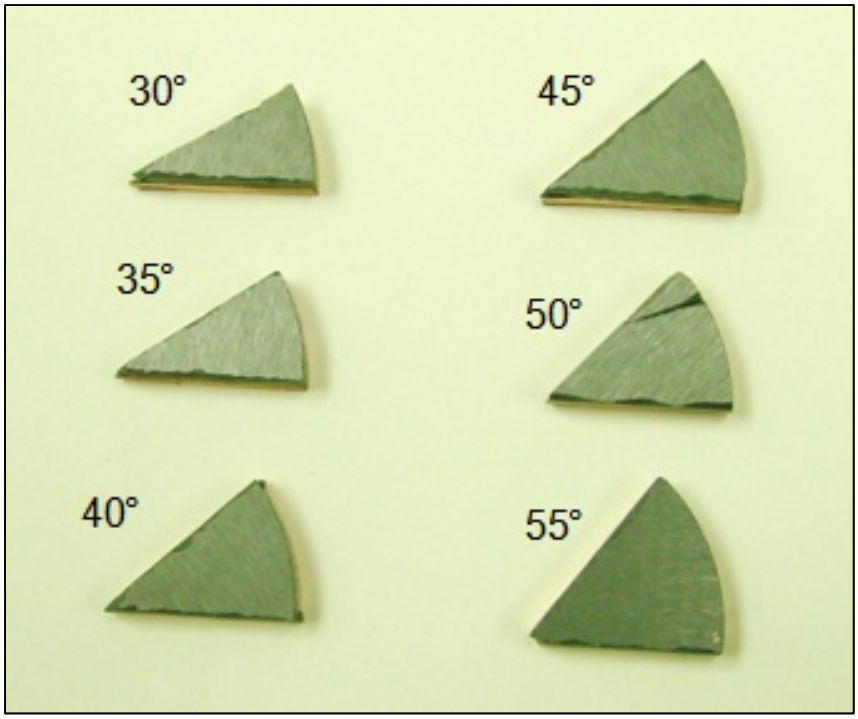

Figure 12 Titanium Dioxide Target Wedges

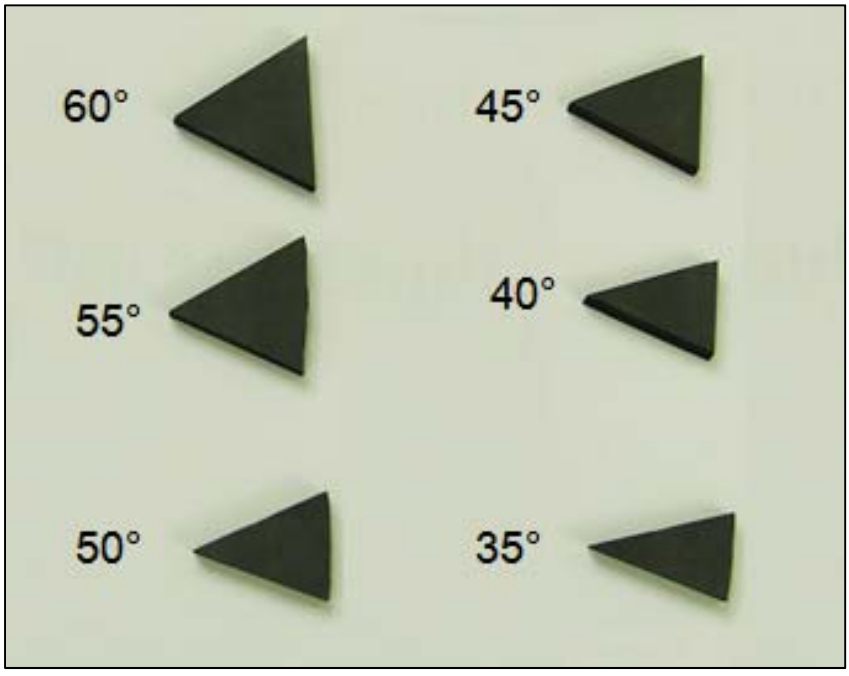

Figure 13 High-Purity Graphite Spacer Wedges

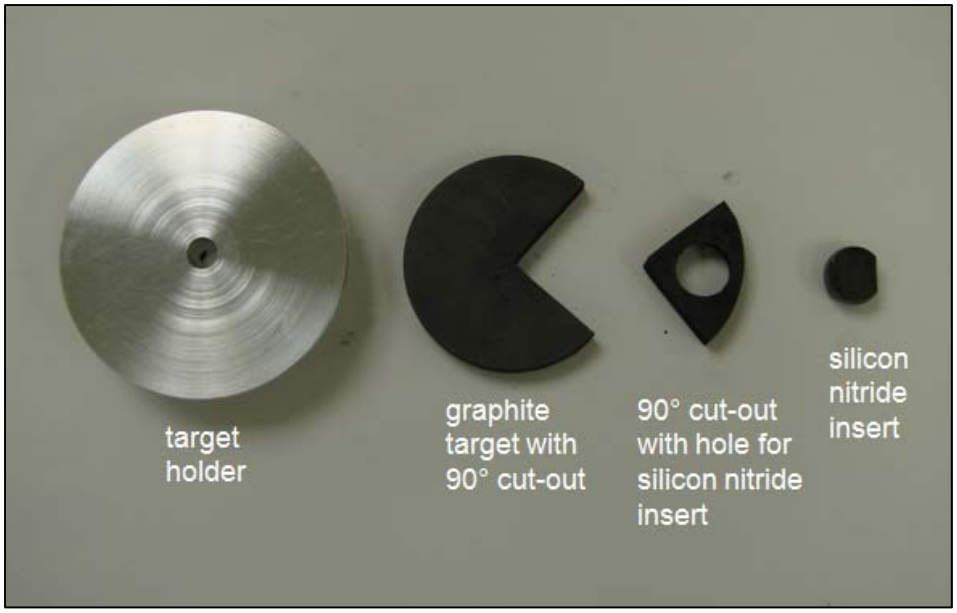

Figure 14 Components of a Silicon Nitride/Graphite Target

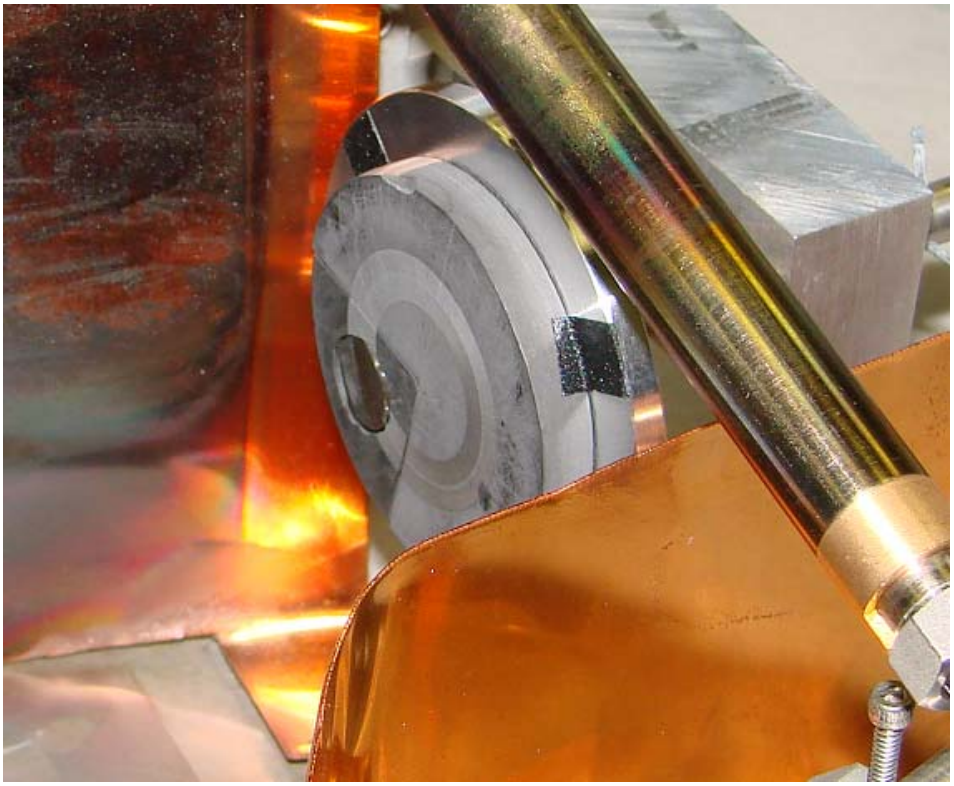

Figure 15 Assembled Silicon Nitride/Graphite Target Installed in the PLD Chamber

Surface Modification of DLC Films

Four films, PLD #s 54-1, 54-2, 54-3, 54-4, were produced simultaneously by pulsed laser deposition on individual fused silica substrates as shown in Figure 7. This was to ensure that the films would have uniform characteristics before surface modification took place.

Film samples PLD #s 54-1, 54-2, 54-3 were cleaned concurrently in a Harrick PDC-32G plasma cleaner (Ithaca, NY) for two minutes. The power applied to the coil was 10.5 W. The RF frequency was 1 MHz. Vacuum was 1 torr.

Film samples PLD #54-2 and PLD #54-3 underwent an additional process, aryl-sulfonation [33]. The films were immersed in 30 mL of 8.4 mMolar sulfanilic acid held in a 50mL beaker at 70°C. Drop-by-drop, with frequent stirring, 1.5 mL of 0.2 M sodium nitrite solution was added. Figure 16 shows the two samples soaking. Sample PLD #54-2 was immersed for two hours; sample PLD #54-3 was immersed for five hours. After removal each sample was rinsed with ultrapure water five times and dried with compressed ultrapure argon. The two aryl-sulfonated samples were then stored in a vacuum oven at 100 °C with a pressure of 100 kPa for two days. PLD #54-4 received no treatment, in order to act as a control.

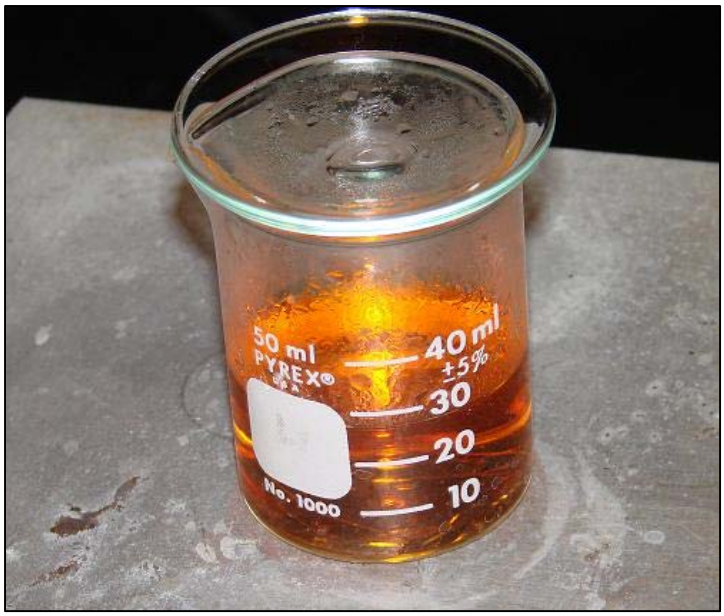

Figure 16 Samples PLD #54-2 and PLD #54-3 Soaking in a Sulfanilic Acid and Sodium Nitrite Solution

Profilometry

Film thickness was measured using an optical profilometer to examine the step height between the film and a masked portion of the substrate, with the step height being equivalent to the film thickness. The optical profilometer used was a Phase Shift Technology Micro XAM surface mapping microscope (Tucson, AZ) connected to a PC with MapVue AE 1.24.1 software. Measurements were made at a minimum of two locations per sample. An average thickness value for each film was reported along with standard error.

Raman Spectroscopy

Raman spectroscopy was performed on all samples using a Renishaw inVia Raman Microscope (New Mills, Wotton-under-Edge, Gloucestershire, GL12 8JR, England). The laser was focused through a 50X lens and had a power of 4 mW. The laser wavelength was 633 nm. Acquisition was for ten seconds with ten accumulations at each location measured.

Soaking Experiments in Simulated Body Fluid

Simulated body fluid (SBF) was prepared as described by Cho et al. [34]. The ion concentrations for the SBF and for human blood plasma are shown in Table 4. Samples were immersed in SBF and incubated at 36.5°C, using a temperature controlled water bath. At varying time intervals, the samples were removed and photographed microscopically. The samples were then placed in fresh SBF and returned to the 36.5°C environment. An example of a DLC sample soaking in SBF is shown in Figure 17.

Contact Angle Measurement

The contact angle of water on the samples was measured using a Krüss DSA20E Easy Drop Standard with a software controlled dosing system (Hamburg, Germany). Typical measurement parameters are shown in Table 5. Measurements were made at five locations per sample. Average contact angle for each film was determined along with standard error.

Table 4 Ion Concentrations of Simulated Body Fluid and Human Blood Plasma [34]

Ion concentrations of the simulated body fluid and human blood plasma

Ion	Concentration (mmol/dm^3)	
	Simulated body fluid (SBF)	Human blood plasma
Na^+	142.0	142.0
K^+	5.0	5.0
Mg^{2+}	1.5	1.5
Ca^{2+}	2.5	2.5
Cl^-	147.8	103.0
HCO_3^-	4.2	27.0
HPO_4^{2-}	1.0	1.0
SO_4^{2-}	0.5	0.5

Source: Cho et al. J. Am. Ceram. Soc., 78 [7] 1769-74 (1995)

Figure 17 DLC Sample Soaking in Simulated Body Fluid

Table 5 Contact Angle Measurement Parameters

Parameter	Value
liquid	ultrapure water (Gebhardt)
dropform	standard (<90°)
dosing volume	2 µL
needle diameter	0.51 mm
drop type	sessile
temperature	approximately 20 °C
relative humidity	approximately 61%

Atomic Force Microscopy

Topography of the samples was measured using a VEECO Nanoscope V Atomic Force Microscope with a Nanoscope V controller (Plainview, NY). The system was equipped with a nitrogen gas vibration isolation stage and an acoustic/Faraday cover. It used a Nanoscope V controller and a computer with Nanoscope 7.30 software installed.

All images were taken under ambient conditions using silicon tips in tapping mode.

Ball-on-flat Tribometer

Tribological measurements were made for samples from the PLD #11 deposition process using a ball-on-flat tribometer as shown in Figures 18 and 19. Silicon nitride coated with DLC and an intermediate silicon bond layer was the ball material; the flat material was DLC coated silicon wafers with an intermediate silicon bond layer. The silicon bond layer was used to help ensure DLC bonded to the silicon nitride spheres. Process parameters for the deposition can be found in the Appendix in Table 19. The test environments were dry nitrogen, air, Mobil 15W30 synthetic motor oil, or bovine serum. Test duration and sliding speed varied and were dependent upon sample performance.

Figure 18 Ball-on-flat Tribometer

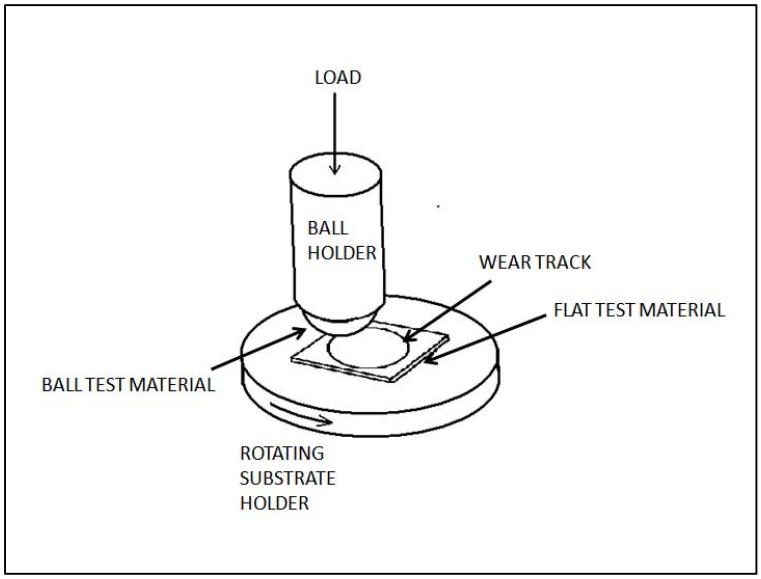

Figure 19 Ball-on-flat Tribometer Set-up

Spectrophotometry

Spectrophotometry data was obtained by using a GenTech Scientific TU-1901 double beam ultraviolet/visible light spectrometer equipped with UVWin5.0 analysis software (Arcade, NY). The transparency of DLC on fused silica substrates was measured between 190 and 900 nm at 1.0 nm intervals. The attenuation effects of the substrate were subtracted from the transmittance plots by using a bare fused silica substrate as reference during the measurements.

CHAPTER III
RESULTS AND DISCUSSION

Undoped Films

The first step in the production of the DLC films was to gain an understanding of how individual process parameters altered the properties of the films produced. To this end, films were produced on three different kinds of substrates: silicon, fused silica, and silicon nitride with varying deposition temperatures and laser fluence. Film thickness was determined by optical profilometry. The films were characterized by Raman spectroscopy, atomic force microscopy, contact angle measurement, and spectrophotometry. Adhesion and stability were checked by soaking the films in simulated body fluid and monitoring the film quality using an optical microscope at varying time intervals.

Profilometry

The thickness and deposition rate results for the DLC on silicon films with varying laser pulse energy are shown in Table 6. The film growth rate increased with increasing laser pulse energy as shown in Figure 20. This is as-expected because increasing pulse energy and greater fluence values will increase the amount of carbon ablated with each pulse.

There is no apparent relationship between deposition rate and laser pulse energy for the DLC films made on fused silica substrates as shown in Table 7 and Figure 21. It is likely, however, that a trend cannot be seen because the precision of the optical profilometer is not adequate to detect the small differences in film thickness one would expect from such short deposition times (15 minutes). Unfortunately, creating thicker films by using longer deposition times led to delamination of the film from the substrate as shown in Figure 23

The thicknesses of the DLC films produced on fused silica with varying deposition temperature are shown in Table 8. The deposition rate for these films can be found in Table 8 and Figure 22. There is no clear relationship between deposition rate and deposition temperature.

Table 6 Film Thickness and Deposition Rate for DLC Produced on Silicon with Varying Laser Pulse Energy at 200 °C Deposition Temperature

Sample	Laser Pulse Energy (mJ)	Thickness (nm)	Deposition Time (minutes)	Deposition Rate (nm/minute)
PLD #24	10.5	170 ± 5	240 ± 2%	0.71 ± 0.03
PLD #29	9.5	139 ± 3	240 ± 2%	0.58 ± 0.02
PLD #32	8.7	100 ± 5	240 ± 2%	0.42 ± 0.02
PLD #26	7.5	82 ± 4	240 ± 2%	0.34 ± 0.02
PLD #21	6.3	97 ± 7	240 ± 2%	0.40 ± 0.03
PLD #22	5.3	52 ± 4	240 ± 2%	0.21 ± 0.02

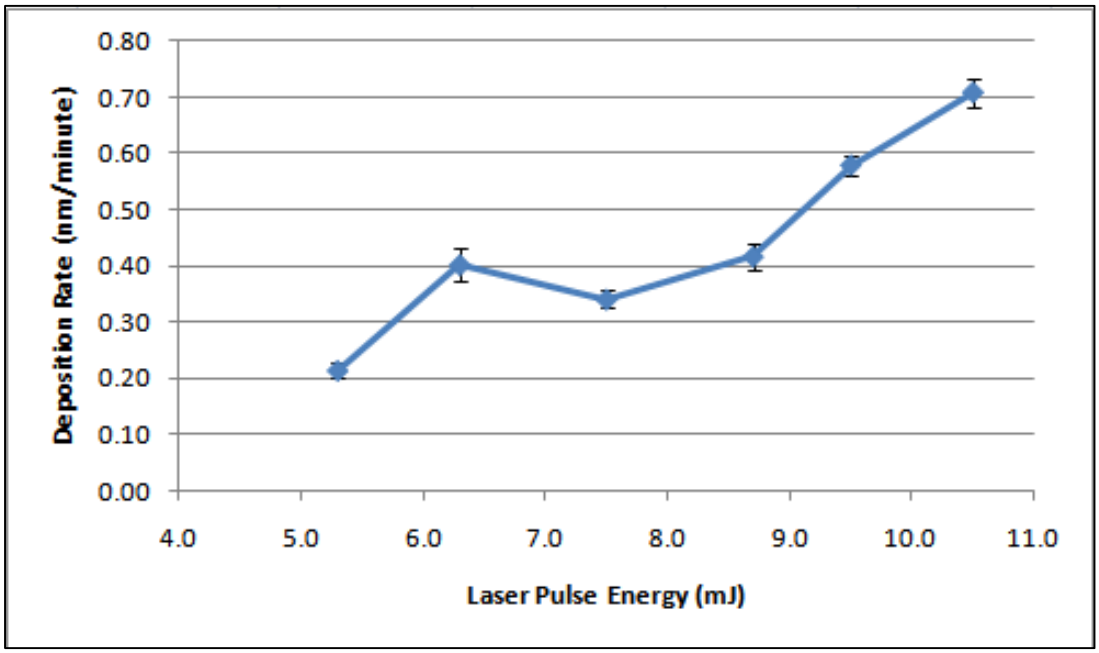

Figure 20 Deposition Rate for DLC Films Produced on Silicon with Varying Laser Pulse Energy at 200°C Deposition Temperature

Table 7 Film Thickness and Deposition Rate of DLC Films Produced on Fused Silica with Varying Pulse Laser Energy at 20 °C Deposition Temperature

Sample	Laser Pulse Energy (mJ)	Thickness (nm)	Deposition Time (minutes)	Deposition Rate (nm/minute)
PLD #40	9.0	27.0 ± 4.8	15 ± 2%	1.8 ± 0.3
PLD #41	8.0	18.0 ± 9.0	15 ± 2%	1.2 ± 0.6
PLD #42	6.9	27.0 ± 1.0	15 ± 2%	1.8 ± 0.1
PLD #43	6.0	20.3 ± 3.2	15 ± 2%	1.4 ± 0.2
PLD #44	5.0	20.5 ± 0.5	15 ± 2%	1.4 ± 0.0
PLD #47	4.0	9.5 ± 1.5	15 ± 2%	0.6 ± 0.1

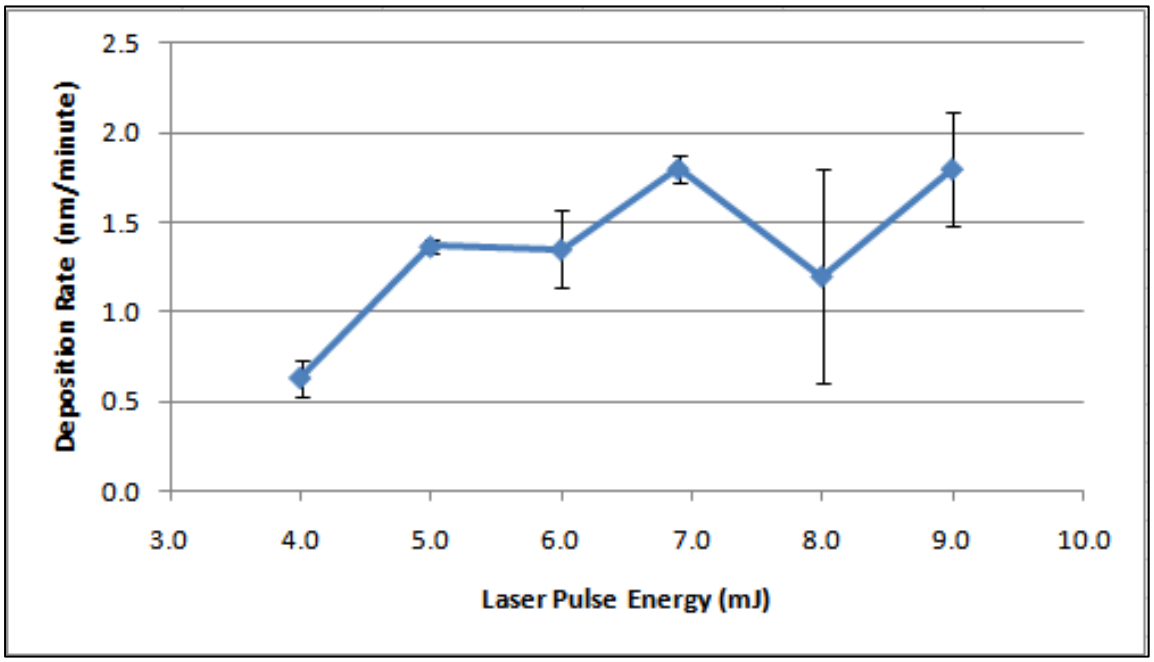

Figure 21 Deposition Rate for DLC Films Produced on Fused Silica with Varying Laser Pulse Energy at 20 °C Deposition Temperature

Table 8 Film Thickness and Growth Rate for DLC Produced on Fused Silica with Varying Deposition Temperature at 7.0 mJ Laser Pulse Energy

Sample	Deposition Temperature (°C)	Thickness (nm)	Deposition Time (minutes)	Deposition Rate (nm/minute)
PLD #42	19 ± 1	27 ± 1.0	15 ± 2%	1.8 ± 0.1
PLD #50	56 ± 1	28.5 ± 1.5	15 ± 2%	1.9 ± 0.1
PLD #49	92 ± 1	32 ± 0.0	15 ± 2%	2.1 ± 0.0
PLD #48	128 ± 1	26.5 ± 1.5	15 ± 2%	1.8 ± 0.1
PLD #46	163 ± 1	27.5 ± 1.5	15 ± 2%	1.8 ± 0.1
PLD #45	202 ± 1	22 ± 1.0	15 ± 2%	1.5 ± 0.1

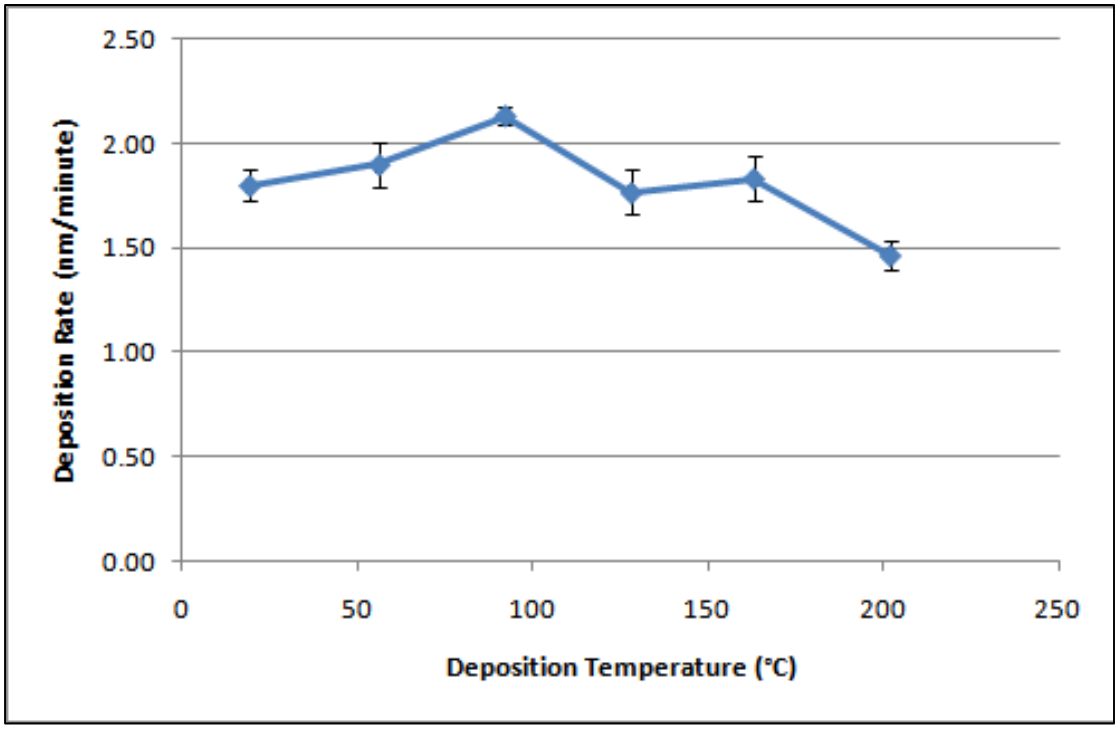

Figure 22 Deposition Rate as a Function of Temperature for DLC Films Produced on Fused Silica with Varying Deposition Temperature at 7.0 mJ Laser Pulse Energy

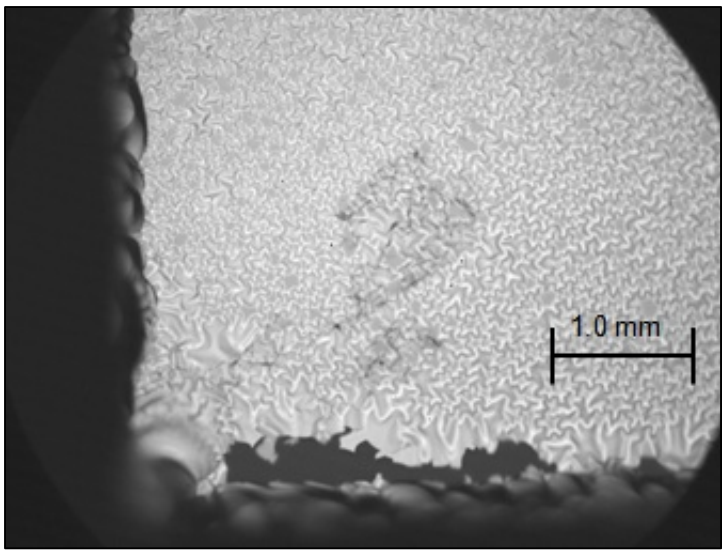

Figure 23 An Optical Micrograph of DLC Deposited on Fused Silica Exhibiting Delamination

Raman Spectroscopy

The Raman spectra for the undoped DLC films produced are shown in Figures 24, 25, and 26. As seen in Figures 24 and 25 the amount of laser pulse energy had little effect on the structure of the DLC films produced. Deposition temperature, however, had a very evident effect on the structure of the films, seen in Figure 26. At a deposition temperature of 202 °C, these films have a noticeable hump on the left side of the peak that gradually diminishes with decreasing temperature.

In Figure 24, there is one nonconforming spectrum belonging to PLD #22. It can perhaps be explained by an error in temperature measurement during deposition, leading to a higher or lower deposition temperature and thus a spectrum unlike all others in the series.

The Raman spectrum for DLC films can be deconvoluted into two Gaussian peaks, known as the D-peak and G-peak, located at approximately 1360 and 1560 cm^{-1}, respectively, when excited by visible light [6]. An example of the two deconvoluted peaks is shown in Figure 27. The relative intensity of these peaks (I_D/I_G) and the full-width half-maximum and position of the G-peak are thought to give insight to the sp^3/sp^2 ratio of hybrid bonding in DLC films. However, Table 9 shows results vary with source.

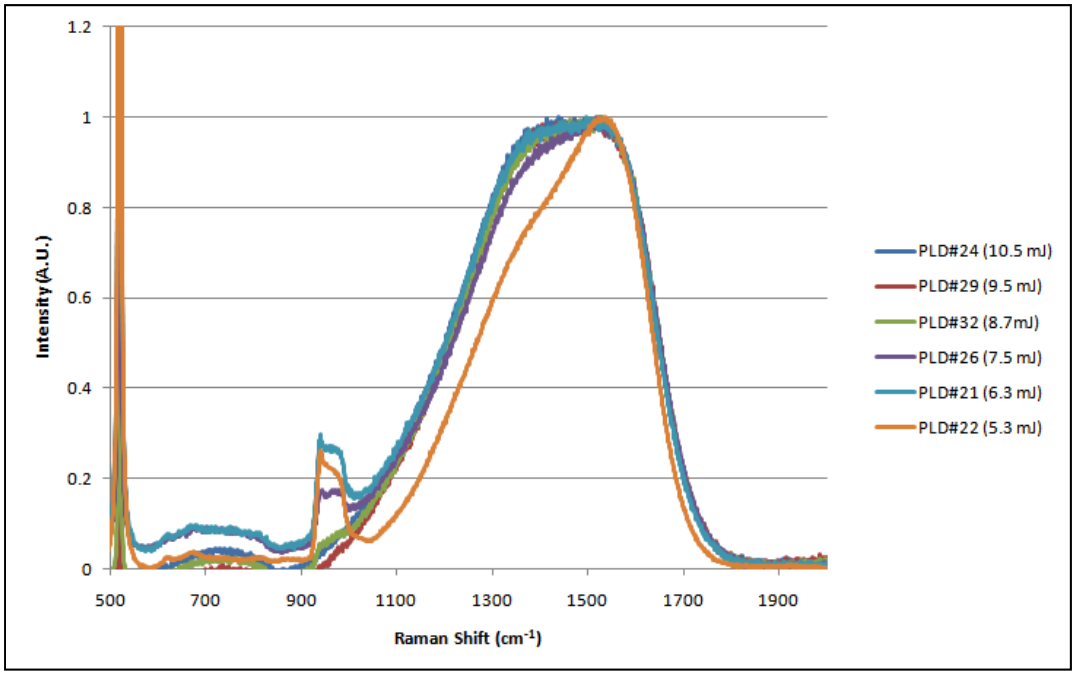

Figure 24 Raman Spectra of DLC Films Produced with Varying Laser Pulse Energy on Silicon Substrates at 200 °C Deposition Temperature

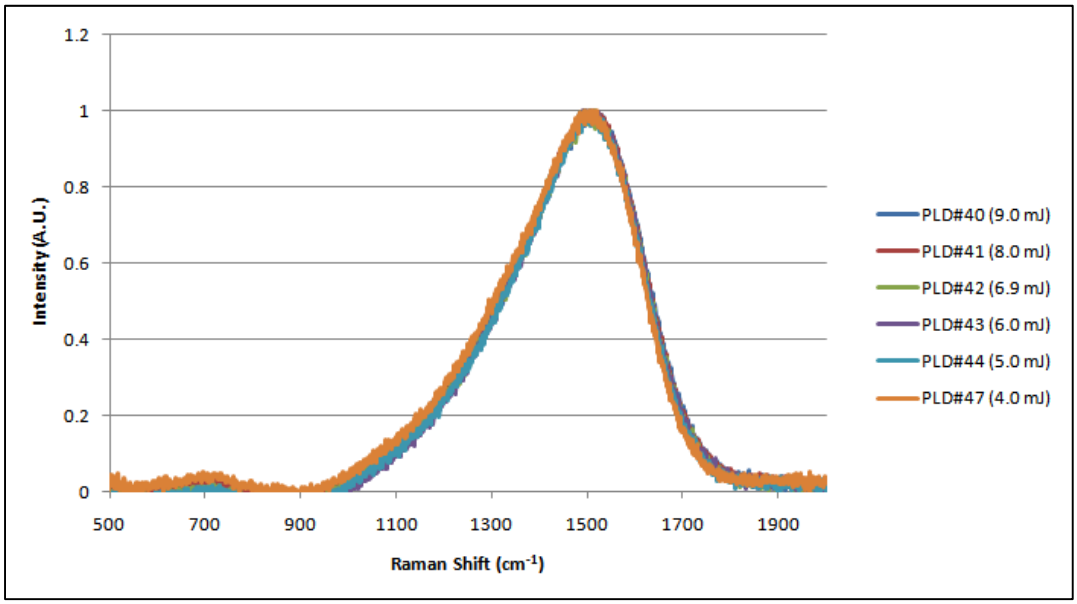

Figure 25 Raman Spectra of DLC Films Produced with Varying Pulse Laser Energy on Fused SIlica Substrates at 20 °C Deposition Temperature

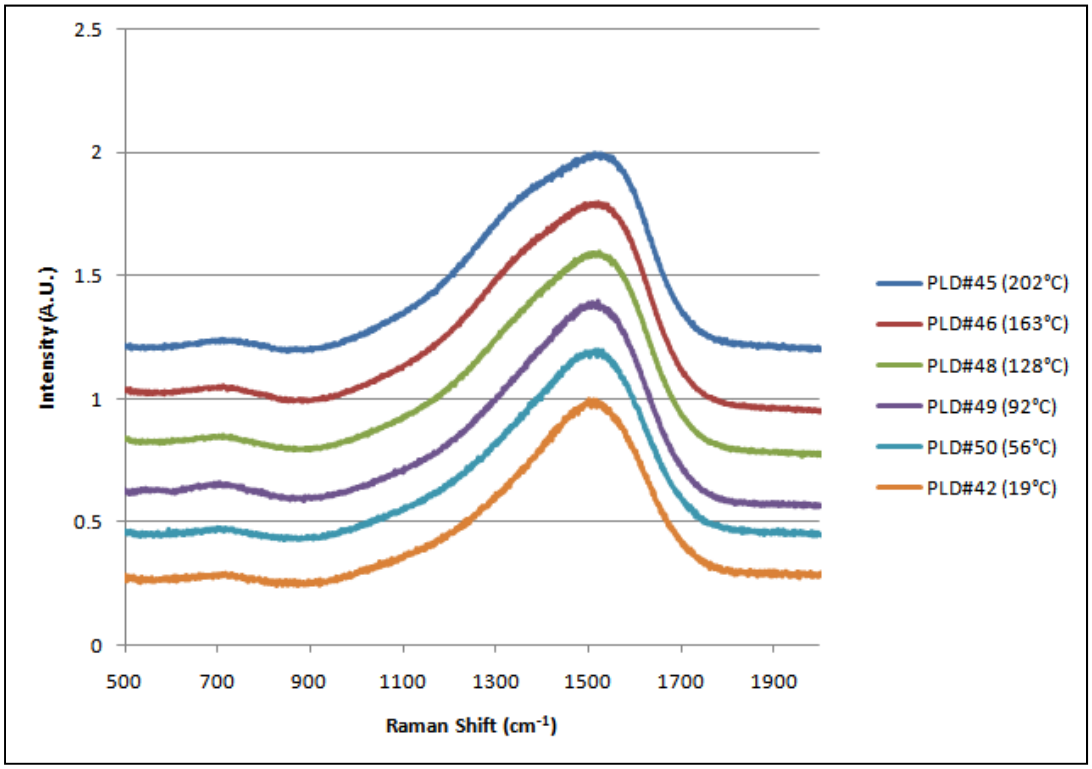

Figure 26 Raman Spectra of DLC Films Produced with Varying Deposition Temperature at 7.0 mJ Laser Pulse Energy

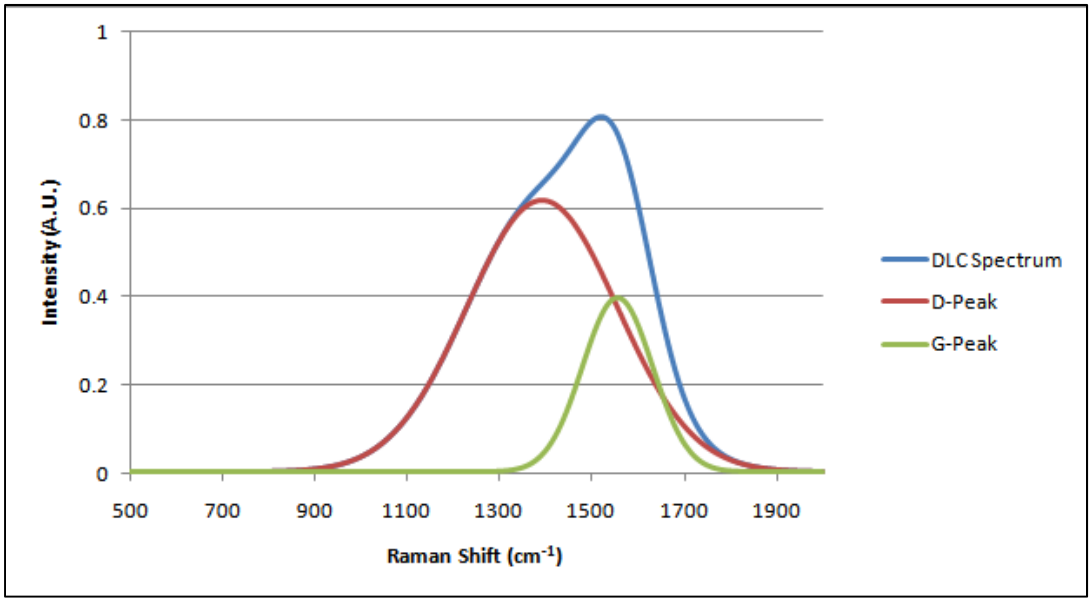

Figure 27 Raman Spectrum of DLC with Deconvoluted D- and G-Peaks Shown

Table 9 Relationship between sp^3 Content, G-Peak Position, I_D/I_G, Full-Width Half-Maximum of the G-Peak, and Deposition Temperature in Literature

Author(s)	Year of Publication	sp^3/sp^2 bonding	G-Peak Position	I_D/I_G	FWHM G-Peak	Temperature (°C)
Balon [35]	2005	↑	↓	↓	↑	↓
Chhowalla [36]	2000	↑	↓	↓	↑	↓
Ding et al. [37]	2009	↑	↓	↓		
Ferrari/ Robertson [8]	2000	↑	↑	↓	↑	
Marchon [38]*	1997	↑	↓			↓
Paul [2]*	2008	↑	↑	↓	↑	
Reuter [39]	2006	↑	−−			
* The DLC films studied were hydrogenated.						

Deconvolution of the spectra in Figure 26 into D and G curves using Origin 8 SRI software, yielded the data in Table 10. Origin 8 SRI software uses the Levenberg–Marquardt algorithm for curve fitting.

The ratio of intensities of the two peaks, I_D/I_G, the full-width half-maximum of the G-peak, and the G-peak position were normalized and are shown graphically in Figure 28. It is of interest that the full-width half-maximum of the G-peak grows in an inverse relationship with I_D/I_G and G-peak position which increases with deposition temperature. This is in agreement with the results found by Balon, Chhowalla, Ding et al., and Marchon, indicating that the films produced become more diamond-like with decreasing temperature [35-38].

Soaking Experiments

For a material to be biocompatible, one requirement is that it must be stable within the human body. In vitro testing in simulated body fluid provides an inexpensive way to determine the stability of the DLC films. DLC sample PLD #36, DLC deposited on fused silica, is shown in Figure 29 after forty-three weeks of soaking in SBF. It is significant that no change can be seen in the film, even at the interface between the DLC and fused silica exposed by a scribe mark that was made before soaking began. Any anomalies seen can be attributed to handling damage, contaminants such as dust, visibility of the microscope stage through the transparent film and substrate, and refraction effects at imperfections on the substrate edge.

Table 10 Raman Spectra Characteristics for DLC Films made at Varying Deposition Temperatures at 7.0 mJ Laser Pulse Energy

Sample	Temperature (°C)	G-Peak Position	I_D/I_G	FWHM G-Peak
PLD #45	202 ± 1	1563.4 ± 0.3	1.68 ± 0.05	172.5 ± 2.4
PLD #46	163 ± 1	1557.4 ± 0.3	1.52 ± 0.05	186.5 ± 3.0
PLD #48	128 ± 1	1553.5 ± 0.3	1.32 ± 0.05	193.3 ± 3.3
PLD #49	92 ± 1	1544.4 ± 0.4	1.04 ± 0.04	208.7 ± 4.0
PLD #50	56 ± 1	1542.6 ± 0.4	0.98 ± 0.04	208.7 ± 3.8
PLD #42	19 ± 1	1537.0 ± 0.9	0.77 ± 0.04	218.4 ± 5.5

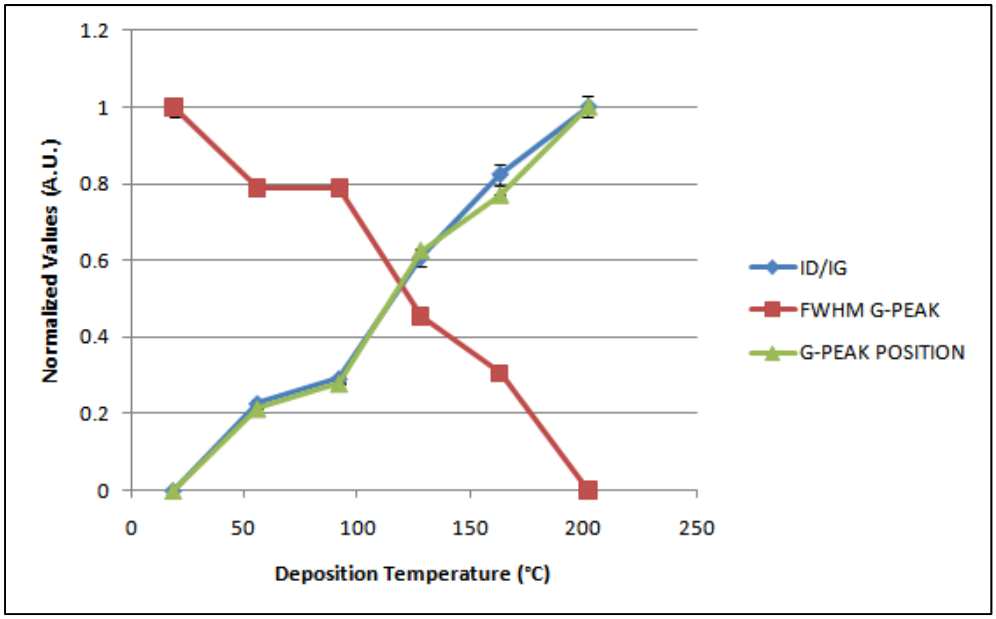

Figure 28 Normalized Raman Spectra Characteristics versus Deposition Temperature

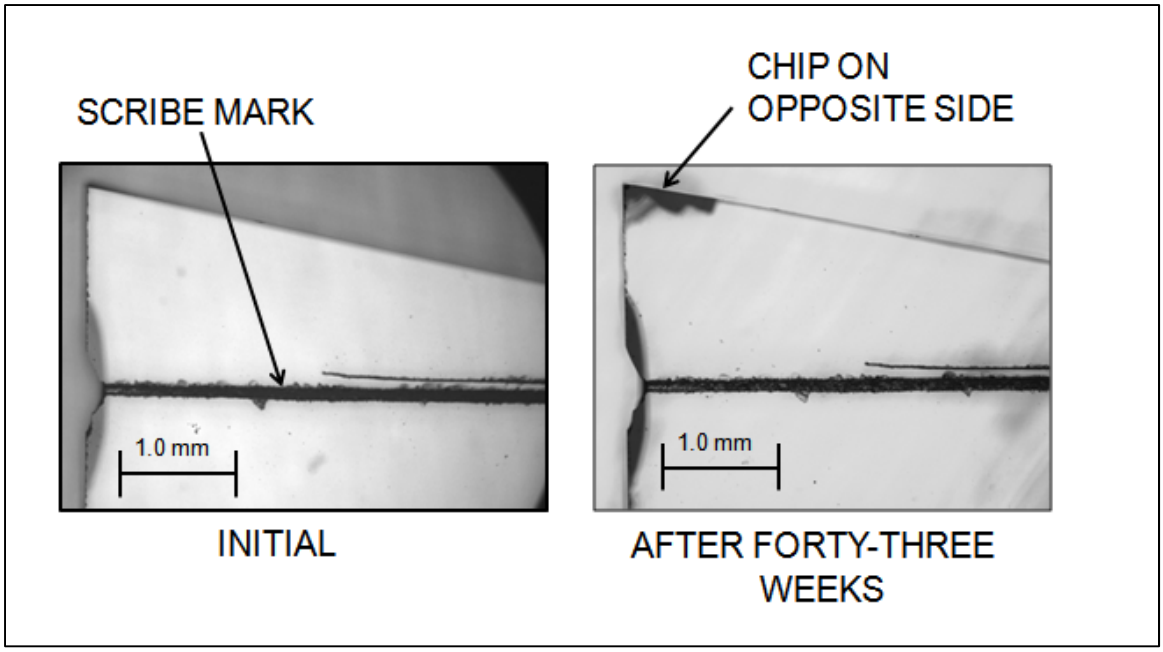

Figure 29 A Micrograph of DLC Film, PLD # 36, Initially and After Forty-Three Weeks of Immersion in SBF

Contact Angle Experiments

It is important to understand the interaction that a biomaterial will have with its environment at the surface. The contact angle that water makes at the surface of a material is a quick way to estimate the surface energy of that material. Figure 30 shows an example of the contact angle of water on a surface. High energy surfaces tend to be hydrophilic, achieving a high degree of wetting, while low energy surfaces tend to be hydrophobic, with water beading up on the surface. Contact angles have been established for water on the surface of the DLC films to determine their suitability for biomedical applications. For heart stent coatings, a low surface energy, super- hydrophobic coating is preferred to decrease the probability of platelet adhesion, which can lead to thrombosis or clotting in the artery. For bronchoscope lenses, a high surface energy, super-hydrophilic surface is required to make the lens anti-fogging. Examples of desired super-hydrophilic and super-hydrophobic surfaces are shown in Figure 31.

Figure 32 shows contact angle versus laser pulse energy for a series of DLC films produced with varying laser pulse energy on silicon substrates with deposition temperature of 200 °C. The films show slightly increased contact angle with increased laser pulse energy, ranging from 79.5° at 5.3 mJ to 87.8° at 10.5 mJ. The reason for this trend is unclear because the Raman spectra for these films show no noticeable change in structure with increasing laser pulse energy. The effects of surface roughness can also be eliminated as a factor

because the films all have similar roughness values, as is shown in the atomic force microscopy section of this work.

For the films deposited on fused silica, there is no clear relation between pulsed laser energy or deposition temperature and contact angle. Figures 33 and 34 show the results of these measurements.

All undoped films produced are neither strongly hydrophilic nor strongly hydrophobic with contact angles ranging from 65° to 88°. Clearly, it will be necessary to change the surface energy to make the films more desirable for bronchoscope (super-hydrophilic) and stent applications (super-hydrophobic). Surface modification and/or doping are two strategies for changing surface energy, which will be discussed in greater detail in subsequent sections.

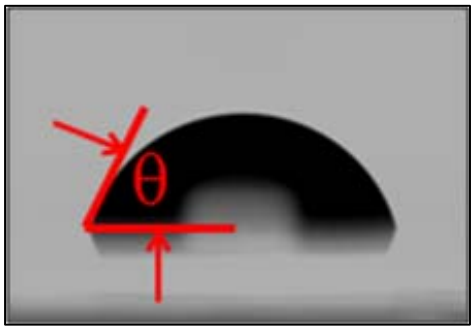

Figure 30 Example of the Contact Angle (θ) of Water on a Surface

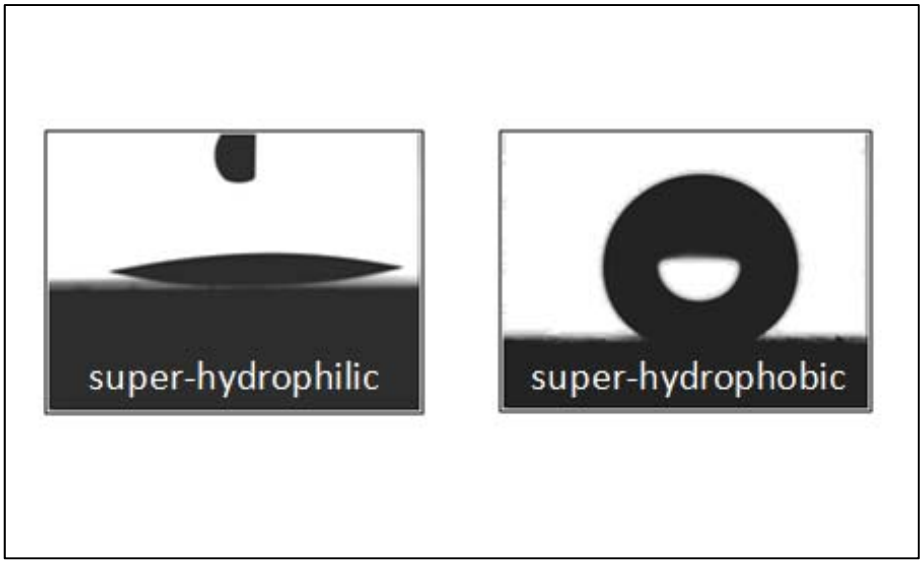

Figure 31 Examples of Super-Hydrophilic and Super-Hydrophobic Surfaces

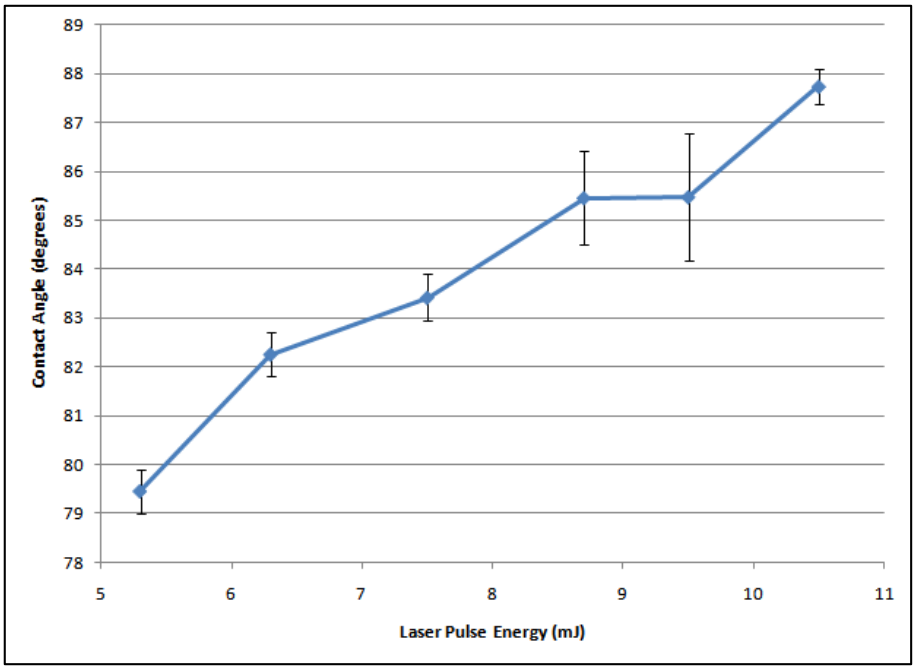

Figure 32 Contact Angle versus Laser Pulse Energy for DLC Films Deposited on Silicon Substrates at 200 °C Deposition Temperature

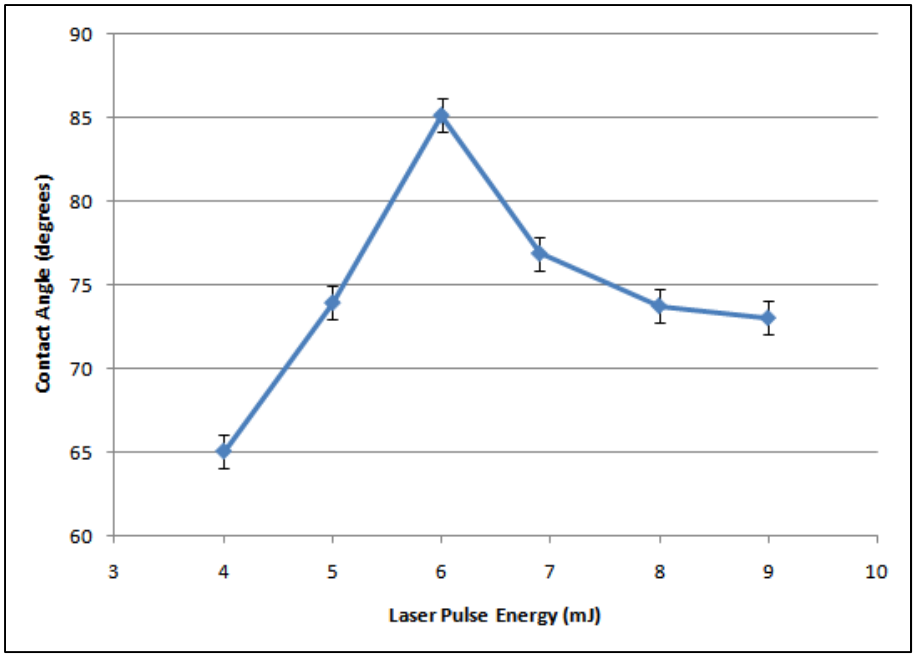

Figure 33 Contact Angles Versus Laser Pulse Energy for DLC Films deposited on Fused Silica Substrates at 20 °C Deposition Temperature

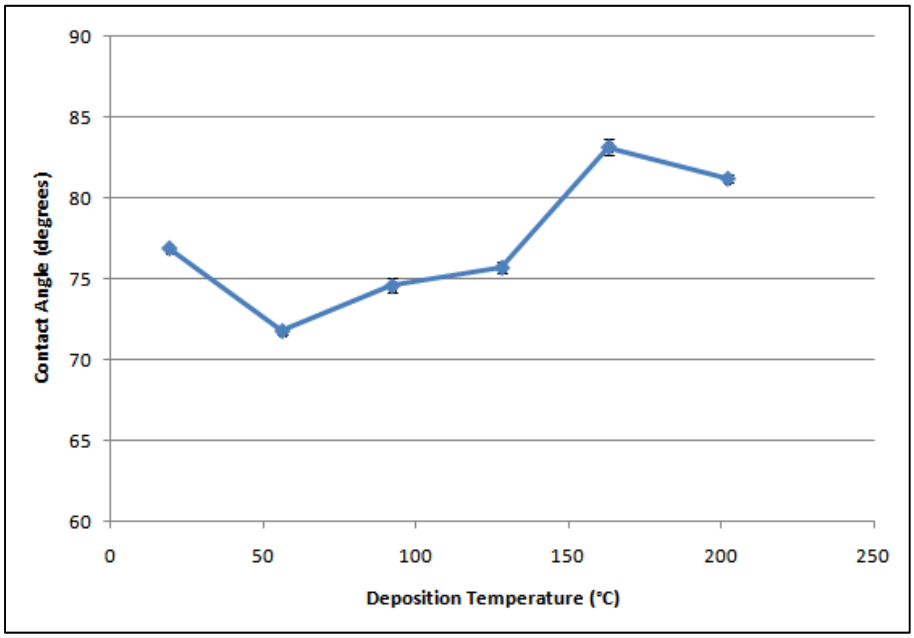

Figure 34 Contact Angle Versus Deposition Temperature for DLC Films Deposited on Fused Silica at 7.0 mJ Laser Pulse Energy

Atomic Force Microscopy

Understanding the morphology and surface roughness of the DLC films produced is important for the three biomedical applications being considered. For coronary stents, increased surface roughness can lead to increased platelet adhesion causing thrombosis. For artificial joints, increased roughness of the wear surface may result in a higher coefficient of friction and increased wear. Roughness can also affect contact angle, making it a consideration in films that may be used as coatings for bronchoscope lenses [40].

The morphology of the DLC films tended to vary greatly depending upon the substrate on which the film was deposited. A representative image for DLC deposited on silicon is shown in Figure 35, which reveals a surface without order. The morphology of DLC deposited on fused silica is quite different, as shown in Figure 36, which has repeating striations running across the surface. These differences are most likely due to the roughness of the underlying substrate. It is quite obvious after measurement that bare fused silica substrates have the same striations found on the samples of DLC deposited on fused silica as shown in Figure 37. This is in contrast to the bare silicon substrates as shown in Figure 38.

In general, the DLC films deposited on silicon were much smoother than those deposited on fused silica as shown in Figures 39, 40, and 41. Also, more variation in roughness was seen in the samples deposited on fused silica. Again this is likely due to the effects of the substrate, as the fused silica substrates were generally rougher (RMS roughness > 0.7 nm) than the silicon substrate (RMS roughness < 0.12 nm).

The results did not show any correlations between laser pulse energy or deposition temperature and RMS roughness.

Figure 36 also shows rounded bumps in the film. Some of the films produced, especially those on fused silica, exhibit delamination. The rounded areas may be where the film has detached from the substrate to release residual stress formed during synthesis. Macroscopic delamination is most common at the thicker portions of the films. This trend could also be seen at the microscopic level during AFM characterization.

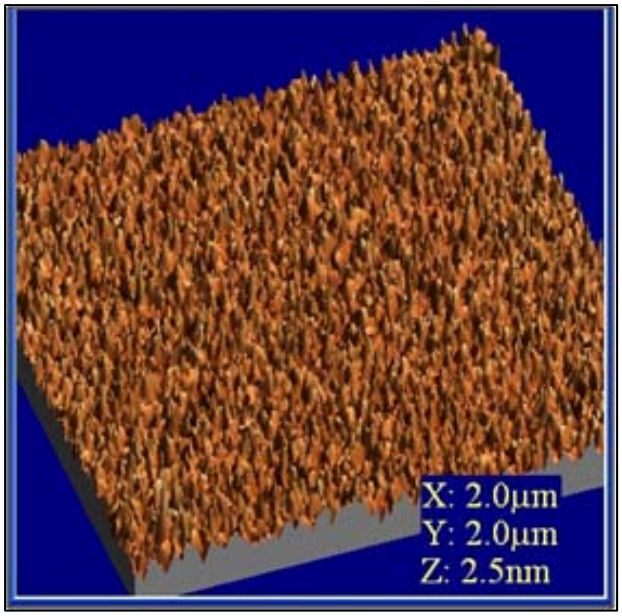

Figure 35 AFM Image of PLD #21, DLC on Silicon, 2 µm x 2 µm Scanning Area

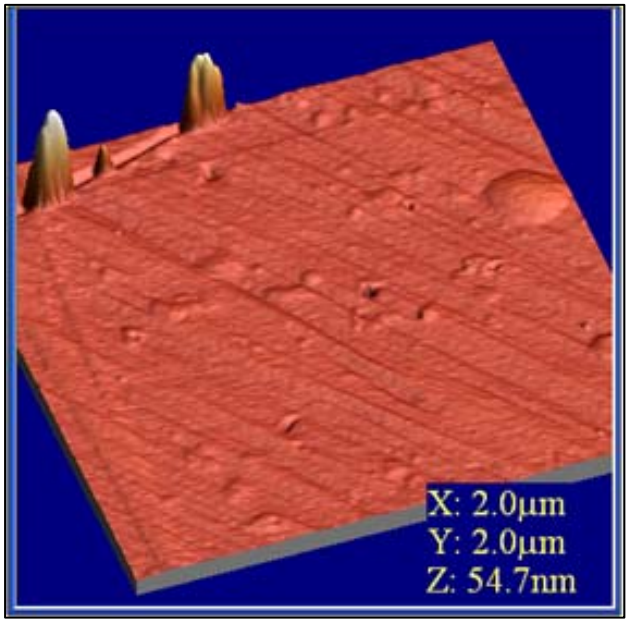

Figure 36 AFM Image of PLD #42, DLC on Fused Silica, 2 µm x 2 µm Scanning Area

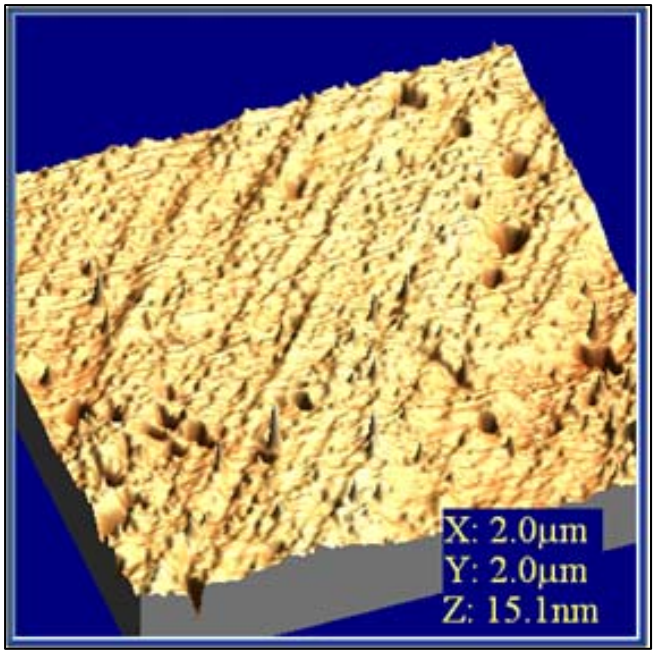

Figure 37 AFM Image of Fused Silica, 2 µm x 2 µm Scanning Area

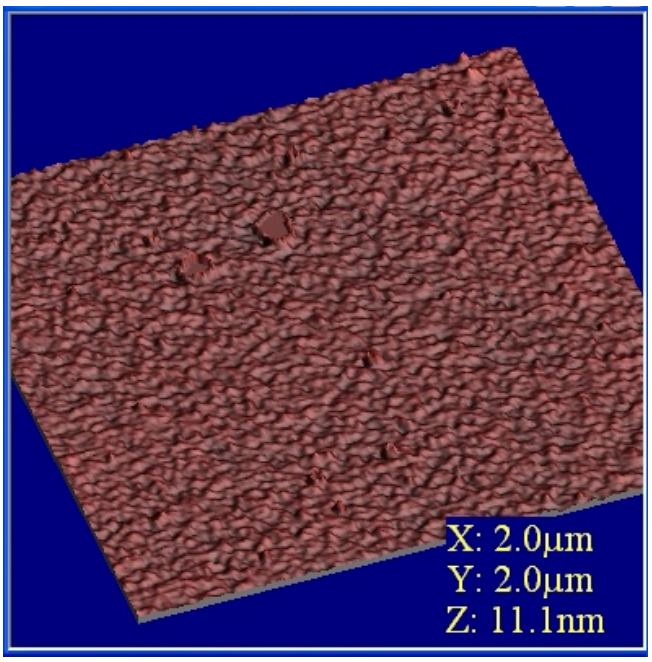

Figure 38 AFM Image of a Silicon Wafer, 2 µm x 2 µm Scanning Area

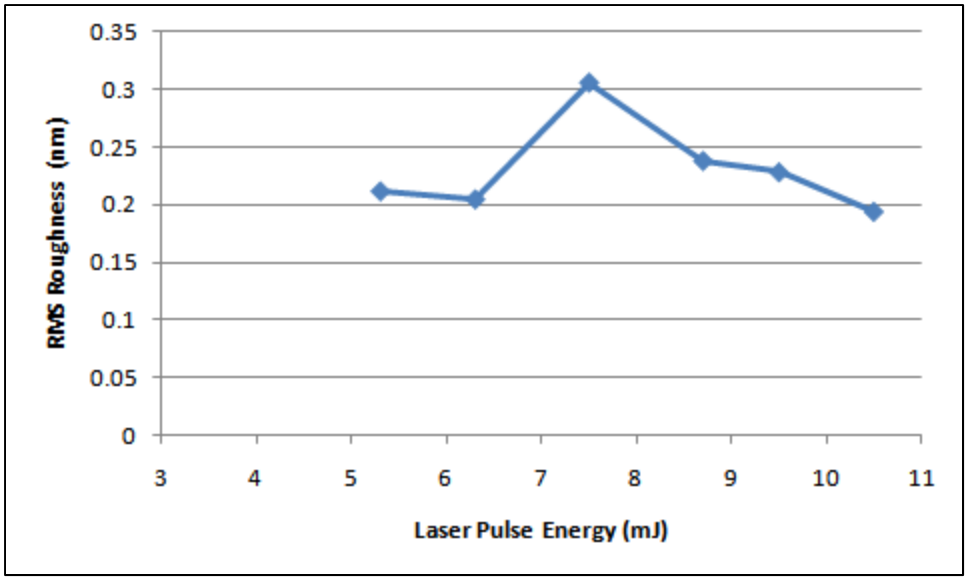

Figure 39 RMS Roughness for DLC Films Produced with Varying Pulse Laser Energy on Silicon at 200 °C Deposition Temperature

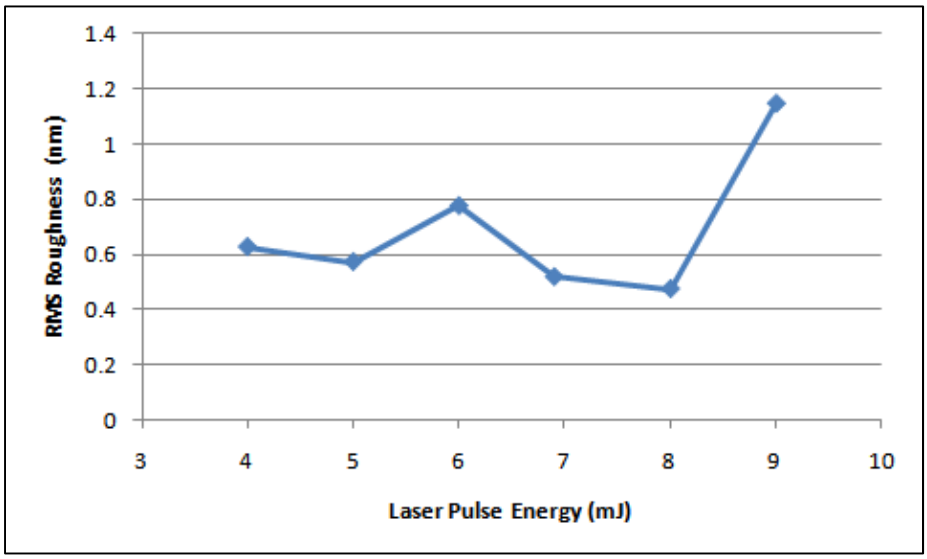

Figure 40 RMS Roughness for DLC Films Produced with Varying Pulse Laser Energy on Fused Silica at 20 °C Deposition Temperature

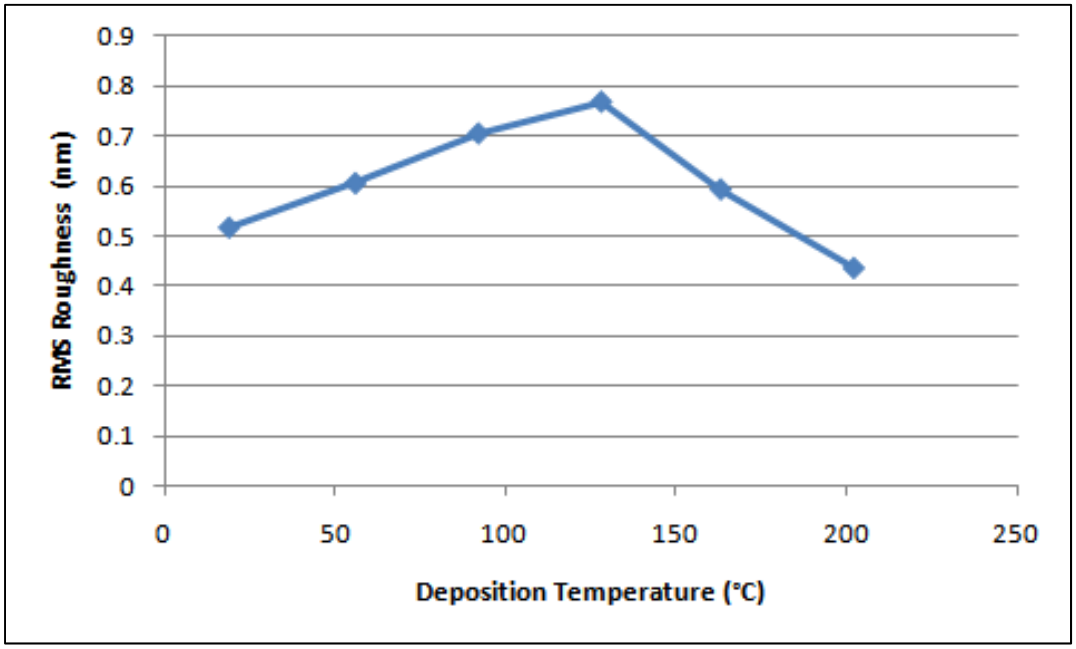

Figure 41 RMS Roughness for DLC Films Produced with Varying Deposition Temperature on Fused Silica at 7.0 mJ Laser Pulse Energy

Ball-on-flat Tribometry

For the DLC coatings to be useful in artificial joints, they must have good wear properties. To this end, one of the DLC films, PLD #11, was tested under a variety of conditions. Parameters for each tribological test performed are shown in Table 11.

The DLC film performed poorly in both dry nitrogen and air. Large wear scars were produced in both environments as shown in Figure 42. The coefficient of friction during testing in nitrogen and air atmospheres can be seen in Figures 43 and 44. As these films are intended for uses in the lubricated environment of the human body, these results are useful mostly as a reference.

For two of the tests, lubrication was used to better simulate the conditions inside the human body. The DLC film tested by the ball-on-flat tribometer with oil lubrication exhibited very light markings with no noticeable wear debris as shown in Figure 45. The coefficient of friction for the DLC film with oil lubrication as a function of time and sliding speed is shown in Figure 46. After an initial wear-in period, the coefficient of friction stabilized at 0.08 ± 0.01. The film maintained this low coefficient of friction during the remainder of the testing at each of the varying sliding speeds. The film's performance was typical of DLC in a lubricated

environment [41]. Lubrication with bovine serum did not yield results as favorable as those using oil. The coefficient of friction during testing with bovine serum lubrication, as a function of time and sliding speed, is shown in Figure 47. A wear track was formed with noticeable debris as shown in Figure 48. Magnification of the wear scar made with bovine serum lubrication shows holes where large amounts of material were removed during testing (See Figure 49). These holes are likely caused by large particles from the silicon bond coat breaking free from the substrate.

The relative motion of joints in the human body is obviously more complicated that the rotational motion seen in ball-on-flat testing. Also, the short test time is only a small fraction of the time that an artificial joint must remain in service in the human body. However, ball-on-flat testing does have merit as it allows for the tribological performance of a material to be quickly evaluated, so that resources are not wasted on inferior films. Additionally, longer test times in future studies will give a more accurate representation of the long-term viability of DLC films. The coating of materials used in actual prostheses would be another future step, as adhesion of the DLC films will vary with substrate. If successful, testing with artificial hip machines would be the next step to more accurately determine the viability of the films.

Table 11 Tribological Test Parameters and Resulting Coefficients of Friction

Environment	Load (N)	Coefficient of Friction of the DLC Film, PLD # 11, at Steady State	Sliding Speed (cm/s)	Test Duration(s)
dry nitrogen	5	n/a – film failure	1	3400
air*	5	n/a – film failure	1	140
oil**	5	0.08 ± 0.01	0.02, 0.1, 1, and 10	4200
bovine serum	5	n/a – film failure	0.4 and 0.1	2400
* at 21% relative humidity ** Mobil 1 5W30 synthetic motor oil				

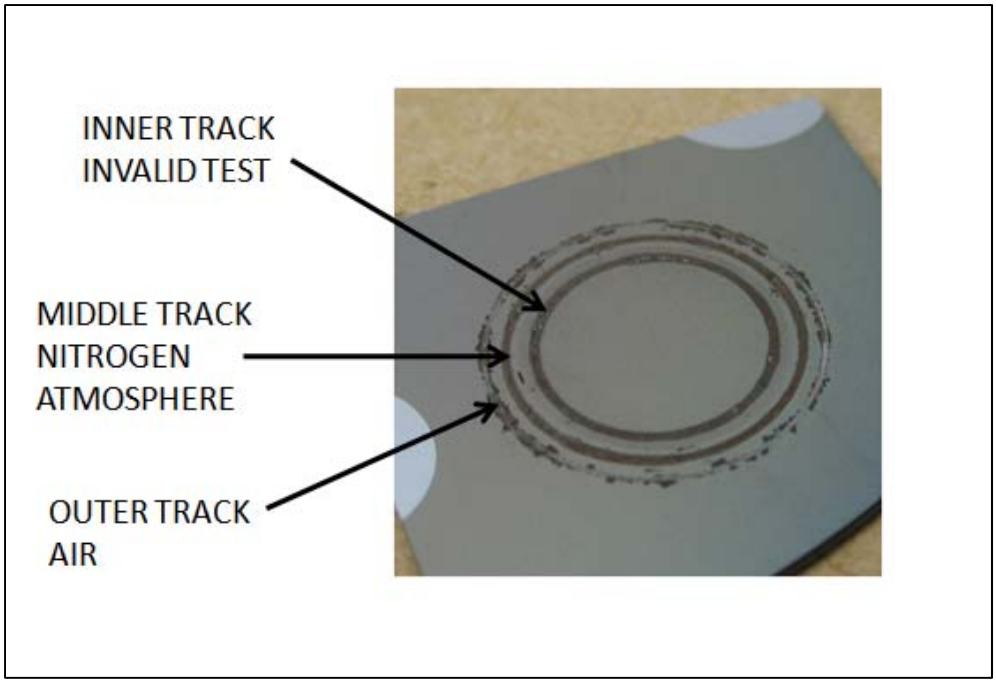

Figure 42 DLC Sample after Tribological Testing in Nitrogen and Air Atmospheres

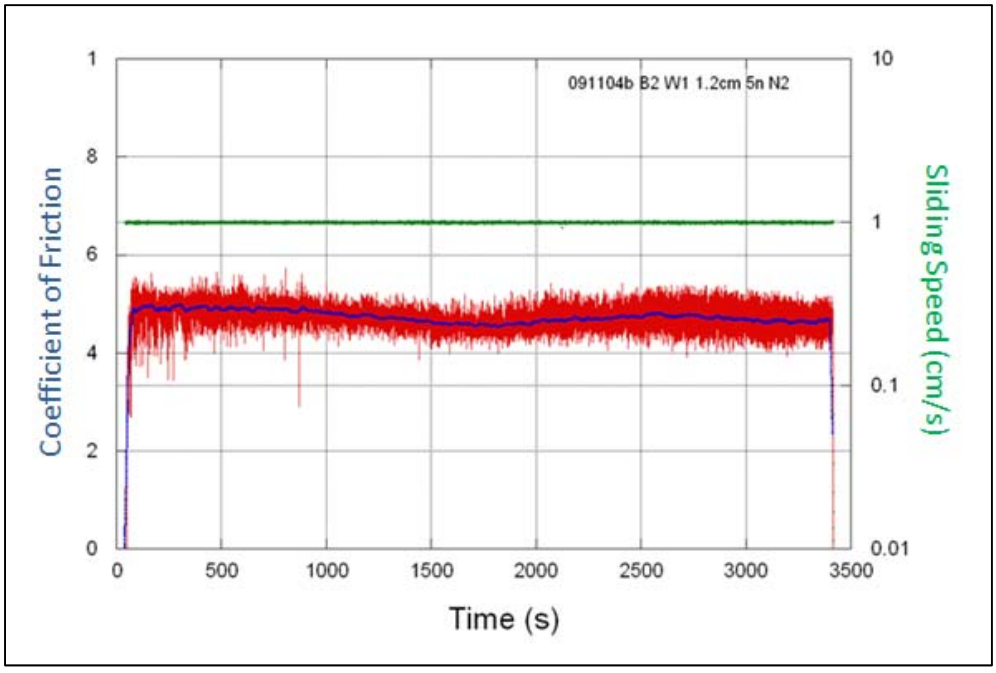

Figure 43 The Coefficient of Friction during DLC against DLC Wear Testing as a Function of Time in a Nitrogen Atmosphere

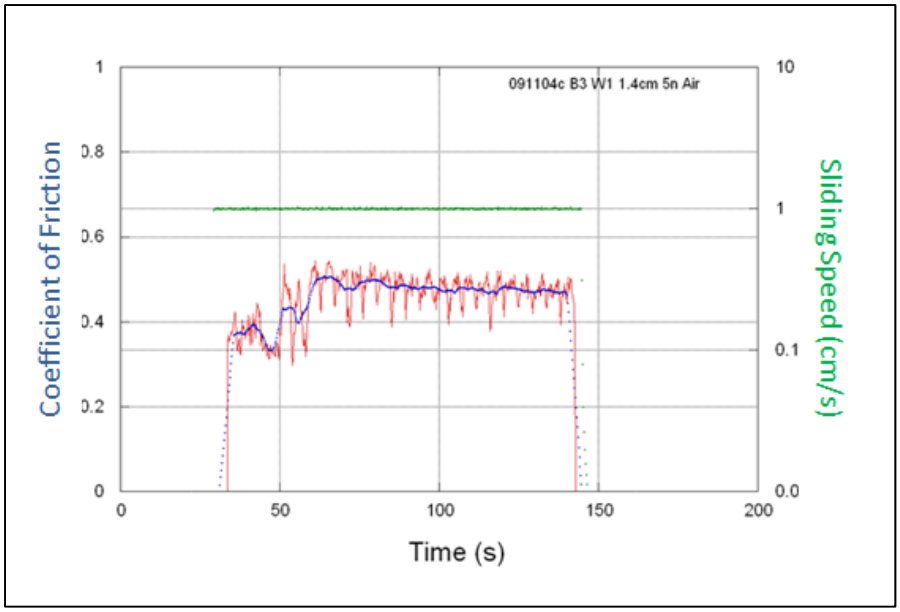

Figure 44 The Coefficient of Friction during DLC against DLC Wear Testing as a Function of Time in an Air Atmosphere

Figure 45 DLC Sample after Wear Testing with Oil Lubrication

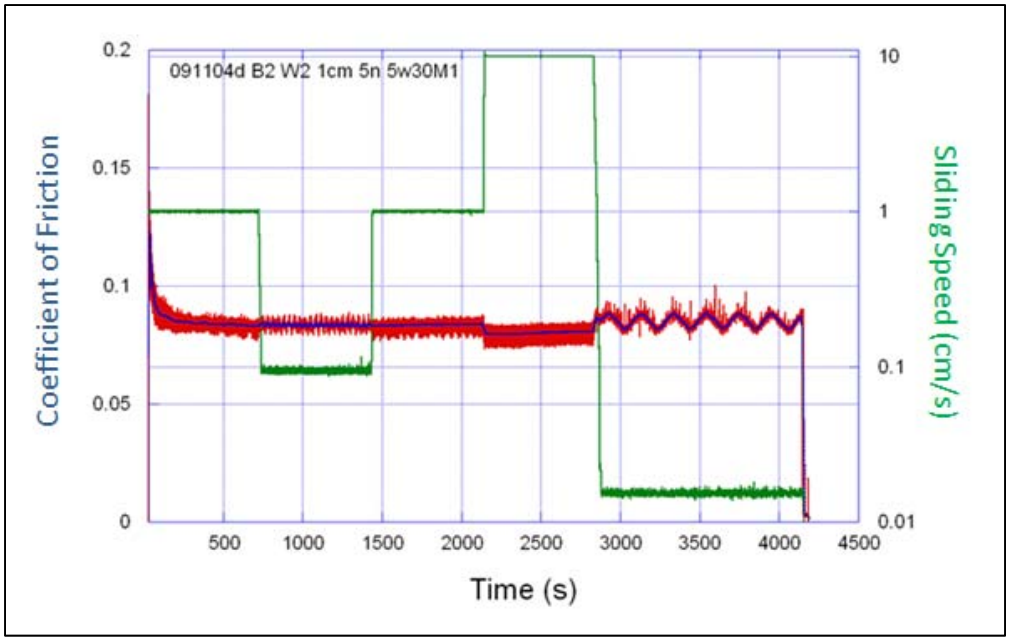

Figure 46 The Coefficient of Friction during DLC against DLC Wear Testing with Varying Sliding Speeds as a Function of Time with Oil Lubrication

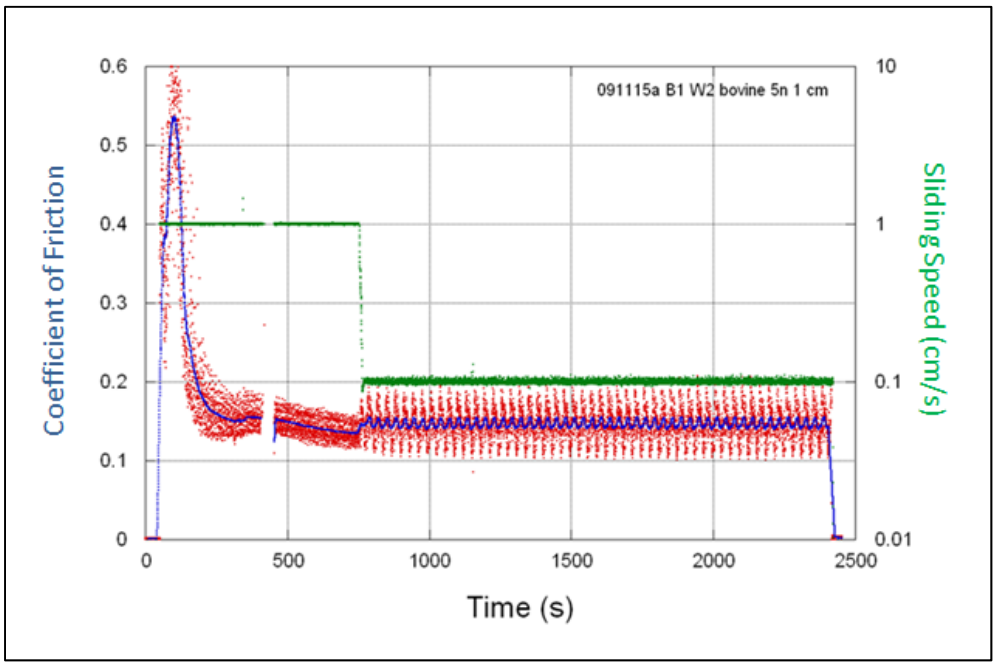

Figure 47 The Coefficient of Friction during DLC against DLC Wear Testing with Varying Sliding Speeds as a Function of Time with Bovine Serum Lubrication

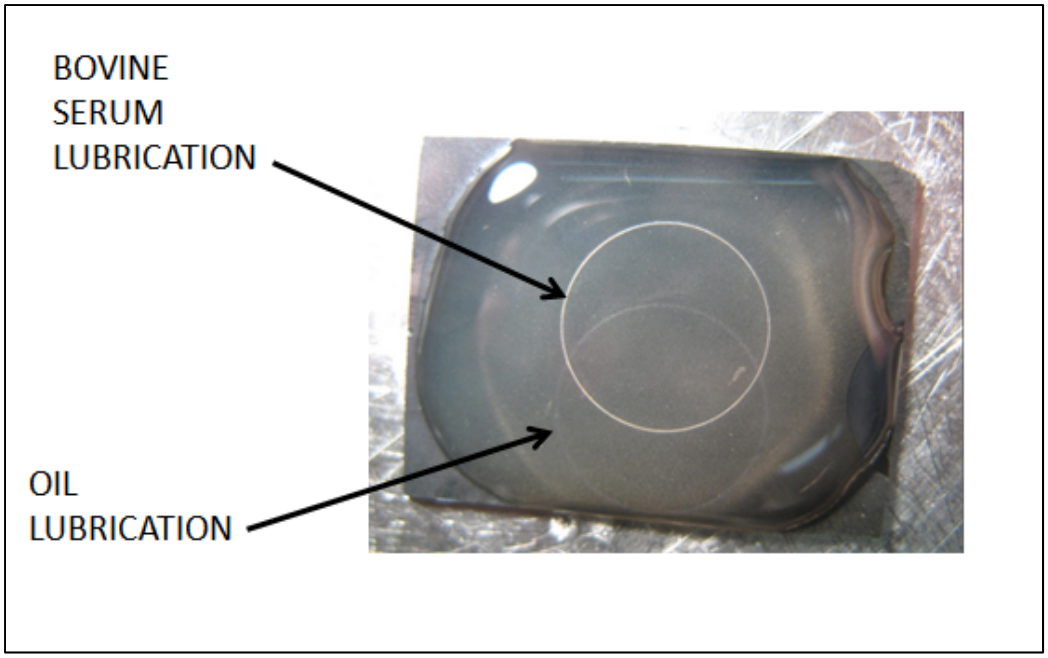

Figure 48 DLC Sample after Wear Testing with Bovine Serum and Oil Lubrication

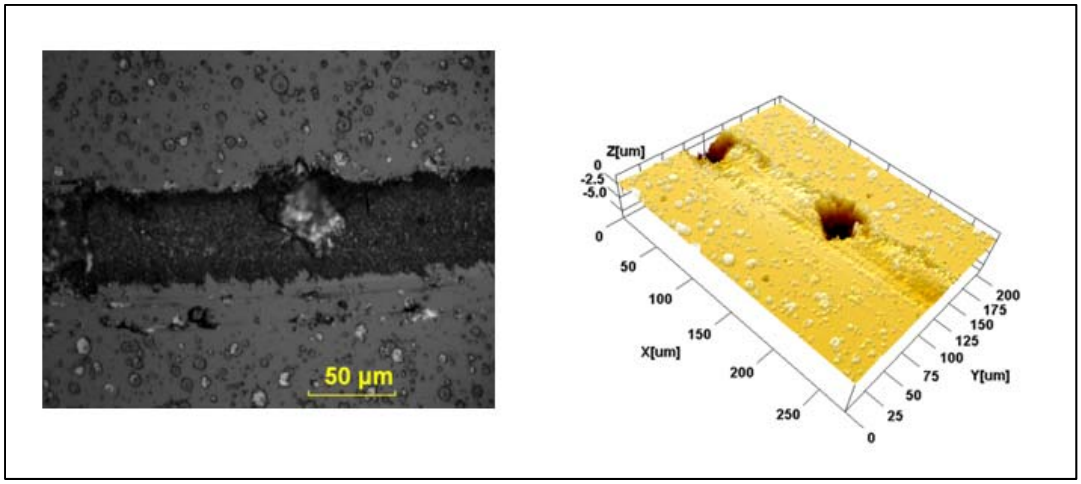

Figure 49 Holes where Large Amounts of Material Were Removed during Tribological Testing of DLC against DLC with Bovine Serum Lubrication

Spectrophotometry

For the films to be useful as protective coatings for bronchoscope lenses, they must be transparent. The DLC films produced are partially transparent as can be seen in Figure 50.

Figure 51 shows that transmission is reduced with increased laser pulse energy, which is likely due to the higher deposition rate leading to thicker films and more attenuation.

As is shown in Figure 52, decreased deposition temperature leads to increased transmission. This is likely due to a change in the structure of films as can be seen in the Raman spectroscopy results in Figures 26 and 28 and Table 10. The results suggest the films become more diamond-like with greater sp^3 content and an increasing band gap with decreasing temperature.

In general, the films allow good transmission of light in the infrared and visible wavelengths. Transmission reduces rapidly at ultraviolet wavelengths, however.

Figure 50 Transparent DLC

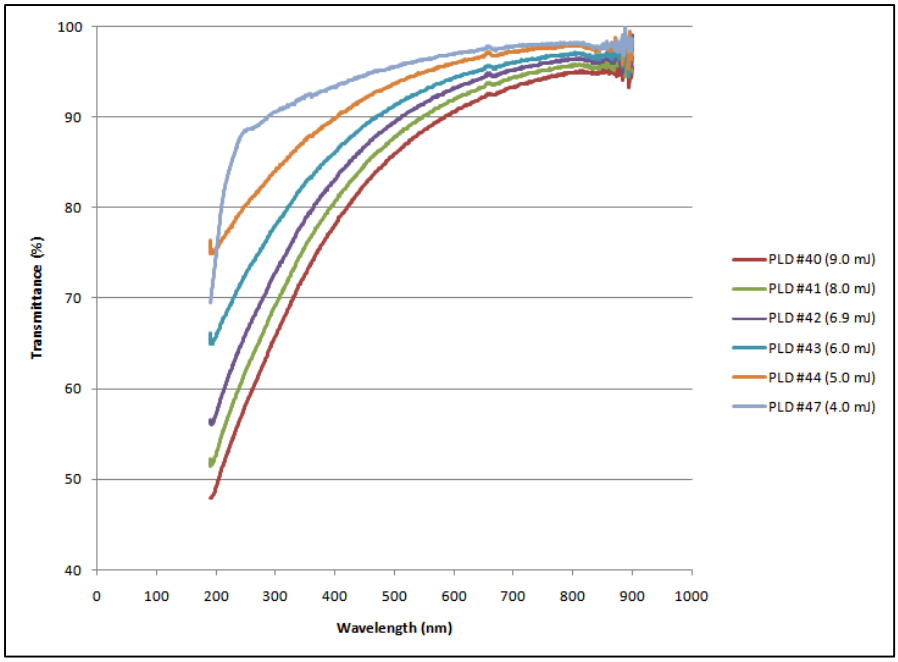

Figure 51 Transmittance of DLC Films Made with Varying Laser Pulse Energy at 20 °C Deposition Temperature

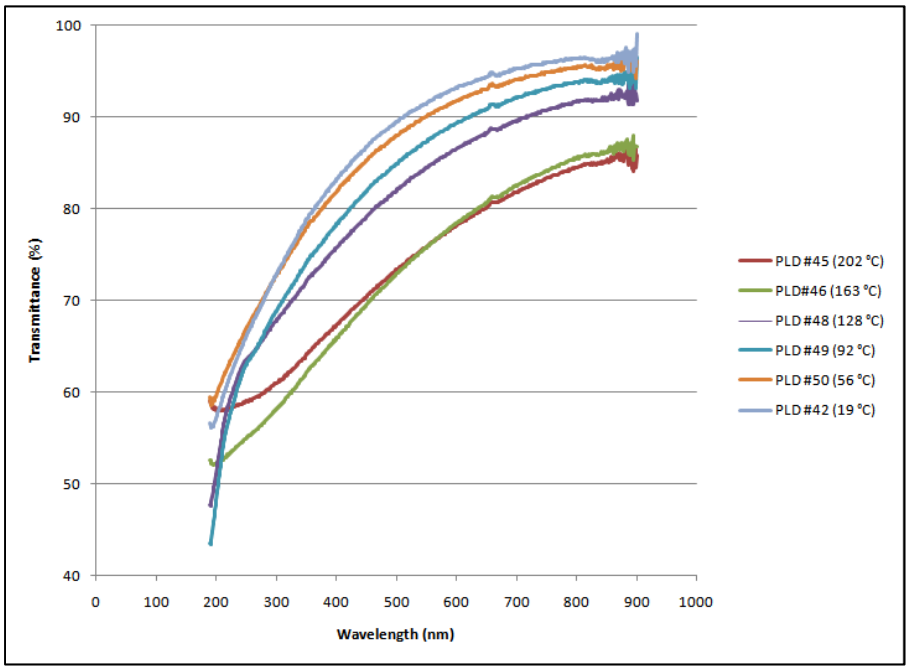

Figure 52 Transmittance of DLC Films Made with Varying Deposition Temperature at 7.0 mJ Laser Pulse Energy

Doped Films

Although the undoped diamond-like carbon films demonstrated many favorable properties, including high transparency, low coefficient of friction, good wear resistance, and stability when immersed in simulated body fluid, the films did not possess all of the characteristics necessary to meet the goals of this project. Thicker films tended to delaminate from the substrate due to residual compressive stresses. Also, the contact angles for the undoped films are neither strongly hydrophobic nor strongly hydrophilic. Experimental results showed that varying process parameters such as substrate temperature and laser fluence had little effect on the delamination problem or the contact angles. Clearly another approach would have to be considered to modify the films' properties so that they might be useful as biomedical coatings. It has been shown that adding dopants to the DLC film matrix can alter contact angle of the films and reduce residual stresses formed during deposition [9] [15] [42]. For this reason the second stage of research focused on the effects of dopants on the film properties.

For this study, potential dopants had to meet certain criteria. First, any dopant considered must be expected to not affect the biocompatibility of the DLC films. Second, the dopant material must exist in solid form and must be capable of being formed into the required shape for use as an ablation target in pulsed laser deposition. Third, the dopant material should not be prohibitively expensive.

In addition to the requirements above, the dopant had to have a reasonable chance of modifying the films in a desired fashion. Surface energy can be given by the following equation:

$$\gamma = \gamma^d + \gamma^p + \gamma^h$$

where γ = surface energy, d = dispersive forces, p = polar forces, h = hydrogen bonding [43]. One strategy to increase overall surface energy is to increase the surface energy due to hydrogen bonding. Nitrogen, oxygen, and fluorine are three elements that are capable of forming hydrogen bonds. Elements or compounds containing these elements might therefore be candidates for increasing surface energy.

Titanium dioxide and silicon monoxide fit the above requirements and were selected as dopants to be evaluated for use in a series of DLC films. Silicon nitride was also evaluated, although due to its hardness and the difficulty in machining it to size, only one group of samples was made. Although it cannot form hydrogen bonds, samples were also made with silicon as a dopant due to its inexpensive nature and availability.

Profilometry

The thickness and growth rate results for the titanium dioxide doped DLC films on fused silica are shown in Table 12. There appears to be little change in deposition rate with increasing dopant wedge size as seen in Figure 53.

Table 13 gives the thickness and growth rate results for the silicon monoxide doped DLC films. There is no clear relationship between the amount of dopant used and film growth rate as shown in Figure 54.

The silicon nitride sample produced, PLD #51, was 8.4 ± 2.0 nm thick, with a deposition rate of 0.56 ± 0.13 nm per minute deposition rate over fifteen minutes of deposition.

The silicon doped sample, PLD #53, was 243 ± 5 nm thick, with a deposition rate of 1.01 ± 0.03 nm per minute deposition rate over four hours of deposition.

The deposition rate for the doped films was considerably less than that for the undoped films produced with similar pulse laser energy (~1.8 nm per minute at 7.0 mJ pulse laser energy).

Table 12 Film Thickness and Deposition Rate for DLC Films Produced on Fused Silica with Varying Amounts of Titanium Dioxide Dopant

Sample	Dopant Wedge Size (degrees)	Thickness (nm)	Deposition Time (minutes)	Deposition Rate (nm/minute)
PLD #57-1	30	165 ± 13	240 ± 5	0.69 ± 0.06
PLD #59-1	35	146 ± 10	240 ± 5	0.61 ± 0.04
PLD #56-1	40	169 ± 13	240 ± 5	0.70 ± 0.06
PLD #60-1	45	194 ± 7	240 ± 5	0.81 ± 0.03
PLD #55-1	50	187 ± 5	240 ± 5	0.78 ± 0.03
PLD #58-1	55	146 ± 14	240 ± 5	0.61 ± 0.06

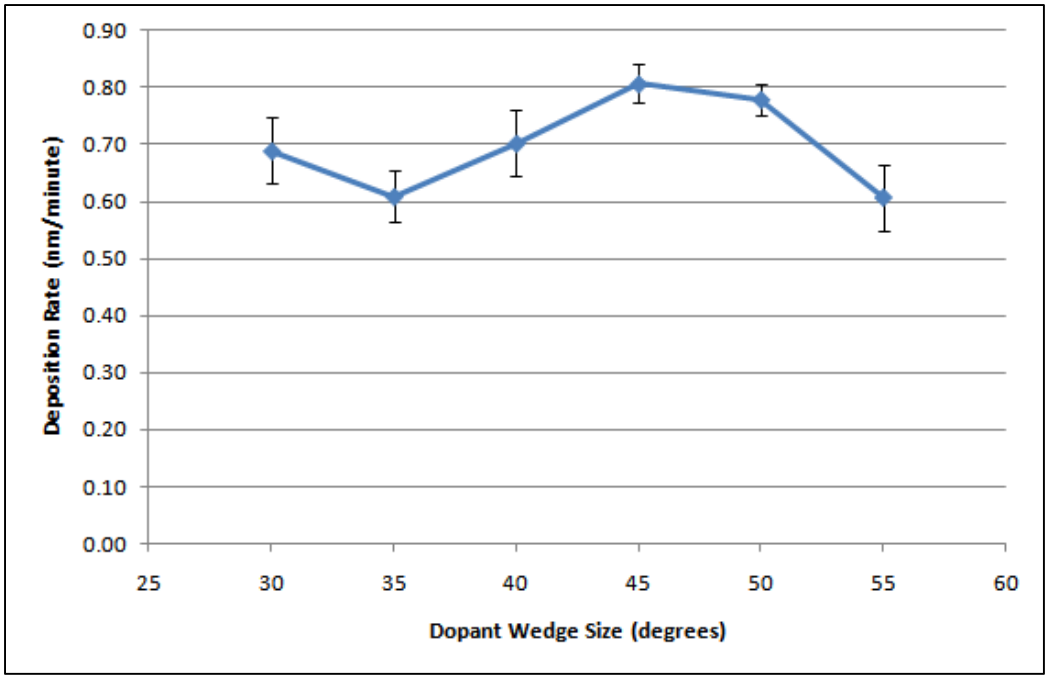

Figure 53 Deposition Rate for DLC Films Produced on Fused Silica with Varying Amounts of Titanium Dioxide Dopant

Table 13 Film Thickness and Deposition Rate for DLC Films Produced on Fused Silica with Varying Amounts of Silicon Monoxide Dopant

Sample	Dopant Wedge Size (degrees)	Thickness (nm)	Deposition Time (minutes)	Deposition Rate (nm/minute)
PLD #63-1	30	191 ± 13	240 ± 5	0.80 ± 0.05
PLD #65-1	35	158 ± 11	240 ± 5	0.66 ± 0.05
PLD #62-1	40	179 ± 4	240 ± 5	0.75 ± 0.02
PLD #61-1	45	217 ± 7	240 ± 5	0.90 ± 0.03
PLD #66-1	50	114 ± 9	240 ± 5	0.47 ± 0.04
PLD #64-1	55	119 ± 10	240 ± 5	0.50 ± 0.04

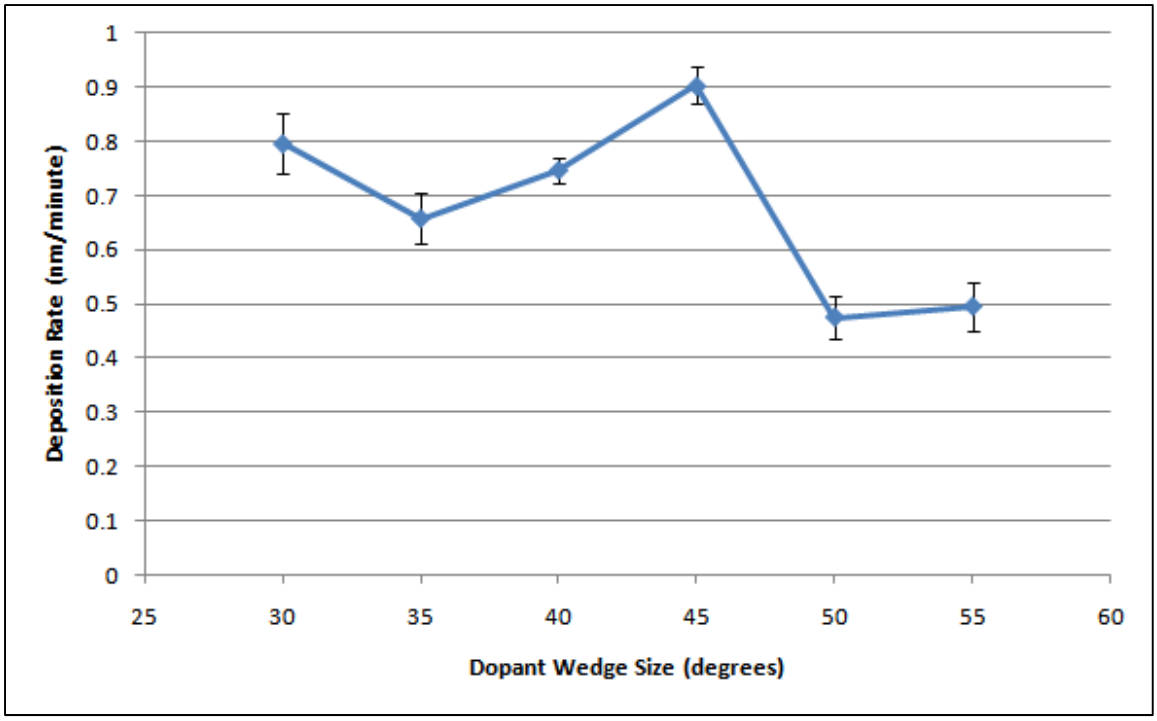

Figure 54 Deposition Rate as a Function of Dopant Wedge Size for DLC Films Produced on Fused Silica with Varying Amounts of Silicon Monoxide Dopant

Raman Spectroscopy

The addition of dopants will not only change the composition of the films but may also alter the nature of the carbon bonding within the films. Examination of the Raman spectra of the doped DLC films can give insight as to whether or not the bonding was affected.

The Raman spectra for titanium dioxide doped DLC films can be seen in Figure 55. Deconvolution of the spectra yields the peak characteristics shown in Table 14. There appears to be little change of peak characteristic with increasing amounts of dopant, as can be seen in a plot of the normalized data in Figure 56. The films all have slightly higher G-peak positions, larger ratios of intensity between the D- and G-peaks, and narrower G-peak widths than the undoped DLC film made under similar conditions, PLD #42, whose characteristics can be seen in Table 10.

For silicon monoxide doped DLC, the Raman spectra for the films are shown in Figure 57. The peak characteristics are shown in Table 15. A plot of the normalized peak characteristics reveals a relationship between increasing dopant content and G-peak position as shown Figure 58, although no such relationship exists between the other characteristics. G-peak position versus dopant wedge

size is shown in Figure 59. The films all have much lower G-peak positions, smaller ratios of intensity between the D- and G-peaks, and broader G-peak widths than PLD #42.

The Raman spectrum for PLD #51, DLC doped with silicon nitride is shown in Figure 60. The deconvoluted spectrum yields a G-peak position of 1498 ± 1 cm^{-1} , a ratio of 0.51 ± 0.1 for the D- and G- Peak intensities, and a value of 231 ± 3 cm^{-1} for the full-width half maximum of the G-peak. Like the silicon monoxide doped films, the silicon nitride films have a much lower G-peak positions, smaller ratios of intensity between the D- and G-peaks, and broader G-peak widths than PLD #42.

Figure 61 shoes the Raman spectrum for PLD #53, DLC doped with silicon. The Raman peak characteristics for this film were a G-peak position of 1517 ± 1 cm^{-1}, a ratio of 0.79 ± 0.1 for the D- to G-peak intensities, and a value of 212 ± 3 cm^{-1} for the full width half maximum of the G-peak. These characteristics are similar to those of PLD #42 with the exception of the full-width half-maximum of the G-peak, which is broader for the silicon doped film. Two large peaks at approximately 520 cm^{-1} and 950 cm^{-1} can be attributed to the first and second order Raman peaks of silicon, respectively.

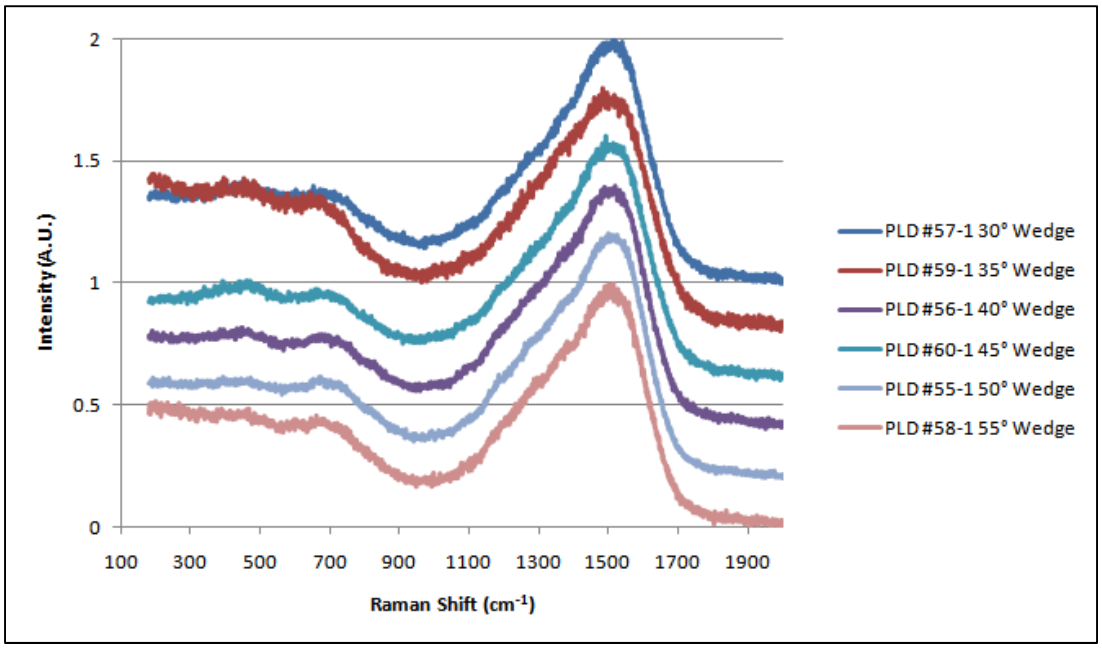

Figure 55 Raman Spectra of DLC Films Doped with Varying Amounts of Titanium Dioxide

Table 14 Raman Spectra Characteristics for Titanium Dioxide Doped DLC Films

Sample	Wedge Angle (degrees)	G-Peak Position (cm^{-1})	I_D/I_G (A.U.)	FWHM G-Peak (cm^{-1})
PLD #57	30	1528 ± 0.3	0.85 ± 0.01	201.8 ± 1.5
PLD #59	35	1529 ± 0.6	1.04 ± 0.04	213.5 ± 4
PLD #56	40	1529 ± 0.3	0.97 ± 0.01	187 ± 1.3
PLD #60	45	1528 ± 0.3	0.88 ± 0.01	201.1 ± 1.4
PLD #55	50	1531 ± 0.3	0.96 ± 0.01	184 ± 1.2
PLD #58	55	1530 ± 0.3	1.02 ± 0.03	209.4 ± 2.8

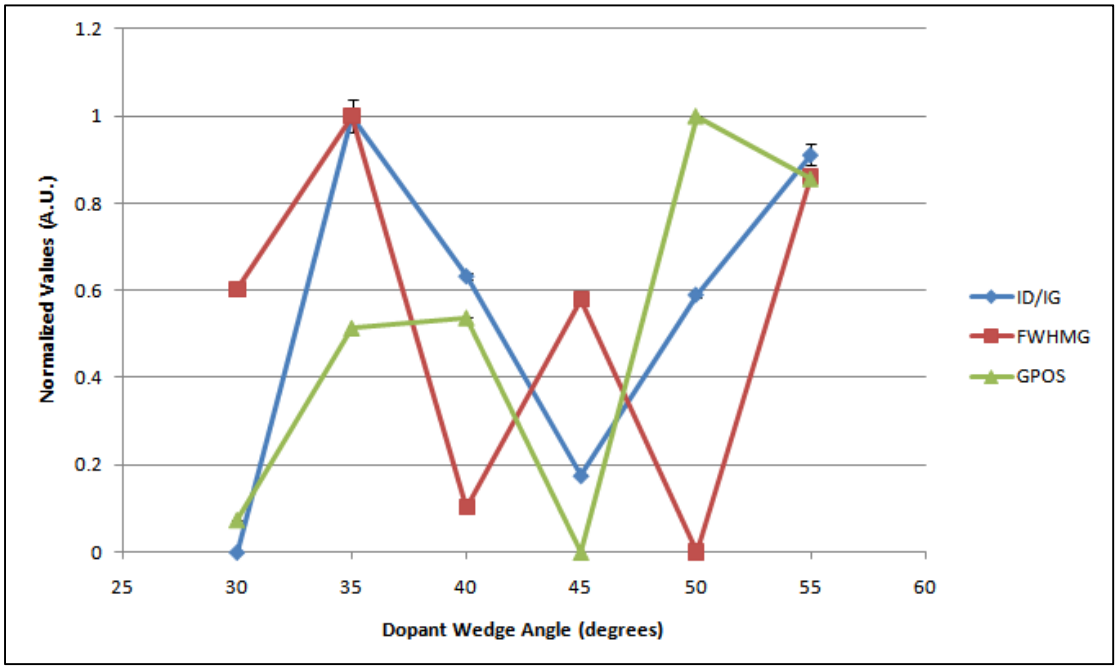

Figure 56 Normalized Raman Spectra Characteristics versus Titanium Dioxide Dopant Wedge Size

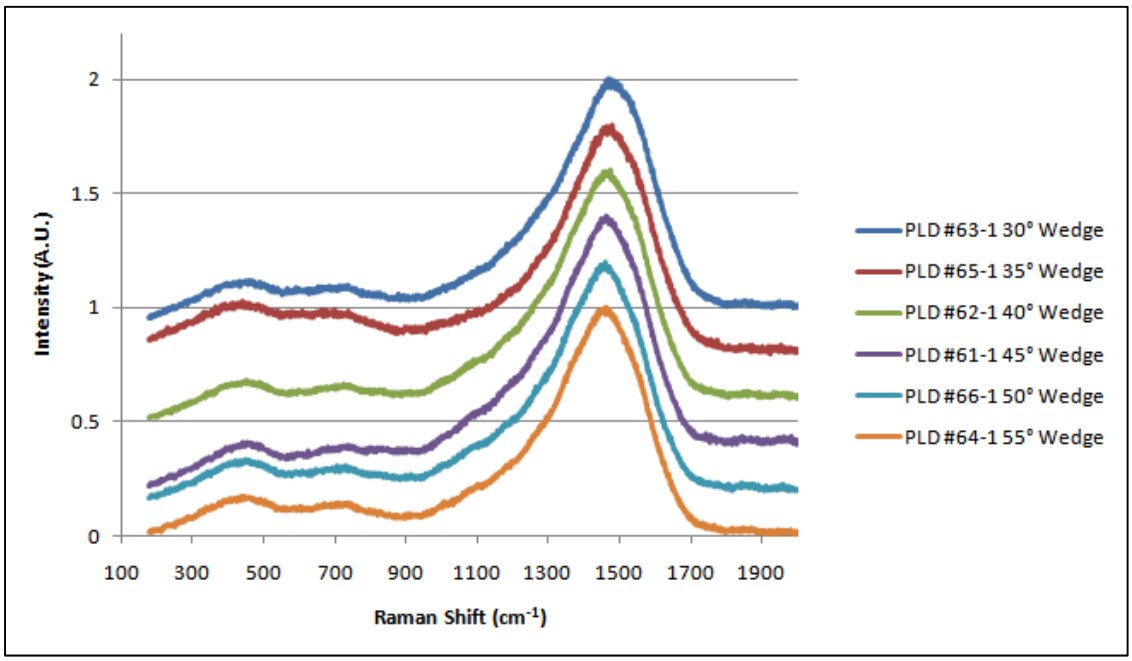

Figure 57 Raman Spectra of DLC Films Doped with Varying Amounts of Silicon Monoxide

Table 15 Raman Spectra Characteristics for Silicon Monoxide Doped DLC Films

Sample	Dopant Wedge Size (degrees)	G-Peak Position (cm^{-1})	I_D/I_G (A.U.)	FWHM G-Peak (cm^{-1})
PLD #63	30	1502.4 ± 1.9	0.48 ± 0.02	220.0 ± 4.1
PLD #65	35	1492.7 ± 4.6	0.43 ± 0.03	206.3 ± 8.2
PLD #62	40	1485.1 ± 1.4	0.44 ± 0.01	229.5 ± 3.8
PLD #61	45	1481.1 ± 0.9	0.77 ± 0.02	209.4 ± 2.8
PLD #66	50	1474.7 ± 1.9	0.40 ± 0.01	224.2 ± 4.0
PLD #64	55	1475.4 ± 2.4	0.40 ± 0.02	219.1 ± 5.0

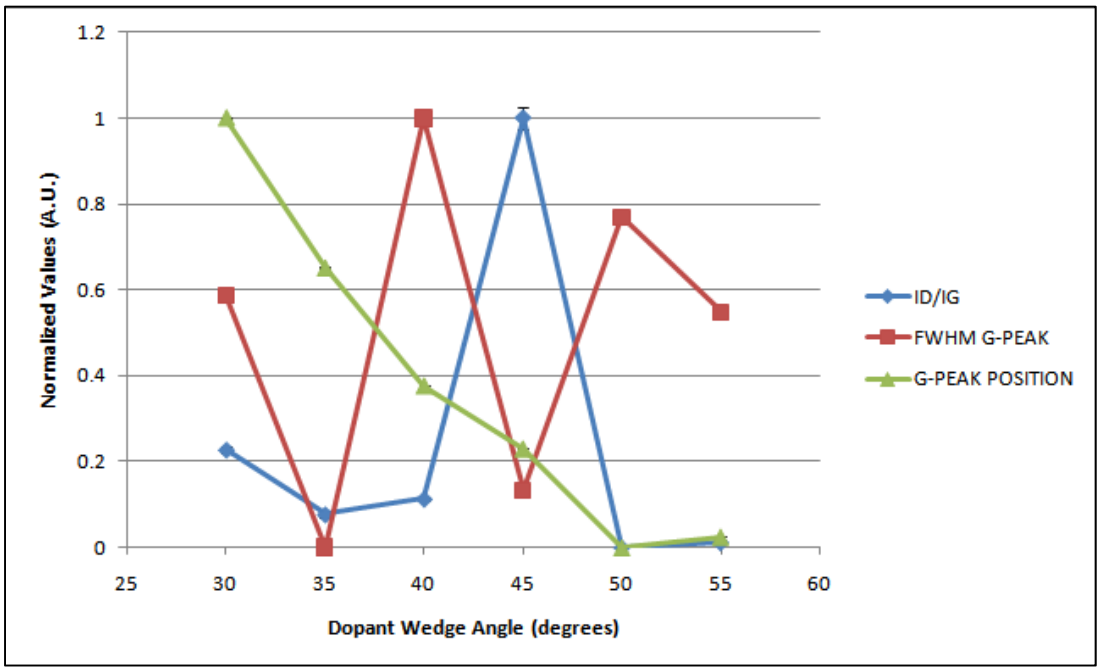

Figure 58 Normalized Raman Spectra Characteristics versus Silicon Monoxide Dopant Wedge Size

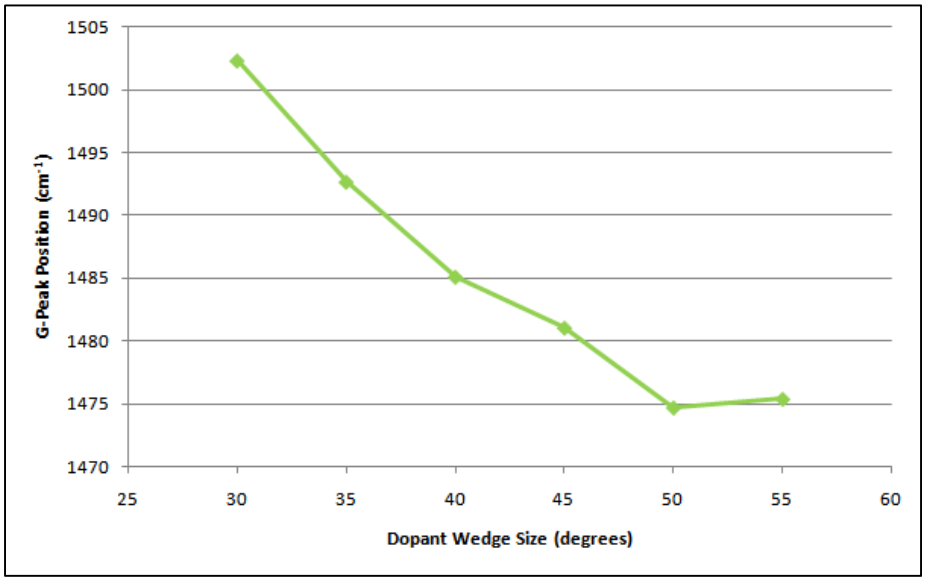

Figure 59 G-Peak Position versus Silicon Monoxide Dopant Wedge Size

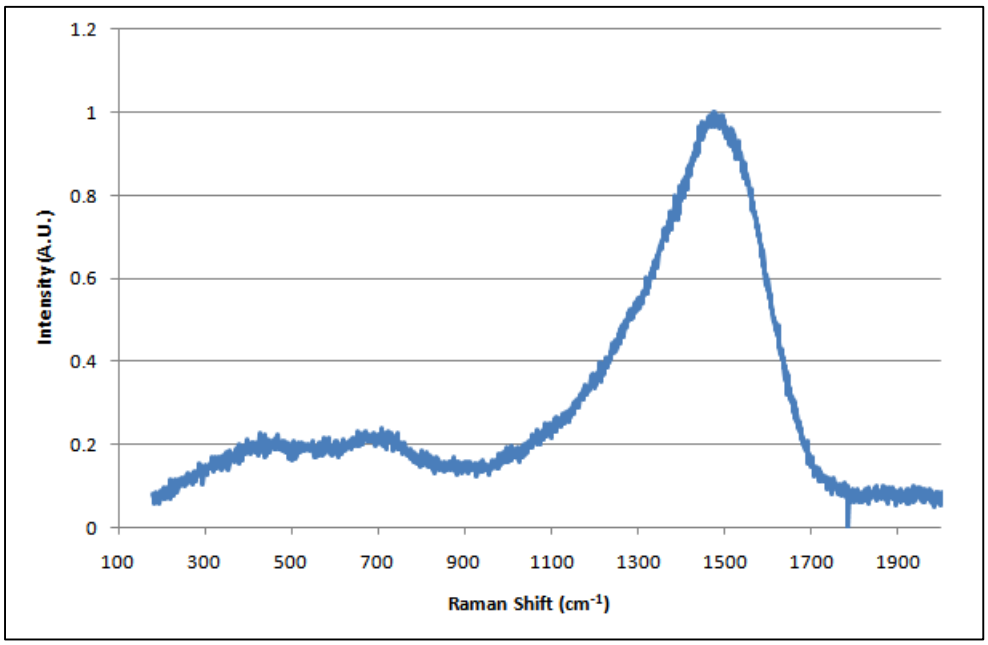

Figure 60 Raman Spectrum for Silicon Nitride Doped DLC

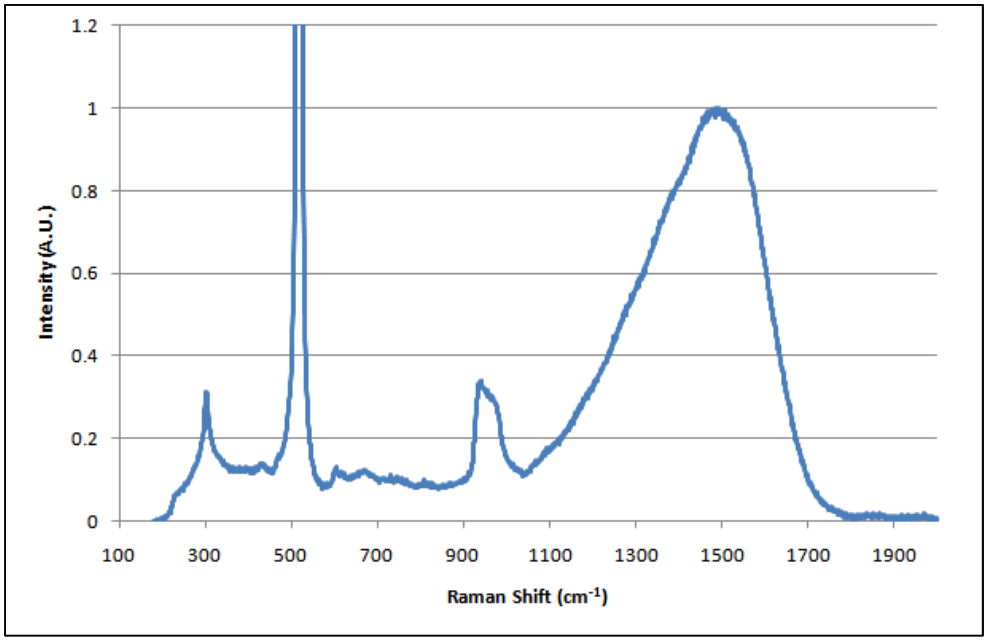

Figure 61 Raman Spectrum for Silicon Doped DLC

Soaking Experiments

Samples of DLC doped with silicon, silicon nitride, titanium dioxide, and silicon monoxide showed little change after immersion in simulated body fluid (SBF) for one week. The appearances of the films before and after the one week of immersion are shown in Figures 62 - 65. All films showed little change in appearance and can be deemed stable for the small amount of time that they were immersed.

One week immersion is obviously not a long enough time to effectively evaluate the films for implantation in the human body, which would require stability for many years. Protective coatings for lenses would likely see hundreds or thousands of hours of intermittent use. Longer testing will be required to determine the suitability of these films for use in wet environments. Furthermore, the doped films' properties such as contact angle and wear resistance should be re-checked to confirm no degradation has occurred, if these films appear to be stable visually after immersion of satisfactory duration.

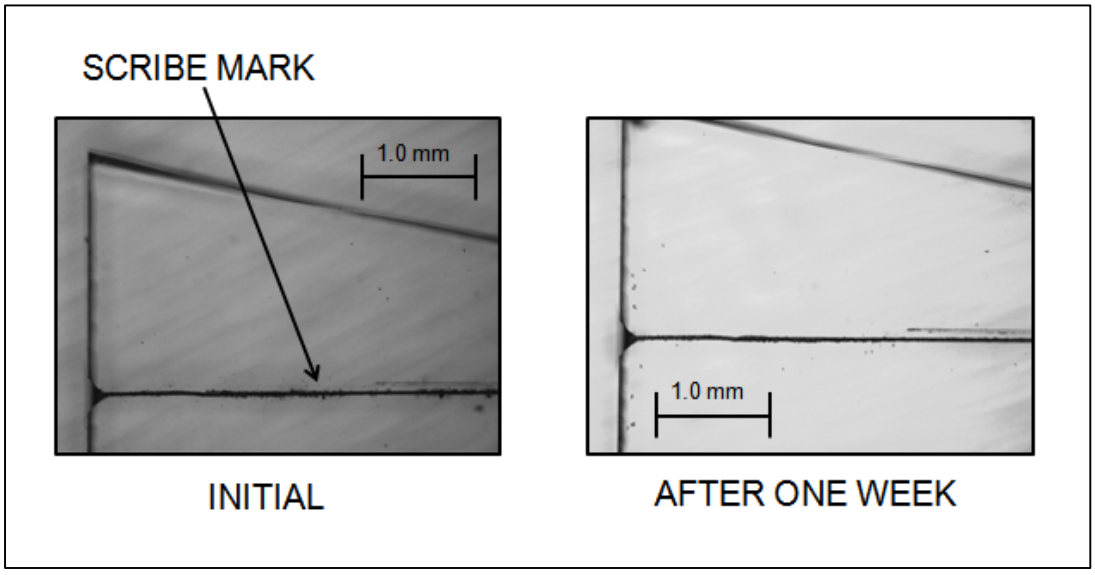

Figure 62 An Optical Micrograph of Silicon Nitride Doped DLC Film, PLD #51, Initially and after one week Immersion in SBF

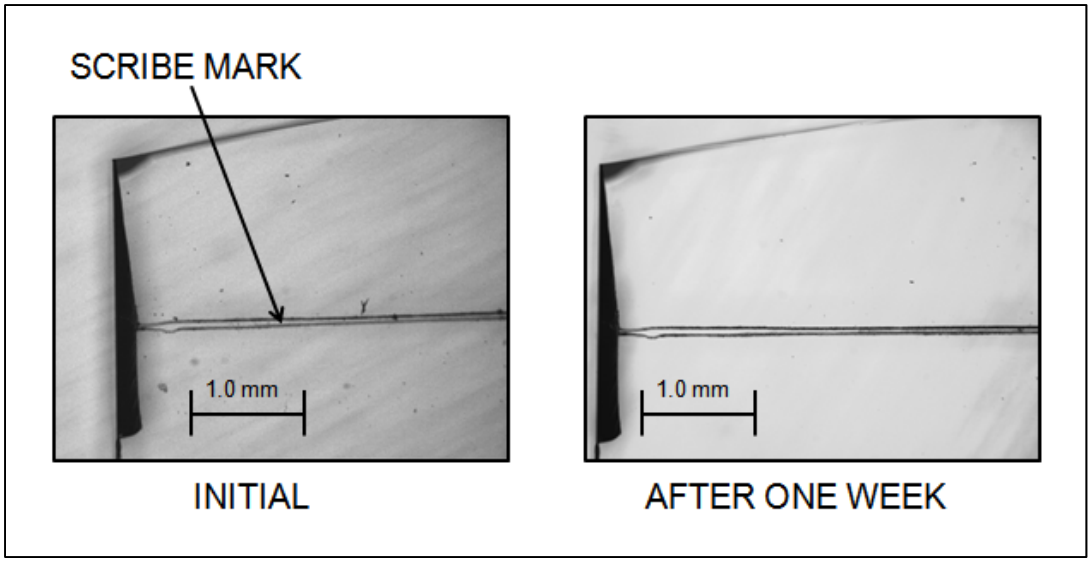

Figure 63 An Optical Micrograph of Silicon Doped DLC Film, PLD #52, Initially and after one week Immersion in SBF

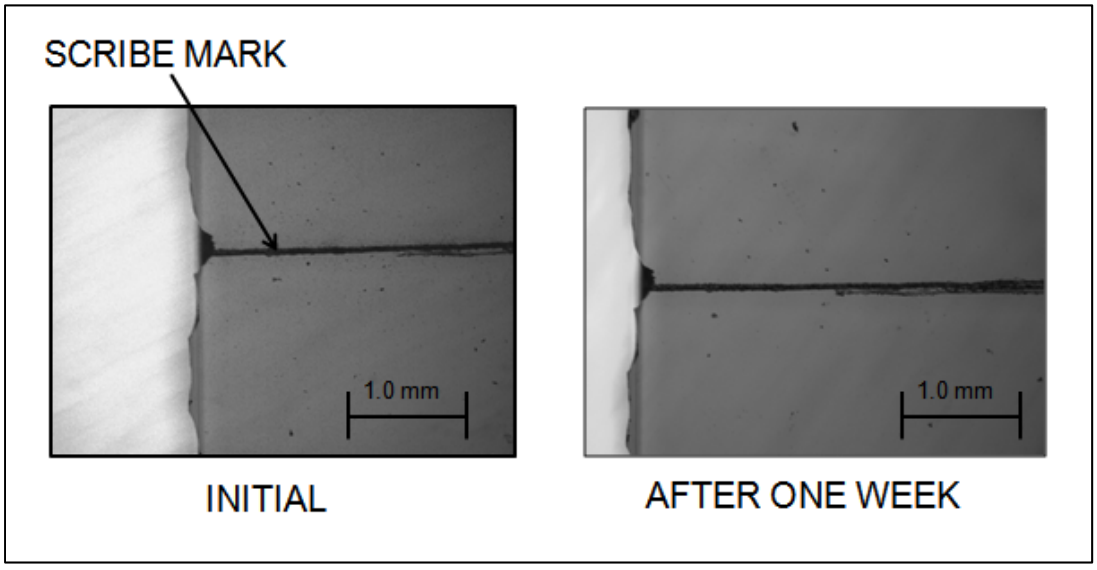

Figure 64 An Optical Micrograph of Titanium Dioxide Doped DLC Film, PLD #60, Initially and after one week Immersion in SBF

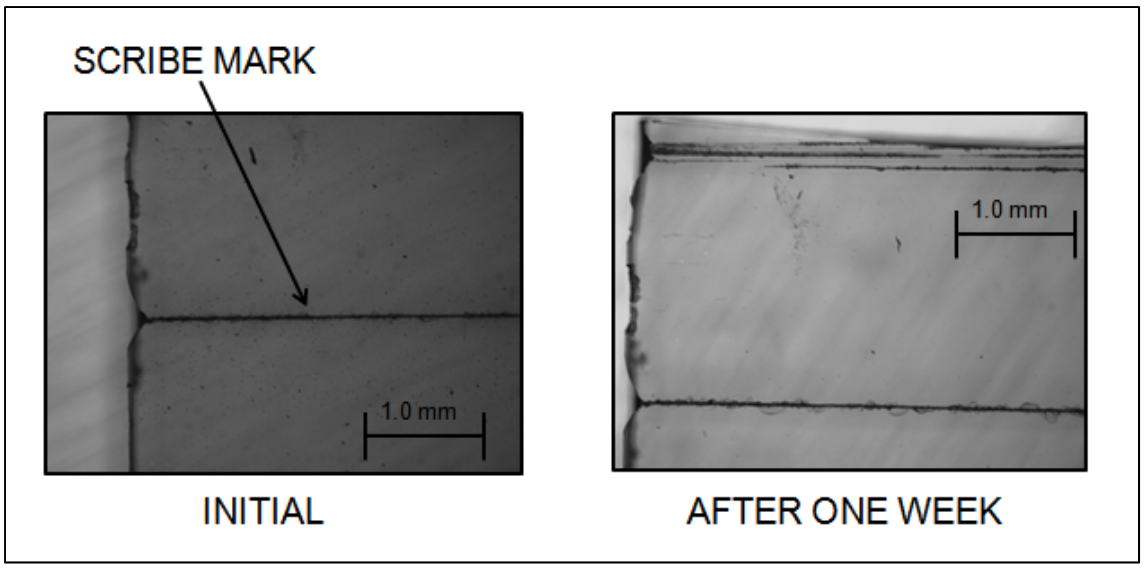

Figure 65 An Optical Micrograph of Silicon Monoxide Doped DLC Film, PLD #61, Initially and after one week Immersion in SBF

Contact Angle Measurement

Earlier experiments with undoped DLC films showed that varying the substrate holder and laser fluence had little effect on the contact angle of the films, with undoped films produced having contact angles between 65° and 88°. It was theorized that the addition of dopants would have a large effect on the contact angle of the films produced.

The results of doping DLC with titanium dioxide can be seen in Table 16 and Figure 66. The results fit within the range of contact angles found in undoped films. Furthermore, there is no pattern of increasing or decreasing contact angle with increased dopant. It could therefore be concluded that the addition of titanium dioxide has no effect on contact angle for DLC films.

The addition of silicon monoxide dopant into DLC films had a marked effect on contact angle as shown in Table 17 and Figure 67. DLC film sample PLD #64 with a 55° silicon monoxide dopant wedge achieved a super-hydrophilic contact angle of 25°. It is encouraging to note that contact angle decreases with increasing silicon monoxide dopant content, meaning that even lower contact angles could possibly be produced by increasing the size of the dopant wedge used in the multi-component ablation target during deposition. Future studies, using larger sizes of dopant wedges, are recommended to understand the full

potential of silicon monoxide doping. Once the effects of increased doping are found, testing on actual bronchoscope lenses would be a logical next step.

The contact angle for the silicon nitride-doped films was 76.6 ± 0.2°. This is similar to the undoped films and does not warrant any further investigation.

The silicon-doped DLC films had a contact angle measuring 53.1 ± 0.3°. This is a significant decrease from the undoped DLC films and deserves some further study. The decrease, however, is not as dramatic as the decrease found with silicon monoxide doping and therefore not as promising. It does indicate, however, that the incorporation of oxygen plays a significant role in the reduction of contact angle. It is also interesting to note that the decrease in contact angle with the incorporation of silicon is opposite to the findings of Grischke et al. for aC:H:Si [9] .

The dopants used in this study either reduced contact angle or had no effect. For stent applications, which require low surface energy and high contact angle, it will be necessary to test different dopants in future studies.

For future research, measuring the contact angle of other probe liquids, in addition to water, on both doped and undoped film surfaces would be beneficial. These measurements using multiple probe liquids would allow the surface energy to be calculated using the theories of Owens/Wendt, Fowkes, or Wu [44].

Table 16 Contact Angle of DLC Films Doped with Titanium Dioxide

Sample	Dopant Wedge Size (degrees)	Contact Angle (degrees)
PLD #42-2	undoped	75.1 ± 0.1
PLD #57-2	30	77.4 ± 0.5
PLD #59-2	35	79.6 ± 0.3
PLD #56-2	40	85.7 ± 0.4
PLD #60-2	45	75.3 ± 0.5
PLD #55-2	50	82.6 ± 0.3
PLD #58-2	55	76.6 ± 1.1

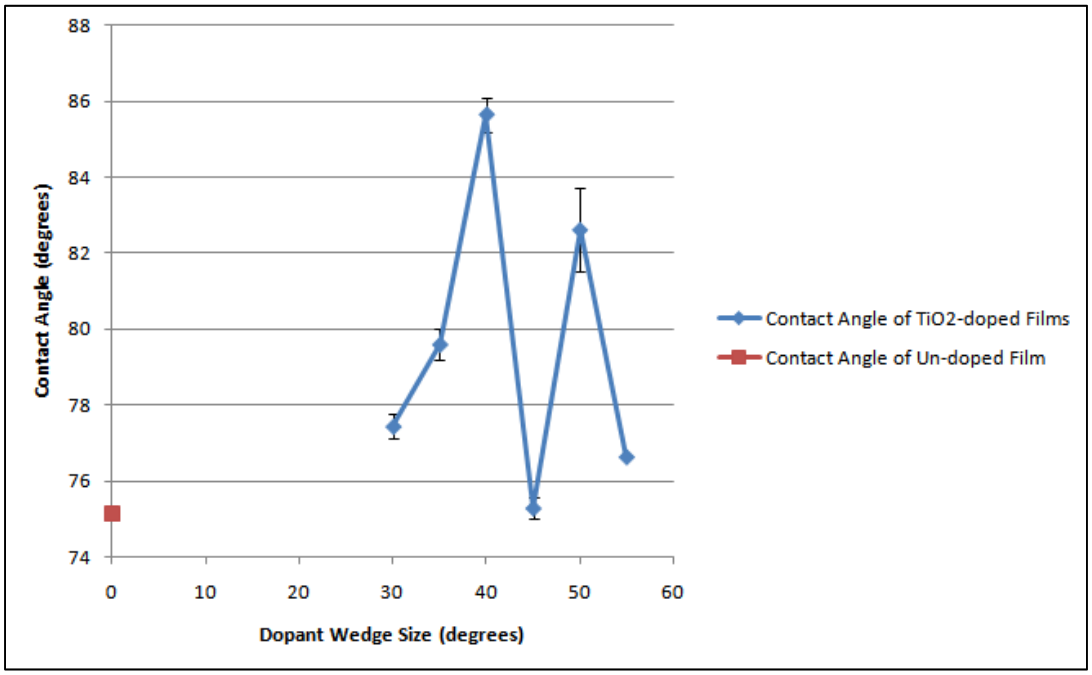

Figure 66 Contact Angle of Titanium Dioxide Doped DLC Films versus Dopant Wedge Size

Table 17 Contact Angles of DLC Films Doped with Silicon Monoxide

Sample	Dopant Wedge Size (degrees)	Contact Angle (degrees)
PLD #42-2	undoped	75.1 ± 0.1
PLD #63-2	30	36.6 ± 0.2
PLD #65-2	35	36.3 ± 0.3
PLD #62-2	40	38.2 ± 0.2
PLD #61-2	45	31.7 ± 1.0
PLD #66-2	50	30.2 ± 0.5
PLD #64-2	55	25.4 ± 0.5

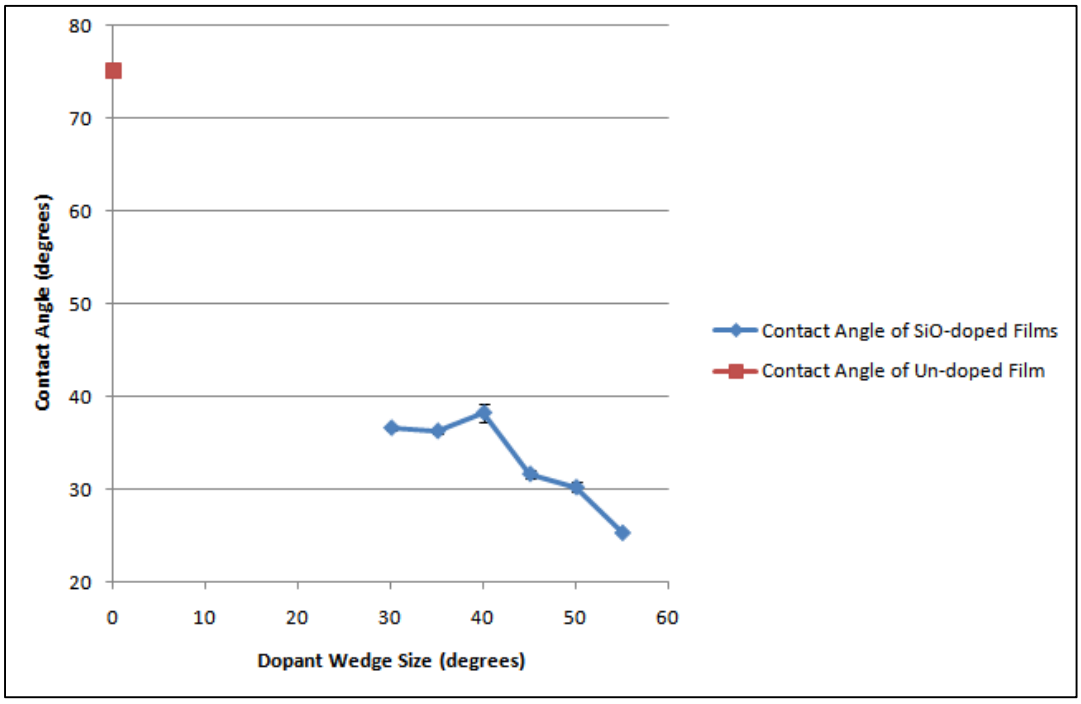

Figure 67 Contact Angle of Silicon Monoxide Doped DLC Films versus Dopant Wedge Size

Atomic Force Microscopy

Atomic force microscopy measurements were made for the doped DLC films. As with the undoped films, striations can be seen across the films' surfaces. This indicates that the roughness of the underlying substrate influences the roughness of the surface of the films. Although not ideal, some general information can be obtained regarding the surface characteristics of the films. To reduce the impact of the substrate characteristics on the measurement results, future films could be deposited on silicon substrates, which would have lower roughness values and also be more consistent.

The silicon doped DLC films had an RMS surface roughness value of 1.34, making them somewhat rougher than the undoped films. Large pits or holes can be seen in the films as shown in Figure 68. These holes seen are likely due to imperfections on the substrate. With this in mind, it is possible that the slightly increased roughness can be attributed to the substrate.

The silicon nitride doped DLC films had an RMS roughness of 1.40 which is also somewhat rougher than undoped DLC. The films had many large bumps on the surface which contributed to this increase in roughness as shown in Figure 69. It is likely that these bumps are due to relatively large particles of silicon nitride formed during the ablation process.

The surface roughness values for titanium dioxide doped films are shown in Figure 70. These values are similar to those found in undoped films. It is of interest to note that small particulates can be seen in the AFM images of these films as shown in Figure 71. These could possibly be particulates of titanium dioxide from the target formed during the ablation process.

Figure 72 shows the RMS roughness values for silicon monoxide doped films. These films also have roughness values similar to that of undoped films. The films contrast with the other doped films produced in that they do not appear to have as many bumps on the surface as shown in Figure 73.

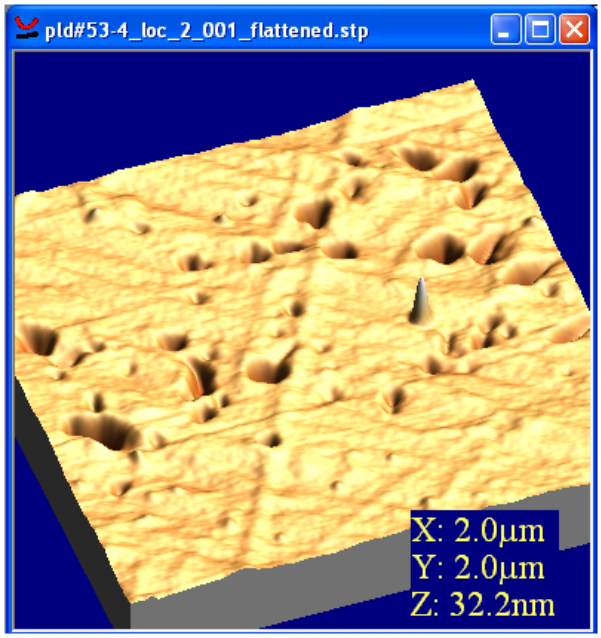

Figure 68 A Representative AFM image of Silicon Doped DLC, PLD #53, 2 µm x 2 µm Scanning Area

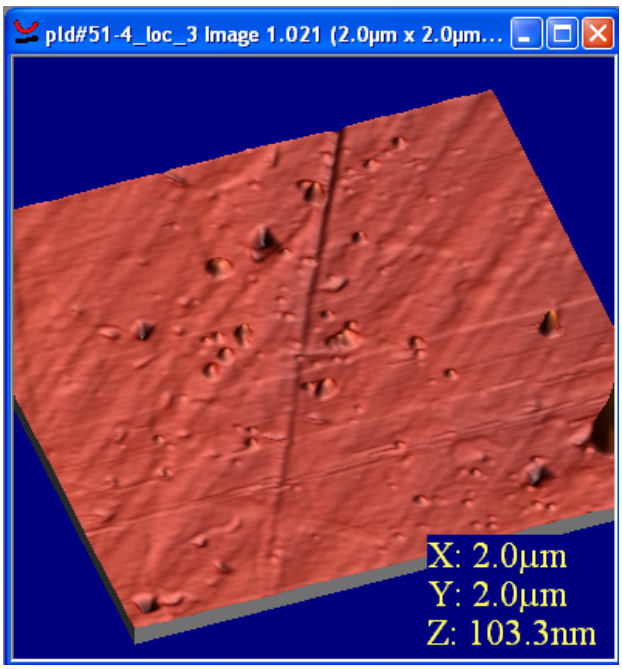

Figure 69 A Representative AFM Image of Silicon Nitride Doped DLC, PLD #51, 2 µm x 2 µm Scanning Area

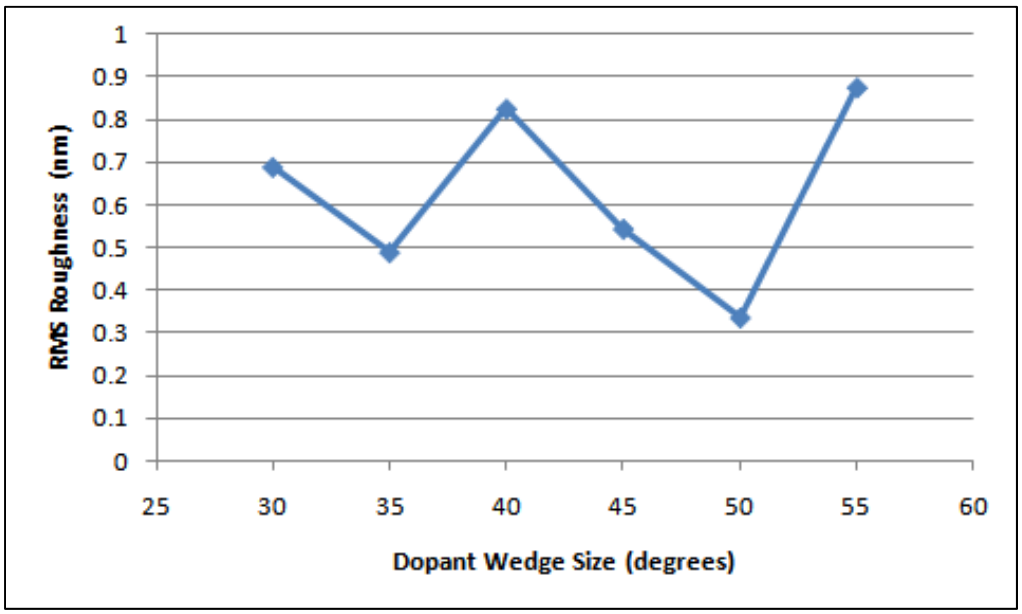

Figure 70 RMS Roughness of Titanium Dioxide Doped DLC

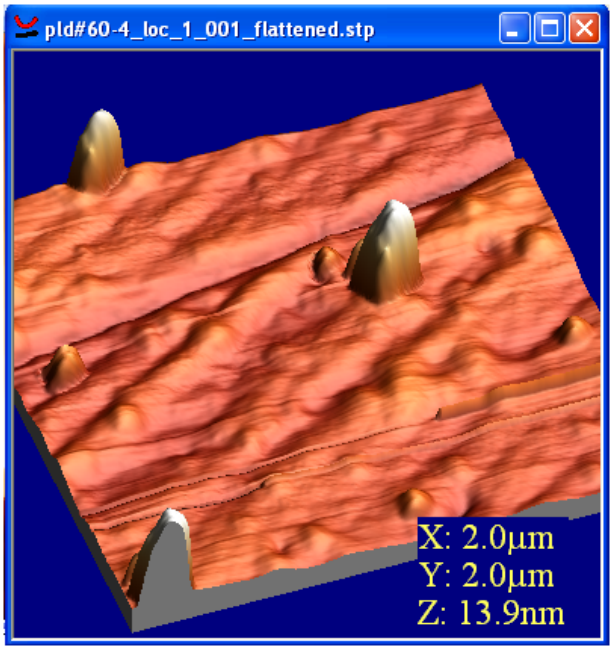

Figure 71 A Representative AFM Image of Titanium Dioxide Doped DLC, 2 µm x 2 µm Scanning Area

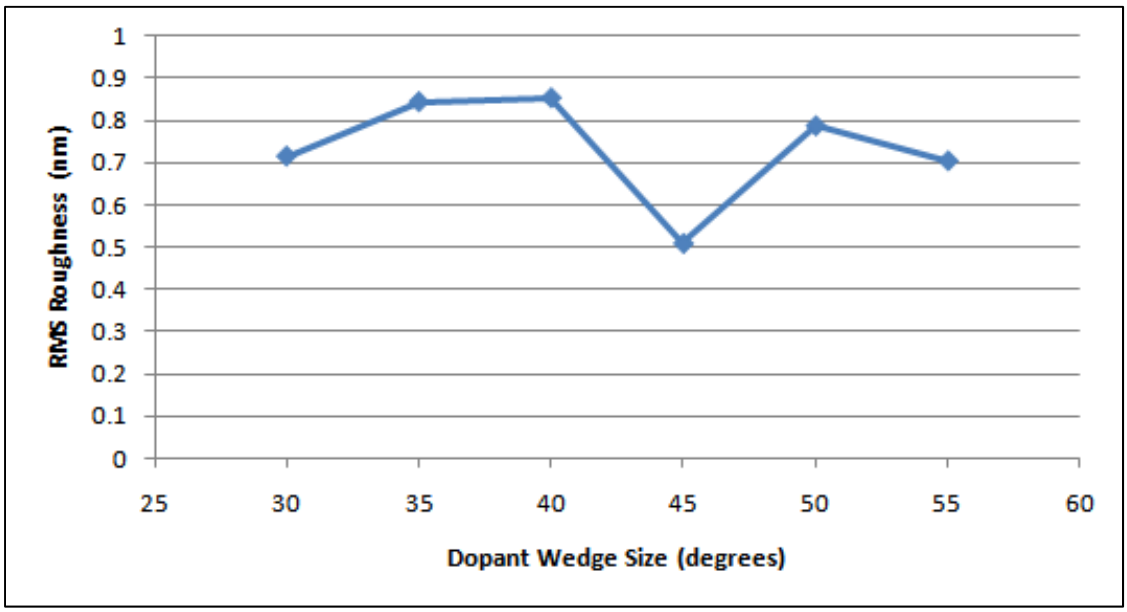

Figure 72 RMS Roughness of Silicon Monoxide Doped DLC Films

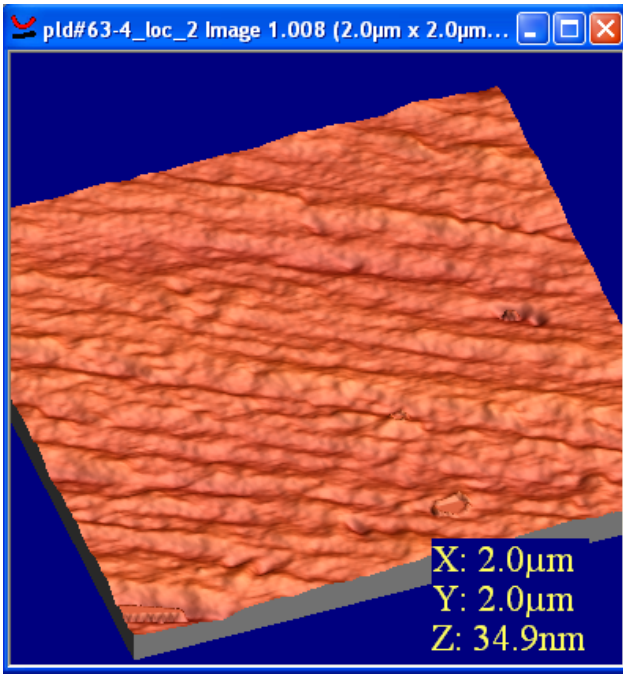

Figure 73 A Representative AFM Image of Silicon Monoxide Doped DLC Deposited on Fused Silica, 2 µm x 2 µm Scanning Area

Spectrophotometry

The transmittance for silicon doped DLC is shown in Figure 74. There is little change in transmittance with decreasing wavelength at or near the infrared portion of the spectrum. At a wavelength of approximately 700 nm, however, transmittance decreases rapidly with decreasing wavelength, possibly because the π- π* band gap energy for the amorphous DLC film has been exceeded.

Figure 75 shows the transmittance of silicon nitride doped DLC. The transmittance of this film tends to decrease gradually with decreasing wavelength until a wavelength of approximately 300 nm where there is sharp decrease in transmittance. This sharp decrease may indicate that the photonic energy at this wavelength exceeds the σ - σ* band gap for the film.

Transmittance for DLC doped with titanium dioxide is shown in Figure 76. At far ultraviolet wavelengths ($\lambda < 200$ nm) the films completely block transmission. This is not entirely unexpected, as one of the uses of titanium dioxide is sunscreen.

DLC films doped with silicon monoxide, a blackish-brown amorphous material, also block the transmission of far ultraviolet light as shown in Figure 77. They, however, transmit much better in the infrared region than the titanium dioxide doped films.

Because these films were produced with varying thicknesses, quantitatively comparing them is problematic. For future studies, a comparison of the differently doped films with samples of equal thickness would be beneficial.

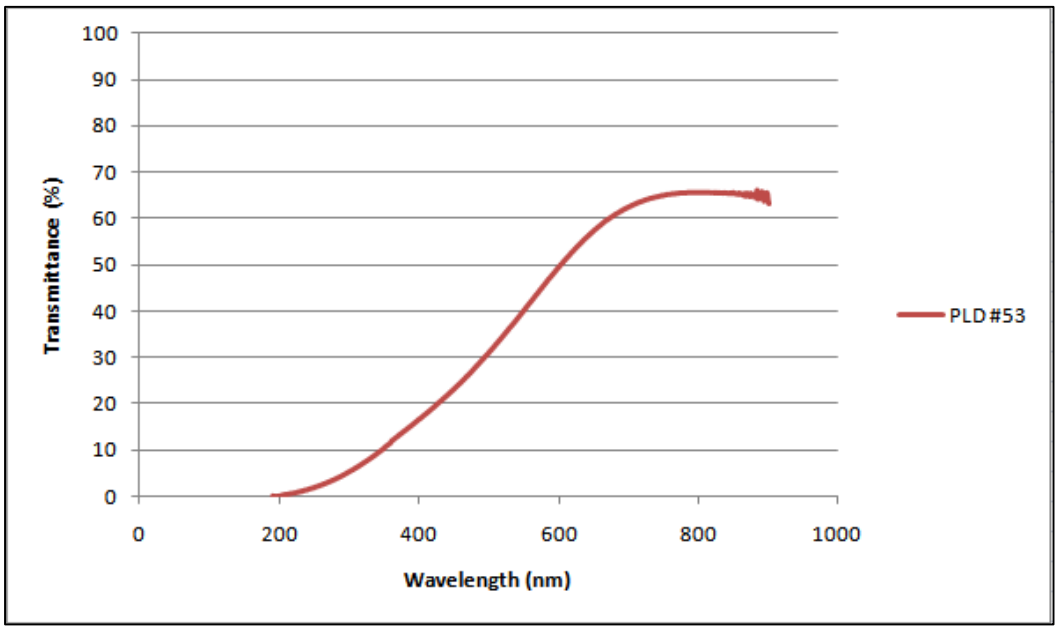

Figure 74 Transmittance of DLC doped with Silicon, PLD #53

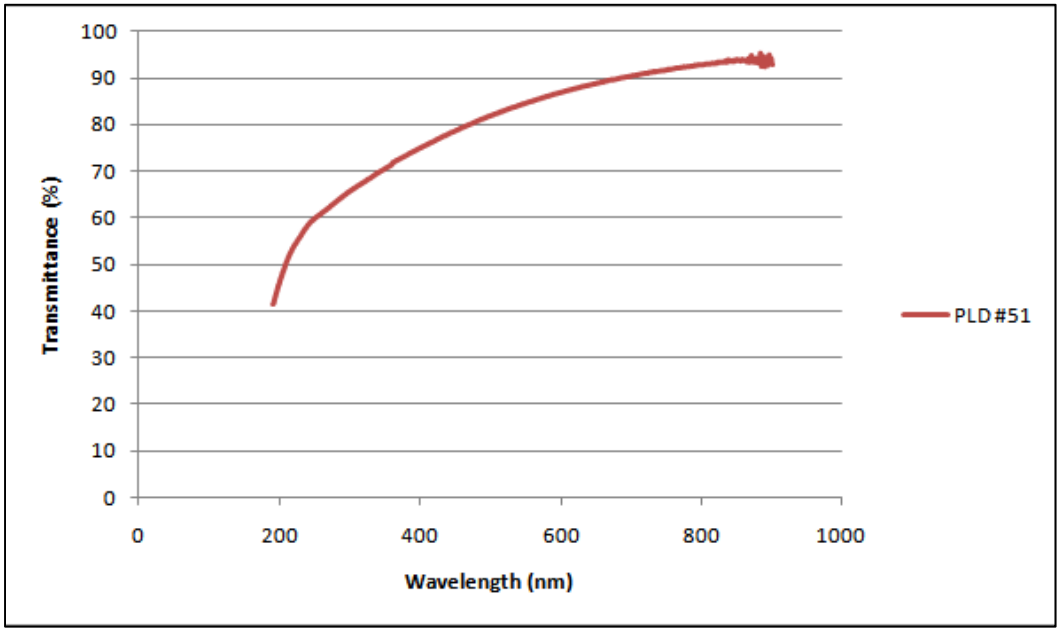

Figure 75 Transmittance for DLC doped with Silicon Nitride, PLD #51

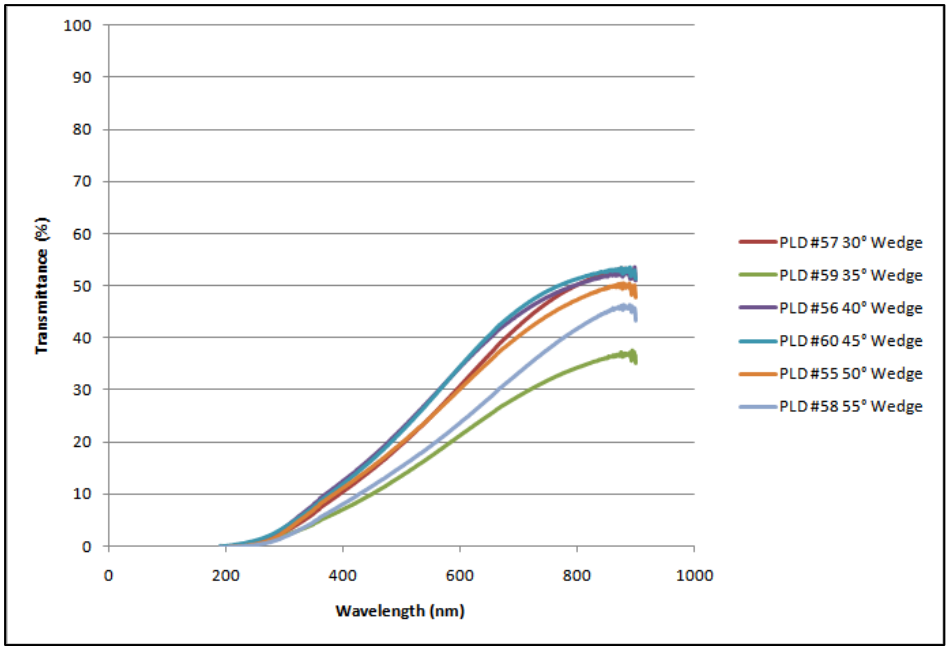

Figure 76 Transmittance of DLC Films doped with Titanium Dioxide

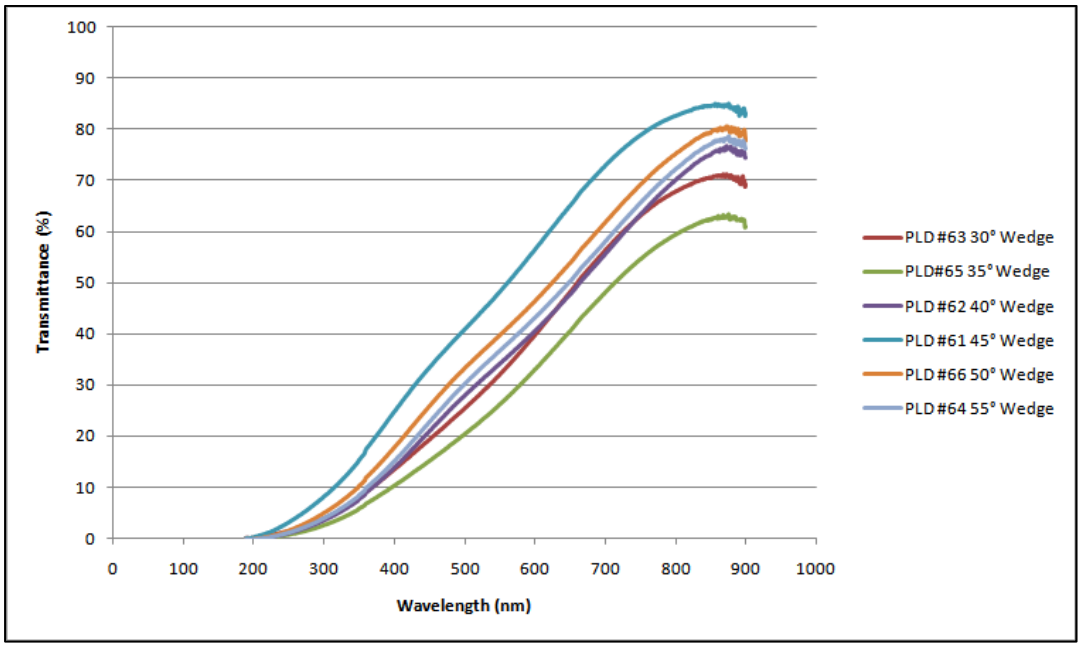

Figure 77 Transmittance of DLC Films doped with Silicon Monoxide

Surface-Modified DLC Films

The contact angles for the surface modified films are shown in Table 18. Aryl-sulfonation, the grafting of aryl sulfonate groups to carbon through diazonium salt intermediates, had little effect on the contact angles of films PLD #s 54-2 and 54-3, when compared to the untreated film PLD #54-4. The results are not in agreement with Yan et al. [33], who reported contact angles as low as 5° after five hours of aryl-sulfonation treatment of carbon films.

The argon plasma treatment alone modified the contact angle the most, producing an angle of 38.7° for PLD #54-1. The reason for this is perhaps due to the cleaning removing any weakly bonded material from the surface, increasing surface energy and therefore increasing hydrophilicity.

A recheck of PLD #54-1 after one week's time showed the contact angle to have grown from 38.7° to 45° indicating that the argon surface treatment is not a permanent one. This may be due to the adsorption of contaminants from the atmosphere into the film's surface.

Table 18 Contact Angle Results for Surface Modified DLC Films

Sample	Surface Treatment	Contact Angle (degrees)
PLD #54-1	argon plasma cleaning	38.7 ± 0.8
PLD #54-2	aryl-sulfonation, 2 hours	65.0 ± 3.9
PLD #54-3	aryl-sulfonation, 5 hours	70.6 ± 4.1
PLD #54-4	none	77.7 ± 1.1

CHAPTER IV
CONCLUSIONS

Diamond-like carbon thin films without dopants were successfully produced on silicon, fused silica, and silicon nitride substrates using a pulsed-laser deposition system. Film thickness was limited by delamination caused by residual stresses. Raman spectroscopy showed that the structure of the films was dependent upon the deposition temperature but independent of the laser pulse energy used. The films were stable after forty-three weeks immersion in simulated body fluid at 36.5 °C, showing no delamination during that time when viewed microscopically. Contact angles for water on the surface of these films varied between 65° and 88°. The films produced were very smooth with RMS roughness values less than 0.35 nm when deposited on silicon, although larger values occurred when the film was deposited on rougher fused silica substrates. Ball-and-flat tribometry showed these films to have excellent wear resistance and a low coefficient of friction (0.08) in an oil-lubricated environment. Spectrophotometry showed that these films have good transparency in infrared and visible light.

Dopants were incorporated into the DLC films by using a multi-component target during deposition. The dopants used, silicon, silicon nitride, titanium dioxide, and silicon monoxide, altered the structure and properties of the films. Residual stress was reduced allowing thicker films to be grown. Doping DLC films with silicon monoxide produced contact angles as low as 25°, with contact angle decreasing with increasing dopant. The doped films were all smooth and transparent. Soaking experiments showed the doped films to have stability in simulated body fluid after one week of test time.

The surface modification techniques tried on the DLC films did not produce a permanent significant change in contact angle. The contact angles for films that underwent aryl-sulfonation were similar to those found in unmodified films. The contact angle for DLC films exposed to argon plasma had a slightly reduced contact angle which increased with time after treatment.

The silicon monoxide doped DLC films show great potential as coatings for bronchoscope lenses. These films have good transparency and have been shown to be stable when immersed in SBF. The low contact angle of water (θ = 25 °) on these films indicates that they may be anti-fogging. Future depositions using greater amounts of silicon monoxide dopant may reduce contact angle further. Using additional probe liquids during contact angle measurement would allow for the calculation of surface energy, giving greater insight to the nature of the surface wetting. Once the effects of increased doping are found, testing on actual bronchoscope lenses is recommended.

The films are candidates for artificial joint coatings due to their favorable wear properties and stability. The test duration was very short in comparison to the lifetime of an artificial joint, however, so longer test times are required to confirm viability of the films for this application. Additionally, films will need to be produced on substrates made from the same materials that would be used in the actual prosthesis.

The films have properties which would make them useful in coronary stent applications. Stability of the films, demonstrated by the soaking experiments in SBF, is a requirement for the long-term implantation of the stents. The smoothness of the films (RMS roughness < 0.35) would help prevent the adhesion of platelets, which could cause clotting. Unfortunately, none of the films produced showed a high contact angle, which is required for the prevention of thrombosis. Further modification of the films, perhaps with new, untried dopants, will be necessary.

LIST OF REFERENCES

1. Ferrari, A., *Determination of bonding in diamond-like carbon by Raman spectroscopy.* Diamond and Related Materials, 2002. **11**: p. 1053-1061.
2. Paul, R., et al., *Synthesis of DLC films with different sp^2/sp^3 ratios and their hydrophobic behavior.* Journal of Physics D: Applied Physics, 2008. **41**: p. 1-7.
3. Pierson, H., *Handbook of Carbon, Graphite, Diamond, and Fullerines*. 1 ed. Materials Science and Process Technology Series, ed. R. Bunshah and G. McGuire. 1993, Park Ridge, New Jersey: Noyes Publications. 399.
4. Ravi, S. and P. Silva, eds. *Properties of Amorphous Carbon*. EMIS Datareviews series EMIS Processing Series, ed. B. Weiss. 2003, INSPEC, The Institution of Electrical Engineers: London, United Kingdom.
5. Sheeja, D., et al., *Low stress thick diamond-like carbon films prepared by filtered arc deposition for tribological applications.* Surface & Coatings Technology, 2002. **154**: p. 289-293.
6. Dearnaley, G. and J. Arps, *Biomedical applicarions of diamond-like carbon (DLC) coatings: a review.* Surface & Coatings Technology, 2005. **200**: p. 2518-2524.
7. Robertson, J., *Diamond-like amorphous carbon.* Materials Science and Engineering R, 2002. **37**: p. 129-381.
8. Ferrari, A. and J. Robertson, *Interpretation of Raman spectra of disordered and amorphous carbon.* Physical Review B, 2000. **61**(20): p. 14095-14107.
9. Grischke, M., et al., *Application-oriented modifications of deposition processes for diamond-like-carbon-based coatings.* Surface Coatings Technology, 1995. **74-75**: p. 739-745.
10. Ahmed, S., D. Banerjee, and K. Chattopadhyay, *The influence of fluorine doping on the optical properties of diamond-like carbon thin films.* Vacuum, 2010. **84**: p. 837-842.
11. Sung, J., M. Kan, and M. sung, *Fluorinated DLC for tribological applications.* International Journal of Refractory Metals & Hard Materials, 2009. **27**: p. 421-426.
12. Qi, j., et al., *Film thickness effects on mechanical and tribological properties of nitrogenated diamond-like carbon films.* Surface Coatings Technology, 2001. **145**: p. 38-43.
13. Sikora, A., et al., *Effect of boron incorporation on the structure and electrical properties of diamond-like carbon films deposited by femtosecond and nanosecond pulsed laser ablation.* Thin Solid Films, 2009. **518**: p. 1470-1474.
14. Cheng, H., W. Wu, and J. Ting, *Microstructure and optical properties of chromium containing amorphous hydrogenated carbon thin films (a-c:H/Cr).* Thin Solid Films, 2009. **517**: p. 4724-4727.

15. Wei, Q., et al., *Improvement of wear resistance of pulsed laser deposited carbon films through incorporation of metals.* Materials Science & Engineering B, 1998. **53**: p. 262-266.
16. Narayan, R., et al., *Anti-microbial Properties of Diamond-like Carbon-Silver-Platinum Nanocomposite Thin Films.* Journal of Materials Engineering and Performance, 2005. **14**(4): p. 435-440.
17. Ahmed, S., M. Moon, and K. Lee, *Effect of silver doping on optical property of diamond like carbon films.* Thin Solid Films, 2009. **517**: p. 4035-4038.
18. Andara, M., et al., *Hemocompatibility of diamond-like carbon-metal composite films.* Diamond & Related Materials, 2006. **15**: p. 1941-1948.
19. Nam, N., et al., *Effect of stress passivation of Si-DLC coating as stent materials in simulated body environment.* Diamond & Related Materials, 2009. **18**: p. 1145-1151.
20. Zhou, Y., et al., *The modifications of the surface wettability of amorphous carbon films.* Colloids and Surfaces A: Physicochemical and Engineering Aspects, 2009. **335**: p. 128.
21. Nagashima, S., et al., *Effect of oxygen plasma treatment on non-thrombogenicity of diamond-like carbon films.* Diamon & Related Materials, 2010. **19**: p. 861-864.
22. Kutsay, O., et al., *Surface properties of amorphous carbon films.* Diamond & Related Materials, 2008. **17**: p. 1689-1691.
23. Weissmantel, S., G. Reisse, and D. Rost, *Preparation of superhard amorphous carbon films with low internal stress.* Surface & Coatings Technology, 2004. **188-189**: p. 268-273.
24. Friedmann, T., et al., *Thick stress-free amorphous-tetrahedral carbon films with hardness near that of diamond.* Applied Physics Letters, 1997. **71**(26): p. 3820-3822.
25. Narayan, R., *Nanostructured diamondlike carbon thin films for medical applications.* Materials Science & Engineering C, 2005. **25**: p. 405-416.
26. Gutensohn, K., et al., *In Vitro Analysis of Diamond-like Carbon Coated Stents: Reduction of Metal Ion Release, Platelet Activation, and Thrombogenicity.* Thrombosis Research, 2000. **99**: p. 577-585.
27. Nakatani, T., et al., *Application of Diamond-Like-Carbon Coating to a Coronary Artery Drug-Eluting Stent.* Journal of Photopolymer Science and Technology, 2007. **20**(2): p. 221-228.
28. Marciano, F., et al., *Diamond-like carbon films produced from high deposition rates exhibit antibacterial activity.* Synthetic Materials, 2009. **159**: p. 2167-2169.
29. Loir, A., et al., *Deposition of tetrahedral diamond-like carbon thin films by femtosecond laser ablation for applications of hip joints.* Thin Solid Films, 2004. **453-454**: p. 531-536.
30. *Stents – All Sections* http://www.nhlbi.nih.gov/health/dci/Diseases/stents/stents_all.html (accessed on 11-10-2010)

31. *Hip Science - NASA Science* http://science.nasa.gov/science-news/science-at-nasa/2002/30oct_hipscience/ (accessed on 11-10-2010)
32. Winslow, T., 2006.
33. Yan, A., et al., *Controlling water contact angle on carbon surfaces from 5 degrees to 167 degrees.* Carbon, 2006. **44**: p. 3113-3148.
34. Cho, S., et al., *Dependence of Apatite Formation on Silica Gel on Its Structure: Effect of Heat Treatment.* Journal of American Ceramics Society, 1995. **78**(7): p. 1769-1774.
35. Balon, F., et al., *Diamond-like carbon thin films for high temperature applications prepared by filtered pulse laser deposition.* Vacuum, 2005. **80**: p. 163-167.
36. Chhowalla, M., et al., *Evolution of sp^2 bonding with deposition temperature in tetrahedral amorphous carbon studied by Raman spectroscopy.* Applied Physics Letters, 2000. **76**(11): p. 1419-1421.
37. Ding, X., Q. Li, and X. Kong, *Effect of repetition rates of laser pulses on microsctructure and optical properties of diamond-like carbon films.* International Journal of Modern Physics B, 2009. **23**(30): p. 5671-5681.
38. Marchon, B., et al., *Photoluminescence And Raman Spectroscopy In Hydrogenated Carbon Films.* IEEE Transactions on Magnetics, 1997. **33**(5): p. 3148-3150.
39. Reuter, S., et al., *Correlation of structural properties of commercial DLC-coatings to their tribological performance in biomedical applications.* Wear, 2006. **261**: p. 419-425.
40. Quere, D., *Rough ideas on wetting.* Physica A, 2002. **313**: p. 32-45.
41. Donnet, C. and A. Erdemir, eds. *Tribology of Diamond-Like Carbon Films*. 2008, Springer Sciece + Business Media, LLC: New York, NY. 157.
42. Damasceno, J. and S. Camargo, *DLC-SiOx nanocomposite films deposited from CH4:SiH4:O2 gas mixtures.* Surface & Coatings Technology, 2006. **200**: p. 6279-6282.
43. Zhang, S. and N. Ali, eds. *Nanocomposite Thin Films and Coatings*. 2007, Imperial College Press: Danvers, MA 01923.
44. Zenkiewicz, M., *Methods for the calculation of surface free energy of solids.* Journal of Achievements in Materials and Manufacturing Engineering, 2007. **24**(1): p. 137-145.

APPENDIX

Table 19 Pulsed Laser Deposition Parameters

Sample	Dopant	Wedge Size (degrees)	Laser Pulse Energy (mJ)	Average Attenuation Factor	Laser Pulse Energy At Target (mJ)	Beam Area (m^2)	Peak Power (W)	Laser Intensity (W/m)	Laser Fluence (J/cm^2)	Repetition Rate (Hz)	Deposition Temperature (°C)	Substrate(s)	Pressure (mTorr)	Deposition Time
PLD#11 DLC	none	n/a	9.2	0.59	5.4	1.30E-07	3.60E+05	2.8E+12	4.2	50	200	silicon wafers and silicon nitride spheres	1.0E-06	4 hours
PLD#11 Si Bond Coating	none	n/a	11	0.59	6.5	1.30E-07	4.31E+05	3.314E+12	5.0	50	200	silicon wafers and silicon nitride spheres	1.0E-06	1 hour
PLD#21	none	n/a	6.3	0.59	3.7	1.30E-07	2.47E+05	1.9E+12	2.8	50	192	silicon wafer	1.0E-06	4 hours
PLD#22	none	n/a	5.3	0.59	3.1	1.30E-07	2.08E+05	1.6E+12	2.4	50	200	silicon wafer	1.1E-06	4 hours
PLD#24	none	n/a	10.5	0.59	6.2	1.30E-07	4.11E+05	3.2E+12	4.7	50	192	silicon wafer	7.5E-07	4 hours
PLD#26	none	n/a	7.5	0.59	4.4	1.30E-07	2.94E+05	2.3E+12	3.4	50	194	silicon wafer	1.0E-06	4 hours
PLD#29	none	n/a	9.5	0.59	5.6	1.30E-07	3.72E+05	2.9E+12	4.3	50	194	silicon wafer	1.1E-06	4 hours
PLD#32	none	n/a	8.7	0.59	5.1	1.30E-07	3.41E+05	2.6E+12	3.9	50	195	silicon wafer	7.7E-07	4 hours
PLD#36	none	n/a	7.8	0.58	4.5	1.30E-07	3.03E+05	2.3E+12	3.5	50	19	fused silica	7.8E-07	15 minutes
PLD#40	none	n/a	9	0.56	5.1	1.30E-07	3.39E+05	2.6E+12	3.9	50	20	fused silica	4.8E-07	15 minutes
PLD#41	none	n/a	8	0.56	4.5	1.30E-07	3.00E+05	2.3E+12	3.5	50	18	fused silica	5.5E-07	15 minutes
PLD#42	none	n/a	6.9	0.57	3.9	1.30E-07	2.61E+05	2.0E+12	3.0	50	19	fused silica	5.5e-7	15 minutes
PLD#43	none	n/a	6	0.57	3.4	1.30E-07	2.29E+05	1.8E+12	2.6	50	21	fused silica	8.1E-07	15 minutes
PLD#44	none	n/a	5	0.57	2.9	1.30E-07	1.91E+05	1.5E+12	2.2	50	17	fused silica	5.6E-07	15 minutes
PLD#45	none	n/a	7	0.57	4.0	1.30E-07	2.67E+05	2.1E+12	3.1	50	202	fused silica	6.5E-07	15 minutes
PLD#46	none	n/a	7	0.57	4.0	1.30E-07	2.67E+05	2.1E+12	3.1	50	163	fused silica	5.2E-07	15 minutes
PLD#47	none	n/a	4	0.57	2.3	1.30E-07	1.53E+05	1.2E+12	1.8	50	18	fused silica	4.6E-07	15 minutes
PLD#48	none	n/a	7	0.57	4.0	1.30E-07	2.68E+05	2.1E+12	3.1	50	128	fused silica	5.0E-07	15 minutes
PLD#49	none	n/a	7.1	0.57	4.1	1.30E-07	2.70E+05	2.1E+12	3.1	50	92	fused silica	6.0E-07	15 minutes
PLD#50	none	n/a	7	0.57	4.0	1.30E-07	2.67E+05	2.1E+12	3.1	50	56	fused silica	5.9E-07	15 minutes
PLD#51	silicon nitride	not a wedge; equivalent to 45 degrees	7	0.57	4.0	1.30E-07	2.67E+05	2.1E+12	3.1	50	16	fused silica	4.8E-07	15 minutes
PLD#52	silicon	45	7	0.58	4.0	1.30E-07	2.69E+05	2.1E+12	3.1	50	18	fused silica	8.7E-07	15 minutes
PLD#53	silicon	45	7	0.58	4.0	1.30E-07	2.69E+05	2.1E+12	3.1	50	19	fused silica	8.7E-07	4 hours
PLD#54	none	n/a	7	0.57	4.0	1.30E-07	2.67E+05	2.1E+12	3.1	50	20	fused silica	6.5E-07	15 minutes
PLD#55	titanium dioxide	50	6.96	0.57	4.0	1.30E-07	2.65E+05	2.0E+12	3.1	50	18.4	fused silica	7.3E-07	4 hours
PLD#56	titanium dioxide	40	7	0.56	3.9	1.30E-07	2.62E+05	2.0E+12	3.0	50	18.2	fused silica	7.2E-07	4 hours
PLD#57	titanium dioxide	30	7	0.58	4.1	1.30E-07	2.71E+05	2.1E+12	3.1	50	18.4	fused silica	7.7E-07	4 hours
PLD#58	titanium dioxide	55	7	0.59	4.1	1.30E-07	2.73E+05	2.1E+12	3.2	50	18.4	fused silica	7.8E-07	4 hours
PLD#59	titanium dioxide	35	7	0.58	4.1	1.30E-07	2.70E+05	2.1E+12	3.1	50	20.4	fused silica	7.2E-07	4 hours
PLD#60	titanium dioxide	45	7	0.57	4.0	1.30E-07	2.67E+05	2.1E+12	3.1	50	18.4	fused silica	1.0E-06	4 hours
PLD#61	silicon monoxide	45	7	0.56	3.9	1.30E-07	2.60E+05	2.0E+12	3.0	50	18.8	fused silica	7.7E-07	4 hours
PLD#62	silicon monoxide	40	7	0.57	4.0	1.30E-07	2.67E+05	2.1E+12	3.1	50	17.6	fused silica	6.7E-07	4 hours
PLD#63	silicon monoxide	30	7	0.57	4.0	1.30E-07	2.67E+05	2.1E+12	3.1	50	18.6	fused silica	7.3E-07	4 hours
PLD#64	silicon monoxide	55	7	0.57	4.0	1.30E-07	2.67E+05	2.1E+12	3.1	50	18.2	fused silica	7.6E-07	4 hours
PLD#65	silicon monoxide	35	7	0.57	4.0	1.30E-07	2.67E+05	2.1E+12	3.1	50	19	fused silica	7.0E-07	4 hours
PLD#66	silicon monoxide	50	7	0.57	4.0	1.30E-07	2.67E+05	2.1E+12	3.1	50	19	fused silica	8.2E-07	4 hours

VITA

Russell Lee Leonard was born in Columbia, Tennessee on June 14, 1973. He was raised in Lewisburg, TN where he graduated from Marshall County High School in 1991. He graduated from Tennessee Technological University with a Bachelor of Science Degree in Mechanical Engineering in 1995. After twelve years working as a project engineer in the die casting industry, he returned to school at the University of Tennessee Space Institute in 2009 to pursue a Master's Degree in Materials Science and Engineering.